1-1-2014

Statistical Characterization of Viscoelastic Creep Compliances of a Vinyl Ester Polymer

Jutima Simsiriwong

Statistical characterization of viscoelastic creep compliances of a vinyl ester polymer

By

Jutima Simsiriwong

A Dissertation
Submitted to the Faculty of
Mississippi State University
in Partial Fulfillment of the Requirements
for the Degree of Doctor of Philosophy
in Aerospace Engineering
in the Department of Aerospace Engineering

Mississippi State, Mississippi

May 2014

Statistical characterization of viscoelastic creep compliances of a vinyl ester polymer

By

Jutima Simsiriwong

Approved:

Rani W. Sullivan
(Director of Dissertation)

Harry H. Hilton
(Committee Member)

Thomas E. Lacy
(Committee Member)

Hossein Toghiani
(Committee Member)

Charles U. Pittman, Jr.
(Committee Member)

Judith A. Schneider
(Committee Member)

J. Mark Janus
(Graduate Coordinator)

Achille Messac
Dean
Bagley College of Engineering

Name: Jutima Simsiriwong

Date of Degree: May 16, 2014

Institution: Mississippi State University

Major Field: Aerospace Engineering

Major Professor: Rani W. Sullivan

Title of Study: Statistical characterization of viscoelastic creep compliances of a vinyl ester polymer

Pages in Study: 130

Candidate for Degree of Doctor of Philosophy

The objective of this study was to develop a model to predict the viscoelastic material functions of a vinyl ester (VE) polymer (Derakane 441-400, Ashland Co.,) with variations in its material properties. Short-term tensile creep/creep recovery experiments were conducted at two stress levels and at four temperatures below the glass transition temperature of the VE polymer, with 10 replicates for each test configuration. Experimental strains in both the longitudinal and transverse directions were measured using a digital image correlation technique. The measured creep strain versus time responses were subsequently used to determine the creep compliances using the generalized viscoelastic constitutive equation with a Prony series representation.

The variation in the creep compliances of Derakane 441-400 was described by formulating the probability density functions (PDFs) and the corresponding cumulative distribution functions (CDFs) of the creep compliances using the two-parameter Weibull and log-normal distributions. The maximum likelihood estimation technique was used to obtain the Weibull shape and its scale parameters and the log-normal location and its scale parameters. The goodness-of-fit of the distributions was determined by performing

Kolmogorov-Smirnov (K-S) hypothesis tests. Based on the K-S test results, the Weibull distribution is a better representation of the creep compliances of Derakane 441-400 when compared to the log-normal distribution. Additionally, the Weibull scale and shape parameters of the creep compliance distributions were shown to be time and temperature dependent. Therefore, two-dimensional quadratic Lagrange interpolation functions were used to characterize the Weibull parameters to obtain the PDFs and subsequently the CDFs of the creep compliances for the complete design temperature range during steady state creep. At each test temperature, creep compliance curves were obtained for CDF values of 0.05, 0.50 and 0.95 and compared with the experimentally obtained lowest, mean and highest creep compliances, respectively. The predicted creep compliances of Derakane 441-400 in the design space are in good agreement with the experimental data.

DEDICATION

This work is dedicated to my parents: Pramoth and Chanikarn Simsiriwong.

ACKNOWLEDGEMENTS

I would like to express my sincere appreciation to my advisor and mentor, Dr. Rani W. Sullivan. She has been the most wonderful advisor and overall role-model that I deeply hope to someday emulate. She has given me the guidance and continuous support throughout this past 6 years. Her confidence in my abilities encourages me to work harder.

This dissertation would not be possible without the help of Dr. Harry H. Hilton. He has opened up my world of viscoelasticity. He generously spent countless hours of his valuable time on the phone answering questions. I greatly admire his professionalism and kindness.

I would like to express my gratitude to the other members of my dissertation committee, Dr. Thomas Lacy, Dr. Hossein Toghiani, Dr. Charles Pittman, and Dr. Judy Schneider for their support and insight.

The experimental portion of this study would not have been accomplished without Mr. Daniel Drake, who introduced me to the Digital Image Correlation Technique. His invaluable assistance is greatly appreciated. Special thanks to Dr. Hossein Toghiani and the Center of Advanced Vehicular Systems (CAVs) for allowing me to use their laboratories to fabricate the test specimens and to perform the tests.

I am fortunate for all of the financial support for my entire graduate study at Mississippi State University. I am very grateful for the valuable assistantships and fellowships from my sponsors including Dr. Rani W. Sullivan, Mr. James W. Bagley, the Office of the Graduate School, and the Department of Aerospace Engineering.

Last but most importantly, I would like to thank my families for their wonderful love and support. To my Thai family, who let me have this opportunity to attend school half way around the world. To my American family, John and Linda, who has given me tremendous love and support throughout the past 12 years. And finally, to my husband, Matt, who has given me a constant encouragement; without them I could never be where I am today.

TABLE OF CONTENTS

LIST OF TABLES

LIST OF FIGURES

LIST OF ACRONYMS AND NOMENCLATURE

BSP	Boltzmann superposition principle
D_{N_0}	Maximum discrepancy for N_0 sample size
$D_{N_0}^{\xi}$	Critical value for Kolmogorov-Smirnov test
C_{1111}	Creep compliance in longitudinal (x_1) direction
C_{1122}	Creep compliance in transverse (x_2) direction
C_{1111}^{0}	Instantaneous creep compliance in longitudinal (x_1) direction
C_{1122}^{0}	Instantaneous creep compliance in transverse (x_2) direction
C_{1111}^{n}	Prony coefficients in the longitudinal creep compliance Prony series representation, $1 \le n \le N_{pr}$
C_{1122}^{n}	Prony coefficients in the transverse creep compliance Prony series representation, $1 \le n \le N_{pr}$
$\underline{C}_{1111}$	Probabilistic creep compliance in longitudinal (x_1) direction
$\underline{C}_{1122}$	Probabilistic creep compliance in transverse (x_2) direction
CCD	Charge-coupled device
CDF, $F(x\|w)$	Cumulative distribution function
DIC	Digital image correlation
DMA	Dynamic mechanic analysis
E	Modulus of elasticity or Young's modulus

E_{1111}	Relaxation modulus in longitudinal (x_1) direction
E_{1122}	Relaxation modulus in transverse (x_2) direction
E^0_{1111}	Instantaneous relaxation modulus in longitudinal (x_1) direction
E^0_{1122}	Instantaneous relaxation modulus in transverse (x_2) direction
$f_\sigma(t)$	Loading function for tensile creep test
$H(t)$	Heaviside unit step function
k	Spring modulus
K	Half of a width of interval
K-S	Kolmogorov-Smirnov test
KV	Kelvin-Voigt model
$L(x\|w)$	Likelihood function
LSQ	Least-squares method
M	Total number of sampling points, $1 \leq m \leq M$
MEKP	Methyl ethyl ketone peroxide
MLE	Maximum likelihood estimation
N_{pr}	Total number of Kelvin elements (length of Prony series), $1 \leq n \leq N_{pr}$
PDF, $f(x\|w)$	Probability density function
PMC	Polymer-matrix composite
Q	Order of the polynomial of loading function $f_\sigma(t)$, $0 \leq q \leq Q$
R^2	Correlation coefficient
RTM	Resin transfer molding
s	Standard deviation
S	Residual sum of squares

t	Time
T	Temperature
t_0	Initial time of the experiment
t_1	Time at the end of the initial loading phase in creep test
t_∞	Time at the end of the experiment
T_g	Glass transition temperature
t_m	Discrete time at which the experimental data is obtained, $1 \leq m \leq M$
VARTM	Vacuum-assisted resin transfer molding
VE	Vinyl ester
w	Distribution parameter
x	Observed data
Y	Non-dimensionalized creep compliance
$z_{\alpha/2}$	A number from the Standard Normal Z-Table for a given confidence level
γ, β	Weibull distribution shape and scale parameters
ε_{11}	Experimental strain in longitudinal (x_1) direction
ε_{22}	Experimental strain in transverse (x_2) direction
$\tilde{\varepsilon}_{11}$	Probabilistic strain in longitudinal (x_1) direction
$\tilde{\varepsilon}_{22}$	Probabilistic strain in transverse (x_2) direction
ε_d	Strain in the damper
ε_s	Strain in the spring
η, ω	Transformed coordinate system for Lagrange interpolation function
Λ	Short-hand notation of the time integral in the Eq. (4.13)
λ, ζ	Log-normal distribution location and scale parameters

μ	Damper viscosity
ξ	Integration variable
ζ	Significance level
σ_0	Constant stress applied for creep loading
σ_{11}	Applied tensile stress in the loading (x_1) direction
$\bar{\sigma}_{11}$	Probabilistic stress in the loading (x_1) direction
σ_d	Stress in the damper
σ_s	Stress in the spring
σ_u	Ultimate tensile stress
τ_n	Retardation times, $1 \leq n \leq N_{pr}$
ϕ_q	Constants for the loading function, $0 \leq q \leq Q$
$\psi(T, t)$	Lagrange interpolation function of time and temperature

CHAPTER I

INTRODUCTION

1.1 Motivation

Polymer-matrix composites (PMCs) have been increasingly adopted in structural applications (Table 1.1) due to their many advantageous properties, such as high strength, high fatigue and durability performances, etc. [1]. The growing use of PMC-based structures is derived in part from the ability to synthesize polymers to achieve the required material properties for a vast range of engineering applications. In some structural applications, PMCs are used in primary and secondary load carrying members where the applied loads are maintained relatively constant throughout the service life of the structure. This constant load produces a time-dependent deformation or creep in the structure. Examples of components which are subjected to sustained loadings include rotors, turbine blades, pressure vessels, heat engines, and other components in power plants and chemical refineries [2].

Long-term viscoelastic behavior (creep response under mechanical and thermal loading) must be considered in the design of PMC structures. Creep can lead to a gradual decrease in the effective stiffness of the structural member and unacceptable deformations. Also, exposure of PMC structures to extreme operational environments can result in changes in material properties that translate into structural changes. These can

have catastrophic effects on the load-bearing characteristics of composite structures, resulting in creep rupture.

Table 1.1 Typical applications of PMCs [1, 3].

Market	Typical Application
Aerospace	Wing leading edges, wing ribs, access doors, interior panels
Marine	Boat bodies, canoes, kayaks
Automotive	Body panels, leaf springs, drive shafts, bumpers, door frames
Sporting goods	Golf clubs, skis, fishing rods, tennis rackets
Biomedical	Medical implants, orthopedic devices, X-ray tables
Electrical	Panels, housing, switchgear, insulators, connectors
Military	Bulletproof vests and other armor parts
Industrial	Chemical storage tanks, pressure vessels, piping, pump bodies, valves

An additional issue that must be considered for PMC structures is the variability of their viscoelastic properties. In contrast to metals, for which elastic properties are ensured to within ± 5% [4], viscoelastic materials, such as high polymers (polymers with high molecular weight) and PMCs, generally exhibit some variations in their material properties (Young's, shear, and bulk moduli/compliances). Such variability can be on the order of 50-100% and is normally attributed to insufficient quality control in the manufacturing process [4, 5]. The stochastic nature of viscoelastic properties of PMCs is primarily due to the viscoelastic response of the polymer matrix [6].

The variability of time-dependent properties of PMCs has been illustrated extensively in the literature. For example, Cook *et al*. [7] conducted creep tests on seven types of fiber-reinforced composite materials using both thermosets (vinyl ester, polyester, and polyurethane) and thermoplastics (polypropylene) and noted significant variation (up to 75%) in the creep strain data. Barbero and Julius [8] obtained similar variations of the creep response of thermoplastic polyvinyl chloride and polyethylene blends and a felt-filled thermoset polyester at various temperatures. Additionally, Gnip *et al.* [9-11] showed substantial experimental variability in compressive creep tests of expanded polystyrene boards. Schwarzl and Zahradnik [12] also observed significant variation in shear creep compliances in the glass-rubber transition region for both thermoplastic (polyvinyl chloride, polystyrene, and polymethyl-methacrylate) and thermoset (polyurethane) polymers. Although stochastic models for strength [13-15] and failure [16-18] of PMCs are available in the literature, statistical studies of experimentally obtained viscoelastic material properties, such as creep compliances or relaxation moduli, are rare. Hilton *et al.* [19] performed an analytical study to include stochastic processes caused by the variations in linear viscoelastic material properties. However, the experimental data used for the statistical analyses in [12] was generated by assuming a normal probability distribution based on the deterministically obtained relaxation moduli of a solid propellant.

Although PMC viscoelastic property variability has been demonstrated, it is largely ignored and deterministic approaches are typically used in obtaining material functions. These functions are subsequently used in PMC structural designs and analyses, which may not represent the actual time-dependent responses of the corresponding PMC

structures. It has been shown that ignoring the stochastic nature of viscoelastic material functions can lead to inaccurate stress-strain analysis, thereby jeopardizing safety [19].

1.2 Objective and Research Overview

The overall objective of this research is to develop a method to predict the creep compliances of a specific vinyl ester (VE) polymer with variations in its material properties for a specified time and temperature range. VEs have mechanical properties that are better than unsaturated polyesters but not as good as epoxies. The cost of VE polymers are also higher than unsaturated polyesters but less expensive than epoxies. Additionally, VEs are easily infused into fiber preforms and can typically be cured at lower temperatures than epoxies. The VE polymer of interest in this study is Derakane 441-400 (Ashland Co.). Figure 1.1 shows a flowchart of this research, which includes both experimental and analytical studies to formulate a model that includes the variability of measured creep strains. To complete the objective of this study, the following tasks were performed.

(1) Short-term creep tests were conducted to obtain the strain versus time histories of cured Derakane 441-400.

- Quasi-static uniaxial tensile tests (Fig. 1.1, Block (a)) were performed at a constant strain rate of 0.001/s until specimen fracture to obtain the ultimate tensile stress σ_u (Fig. 1.1, Block (b)) The tests were performed at four temperatures (24°C, 40°C, 60°C, 80°C) below the glass transition temperature (135°C) of Derakane 441-400 to establish the short-term creep test parameters.

- Short-term tensile creep/creep recovery experiments were conducted at 60% and 70% of σ_u at each of the four temperatures (24°C, 40°C, 60°C, 80°C) with ten replicates for each test configuration (Fig. 1.1, Block (c)).
- Experimental strain versus time responses of cured Derakane 441-400 were obtained in both the longitudinal and transverse directions using a digital image correlation (DIC) technique (Fig. 1.1, Block (d)).
- Isochronous stress-strain curves for each test configuration were developed to determine viscoelastic linearity (Fig. 1.1, Block (e)); nonlinear data was not considered (Fig. 1.1, Block (f)).

(2) Creep compliances of cured Derakane 441-400 were characterized using a Prony series representation (Fig. 1.1, Block (h)).

(3) Statistical analyses of creep compliances of cured Derakane 441-400 were performed using a two-parameter Weibull distribution (Fig. 1.1, Block (j)).
- Weibull shape and scale parameters were obtained at each time using the maximum likelihood estimation (MLE) method.
- The probability distribution functions (PDFs) and the corresponding cumulative distribution functions (CDFs) of the creep compliances were obtained for each time ($0 \leq t \leq 7000\ s$).

(4) Creep compliances of cured Derakane 441-400 were predicted using Lagrangian interpolation functions over the complete time and temperature design space (Fig. 1.1, Block (k)).

- Weibull shape and scale parameters were obtained for steady state creep (1000 $s \leq t \leq 7000$ s) and temperature range (24°C $\leq T \leq$ 60°C) using two-dimensional quadratic Lagrangian interpolation functions.
- PDFs and CDFs of creep compliances of cured Derakane 441-400 for the complete time and temperature range were computed.
- For steady-state creep and constant CDFs, creep compliances of cured Derakane 441-400 were computed over the temperature design space.

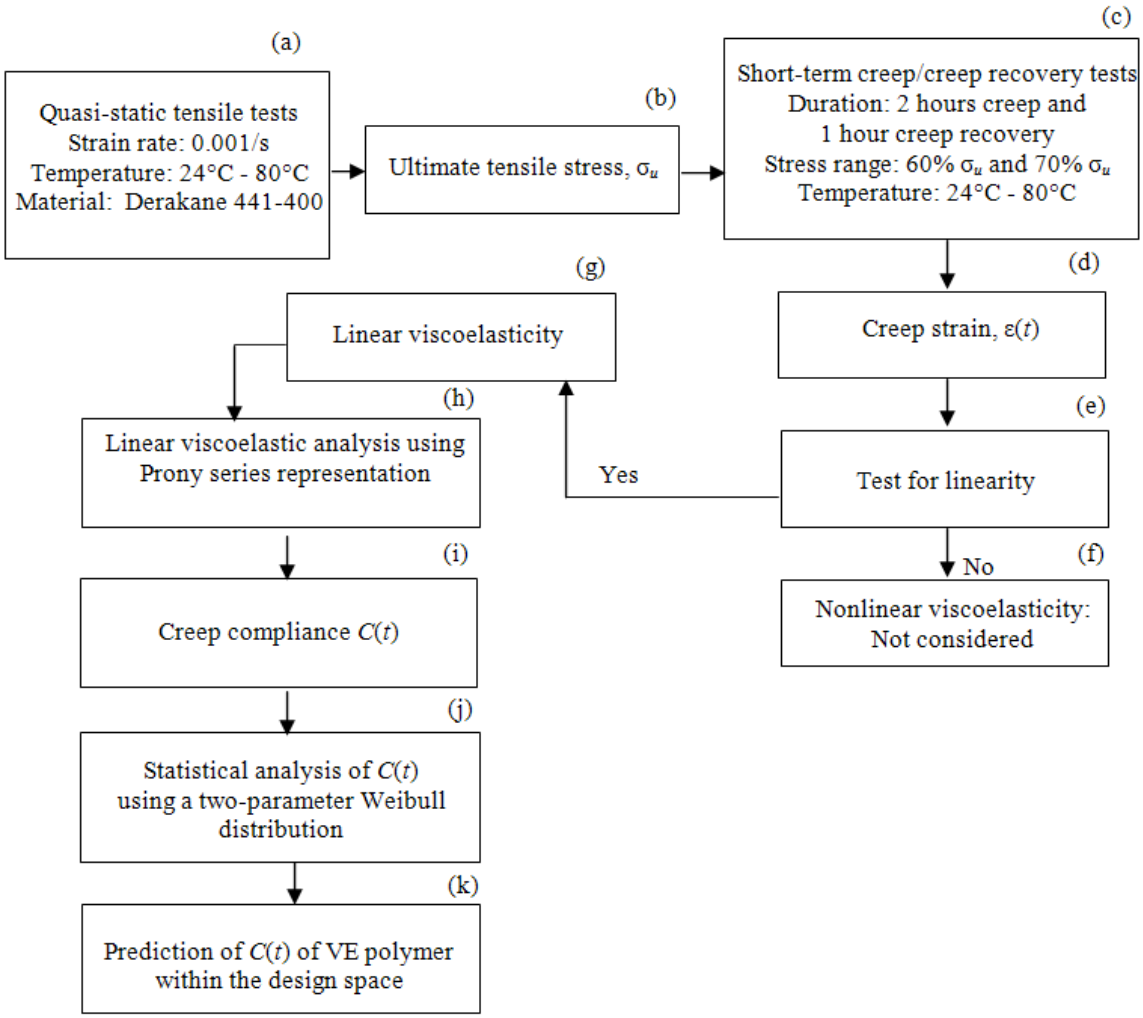

Figure 1.1 An overview of the model development that includes the variability in experimentally obtained creep compliances of a vinyl ester (VE) polymer (Derakane 441-400).

In subsequent chapters of this dissertation, a brief overview of linear viscoelasticity is presented, followed by a literature review of creep studies of VE polymers. The experimental program for determining a thermoset VE polymer's viscoelastic properties is described. The development of the creep compliance versus time responses of a VE polymer using the generalized viscoelastic constitutive equation

with a Prony series representation is given. The statistical approach to determine the Weibull PDFs for the experimentally derived creep compliances is presented. The Weibull distribution parameters are subsequently used to form a predictive model for the time and temperature design range.

CHAPTER II

BACKGROUND ON LINEAR VISCOELASTICITY AND A REVIEW OF EXPERIMENTAL CREEP STUDIES OF NEAT VINYL ESTER POLYMERS

This chapter presents a brief introduction on the theory of linear viscoelasticity. Experimental creep studies of neat vinyl ester (VE) polymers are reviewed.

2.1 Linear Viscoelasticity

Viscoelasticity theory is used to describe materials that exhibit characteristics of both elastic solids and viscous fluids. The constitutive behavior of linearly elastic solids is described by Hooke's law, in which stress is proportional to strain. Elastic solids also have the capability of storing energy under an applied load, enabling them to recover their undeformed state after the load is removed. In contrast to elastic solids, viscous fluids obey Newton's law, which states that the stress is proportional to the strain rate. Ideal Newtonian fluids are capable of energy dissipation but not energy storage [20]. Viscoelastic or time-dependent materials are capable of both energy storage and energy dissipation under applied loads [21]. All materials exhibit some viscoelastic behavior depending on the time and/or temperature scale. For example, polymeric materials can exhibit viscoelastic behavior at room temperature and their viscoelastic response becomes more pronounced as the temperature approaches the glass transition temperature (T_g) of

the material [20]. Other examples of viscoelastic materials include polymer composite materials, glass, asphalt, ice, etc.

Two important physical manifestations of viscoelastic behavior include creep and stress relaxation. Creep is a continuous deformation of a material under continuous loading whereas stress relaxation is a progressive reduction of stress while a material is under constant deformation [21]. Although creep and stress relaxation can occur in axial, shear, or volumetric deformation, creep behavior for one-dimensional tensile loading is investigated in this study.

2.1.1 Creep Testing for Viscoelastic Characterization

A creep test, in which an instantaneous constant stress σ_0 is applied to a specimen and maintained throughout the duration of the test, is often used to characterize viscoelastic behavior in a material. The resulting deformation or creep strain $\varepsilon(t)$ is measured as a function of time and can be represented by

$$\varepsilon(t) = C(t)\sigma_0 \tag{2.1}$$

where the viscoelastic creep compliance $C(t)$ is the ratio of the creep strain per unit applied stress [22]. A typical isothermal creep strain versus time response under constant stress in the longitudinal (x_1) direction for a polymeric material is described in three stages: primary creep, secondary creep, and tertiary creep (Fig. 2.1). In the primary creep phase, there is an initial deformation due to the instantaneous loading. Under constant stress, the strain rate decreases and becomes steady in the secondary or steady-state creep phase. In the tertiary phase, the strain rate increases rapidly until rupture of the test

specimen [23]. In this study, the creep responses of a neat cured VE resin in the secondary creep phase are investigated.

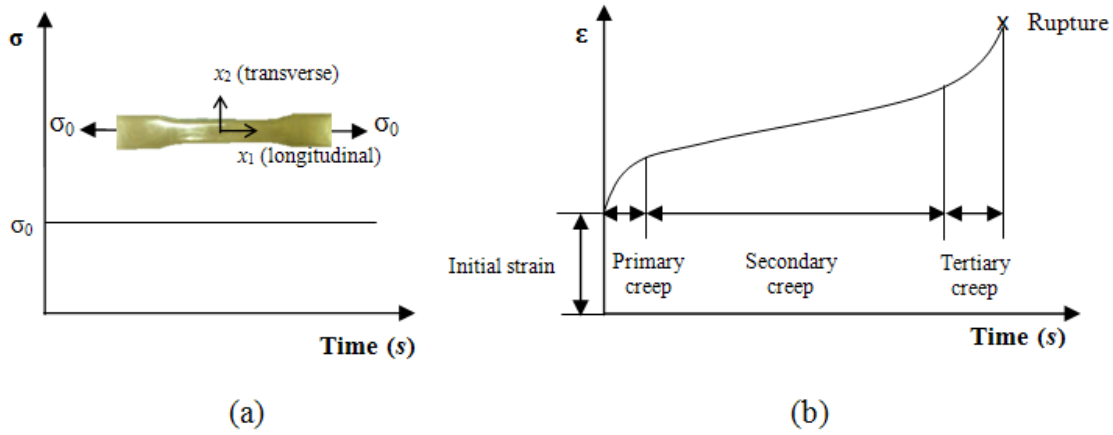

Figure 2.1 Applied constant stress and creep strain history of an isothermal tensile creep test.

(a) Constant stress applied to a tensile creep specimen and (b) the primary, secondary, and tertiary stages of creep strain.

2.1.2 Boltzmann Superposition Principle

The relation between stress and strain for linear viscoelastic materials is described by the Boltzmann Superposition Principle (BSP), which states that the sum of the strains resulting from each increment of stress input is the same as the total strain resulting from the combined stresses. Figure 2.2a shows a one-dimensional loading of an isotropic, homogenous linearly viscoelastic material by the increments in stress $\Delta\sigma_1$, $\Delta\sigma_2$, $\Delta\sigma_3$ at times $t = \xi_1$, $t = \xi_2$, $t = \xi_3$, respectively.

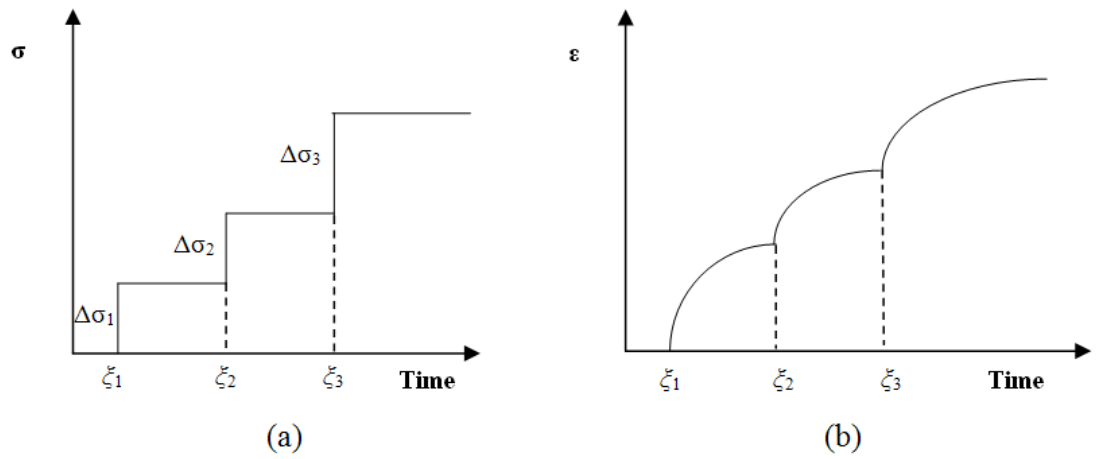

Figure 2.2 Variable stress inputs and creep strain history in one-dimensional loadings of a linear viscoelastic material.

(a) Variable stress inputs with increments in stress $\Delta\sigma$ and (b) creep strain responses.

According to the BSP, the effects of the stress history on strain are linearly additive, and therefore, the strain versus time response $\varepsilon(t)$ of a linear viscoelastic material due to a variable stress can be approximated as [20]

$$\varepsilon(t) = C(t-\xi_1)\Delta\sigma_1 + C(t-\xi_2)\Delta\sigma_2 + C(t-\xi_3)\Delta\sigma_3 \tag{2.2}$$

If the applied stress is varied with time, the stress input can be represented in series form as

$$\sigma(t) = \sum_{p=1}^{P} \Delta\sigma_i H(t-\xi_p) \tag{2.3}$$

where P denotes the last constant stress increment and $H(t)$ is the Heaviside unit step function defined as

$$H(t) = \begin{cases} 0 & t < 0 \\ 1 & t \geq 0 \end{cases} \tag{2.4}$$

Substituting Eq. (2.3) and Eq. (2.4) into Eq. (2.2), the strain output under variable stress $\sigma(t)$ can be written as

$$\varepsilon(t) = \sum_{i=1}^{I} \Delta\sigma_i C(t-\xi_i) H(t-\xi_i) \tag{2.5}$$

For a continuous stress application, the strain versus time response $\varepsilon(t)$ in Eq. (2.5) can be expressed in a generalized form by an integral representation as [22]

$$\varepsilon(t) = \int_0^t C(t-\xi)\frac{d\sigma}{d\xi}d\xi \tag{2.6}$$

where $C(t)$ is the creep compliance, σ is the applied stress, and ξ denotes the time offset. Equation (2.6) is known as the Boltzmann integral or hereditary integral, which can be used to obtain creep strains under a given stress history. As depicted by the Boltzmann integral, a viscoelastic material has "memory", i.e., its current state of strain depends on the current stress as well as the complete loading history [24].

2.1.3 Isochronous Stress-strain Relationships to Determine Viscoelastic Linearity

Similar to elastic materials, viscoelastic materials can be either linear or nonlinear depending on various factors such as temperature, stress level, moisture content, geometry, etc. The time-dependent behavior of viscoelastic materials is linear if the creep compliance is independent of stress [24]. A typical technique to distinguish between linear and nonlinear behavior is to construct isochronous (constant time) plots of the stress-strain curves. The isochronous curves are generated from a series of creep experiments at different stress levels in tension, compression, or shear [21]. For example, Fig. 2.3 shows idealized isochronous curves obtained from idealized uniaxial tensile creep tests in which the strain responses from three separate tests with applied constant

stresses σ_1, σ_2, σ_3 are obtained at times t_1, t_2, t_3, respectively. When stress and strain values are plotted for constant times, material linearity is depicted by the straight lines shown in Fig. 2.3a. For nonlinear behavior, isochronous plots result in curved lines as shown in Fig. 2.3b [24].

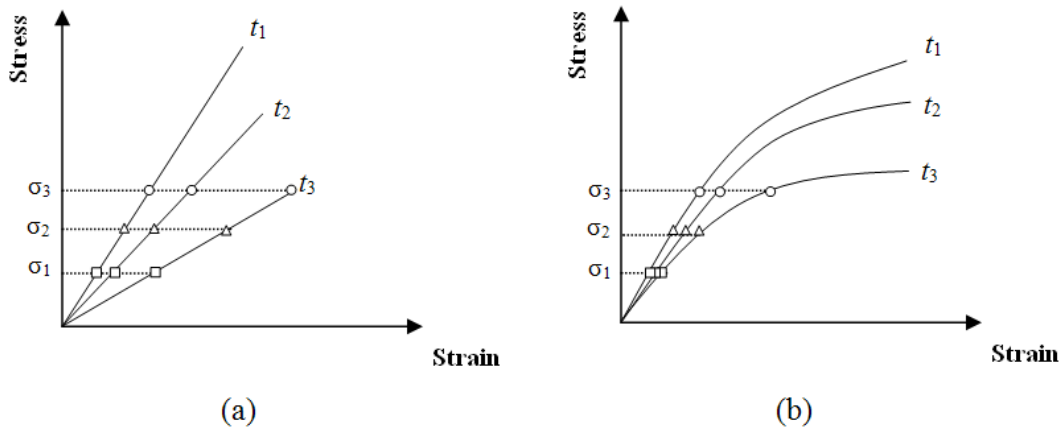

Figure 2.3 Idealized isochronous stress-strain curves for viscoelastic linear and nonlinear materials.

(a) Viscoelastic linear and (b) nonlinear materials' isochronous stress-strain curves from a series of creep experiments at different stress levels.

Linearity can be mathematically examined by considering the viscoelastic constitutive relation (Eq. (2.6)) with applied stress $\sigma(t)$ of constant magnitude σ_0 for uniaxial tensile creep expressed as

$$\sigma(t) = \sigma_0 H(t) \tag{2.7}$$

Using Eq. (2.7) in Eq. (2.6), the creep strain $\varepsilon(t)$ is written as

$$\varepsilon(t) = \sigma_0 \left(\int_0^t C(t-\xi) d\xi \int_0^t H(\xi) d\xi \right) \tag{2.8}$$

By normalizing the left side of Eq. (2.8) by a unit strain (ε = 1 % strain) and the right side by a unit creep compliance (C = 1 Pa^{-1} or C = 1 psi^{-1}) and time (t = 1 s), Eq. (2.8) can be expressed as [25]

$$\hat{\varepsilon}(t) = \hat{\sigma}_0 \left(\int_0^t \hat{C}(t-\xi) d\xi \right) = \hat{\sigma}_0 \hat{\Upsilon}(t) \tag{2.9}$$

where

$$\hat{\Upsilon}(t) = \int_0^t \hat{C}(t-\xi) \widehat{d\xi} \tag{2.10}$$

Equation (2.9) indicates that for linearly viscoelastic materials, non-parallel linear plots of stress versus strain will be obtained. Taking the logarithm of both sides of Eq. (2.9),

$$\log\left[\hat{\varepsilon}(t)\right] = \log\left[\hat{\Upsilon}(t)\right] + \log\left[\hat{\sigma}_0\right] \tag{2.11}$$

For linearly viscoelastic materials and constant time t, Eq. (2.11) produces parallel lines of unit slope horizontally displaced by $\log\left[\hat{\Upsilon}(t)\right]$ for different applied constant creep stresses σ_0. In this study, isochronous plots were produced for all data to determine material linearity.

2.2 An Overview of Neat Vinyl Ester Polymers Creep Studies

The creep behavior of PMCs is dominated by the resin matrix and this behavior is most pronounced in off-axis or shear loading [6] [20]. Therefore, this research focuses upon the creep behavior of a neat VE polymer (Derakane 441-400, Ashland Co.). VE is a thermoset polymer, which is cross-linked. The chain growth and cross-linking is irreversible. As a result, these polymers cannot be recycled [24]. VE polymers are used as the matrix component in composite structures with glass, aramid, carbon fibers, and

vapor-grown carbon nanofibers [26-30]. VE resins can be processed using a variety of molding methods such as compression molding, resin transfer molding (RTM), and vacuum-assisted RTM (VARTM), which are subsequently cured to solids [31]. VEs are typically used in transportation, wind energy, and infrastructure applications, such as rail cars, automobiles, and bridge deckings. Additionally, these polymers have superior chemical resistance and are often used in applications involving highly corrosive and thermal environments [32-34]. In some of these applications, VE composite structures are subjected to long-term mechanical loadings, which result in creep deformations. The mechanisms associated with creep are related to the deformation of the polymer's molecular structure. Continuous loading causes segmental motions such as bond rotations, which "unwinds" coiled segments to accommodate the load. This induces strain accumulation in creep [24].

Despite the expanding market and development of VE composite structures, only limited experimental studies of the creep behavior of VE resins are available, especially when compared to the number of creep studies on unsaturated polyesters and epoxy resins [35-42]. A summary of creep experiments from both quasi-static creep tests and dynamic mechanical measurements on several types of neat VE polymers is presented in Table 2.1. The VE polymer materials used in these studies, along with their styrene content and tensile mechanical properties, are identified in Table 2.2.

As seen in Table 2.1, seven experimental studies have been performed to investigate the creep responses of neat VE polymers. These studies include a variety of topics, such as physical aging, testing temperature, specimen curing condition and geometry, and inclusion of nanofiller. Sullivan *et al.* [6, 43, 44] studied the physical

aging and temperature effects on the tensile and torsional creep behaviors of a series of VE resins (Derakane 470-36 and Derakane 411-C50) and E-glass fiber reinforced composites. Generally, physical aging in polymers refers to the change in mechanical properties when they are initially cooled from the glass transition temperature T_g to a temperature below T_g. When a polymer is cooled below its T_g, the polymer's molecular structure is not in thermodynamic equilibrium because there is a significant loss in the rate of polymer chain and polymer segment mobility. This "locks in" conformational morphologies that are not at equilibrium. Therefore, physical aging is the slow evolution of the polymer structure to its thermodynamic equilibrium [6, 43, 44]. In [6, 43, 44], short-term experiments were performed in the frequency domain using dynamic mechanical analysis (DMA) to predict the long-term creep versus time responses of both neat VE resins and their composites. These studies [6, 43, 44] show that the matrix-dominated material properties of continuous fiber-reinforced PMCs are affected by physical aging in a manner similar to the neat VE polymers. The effects of physical aging are dominant in long-term creep behavior. Since only short-term (2-hour) creep responses of Derakane 441-400 are considered in this study, physical aging effects are assumed to be minimal and therefore, neglected.

Bradley *et al.* [45] studied the creep behavior of Derakane 441 as a function of curing conditions by conducting flexural creep tests for up to 10,000 hours at room temperature. The comparison of creep compliances was performed on a partially cured neat VE (cured at room temperature) and a post-cured neat VE (post-cured at 93°C). The partially cured neat VE had a greater creep exponent (lower creep strain resistance) than

that of the post-cured neat VE. The total creep compliances decreased as the time and/or temperature of curing increased [45].

Stahlberg *et al.* [46] have shown the dependence of apparent mechanical properties of Derakane 441-C50 on the size and shape of a test specimen. Creep tests in compression and tension were conducted on cylindrical samples with different radii and lengths. One hour creep and four hour creep recovery tests were conducted and it was shown that the creep strain decreases when the length of the specimen is reduced.

Plaseied and Fatemi [47] examined linear viscoelastic behavior of a neat VE resin (Hetron 942/35) and VE carbon nanofiber reinforced composites. Quasi-static tensile creep experiments were performed at various stress levels and temperatures below the T_g of Hetron 942/35. At lower temperatures (23.8°C-46.5°C), the measured creep compliances of the neat Hetron 942/35 were higher than those of the Hetron 942/35 with dispersed carbon-nanofibers. However, at higher temperatures (46.5°C-69.2°C), the nanocomposites exhibited more creep than the Hetron 942/35.

A similar study in [48] examined the creep response of Derakane 411-350 and nanocomposites. The creep and stress relaxation behavior of the neat Derakane 411-350 and the composites containing nanoclay and graphite platelet reinforcements were obtained by conducting DMA tests at various temperatures (28°C-100°C). At lower temperatures (28°C-52°C), creep compliances of the neat Derakane 411-350 were found to be higher than those of the nanocomposites. At temperatures close to the T_g, higher creep compliances were observed for the nanocomposites. Out of seven studies shown in Table 2.1, only the work in [48] reported that multiple (2) samples were tested at each test configuration; all other studies tested only (1) sample for each test configuration.

Therefore, variation in the measured viscoelastic properties obtained at the same conditions on the same VE polymer system was not demonstrated and subsequently not included.

Table 2.1 Summary of published studies on experimental creep of neat vinyl ester (VE) resins.

Citation	Material	Experiment				Topics
		Type of testing	Temperature	Duration of tests (or frequency range in DMA tests)	Number of samples for each test configuration	
Sullivan (1990) [6]	Derkane 470-36	Tensile DMA	RT and 40°C-120°C	Not available	1	Physical aging and temperature effects
Sullivan et al. (1993) [43]	Derkane 470-36 Derakane 411-C50	Torsional DMA	$T_g \pm 30$ °C	Frequency 0.1-100 rad/sec	1	Physical aging effects
Sullivan et al. (1995) [44]	Derkane 470-36 Derakane 411-C50	Torsional DMA	$T_g \pm 30$ °C	Frequency 0.1-100 rad/sec	1	Shift factors for temperature, aging shift rate, vertical shift factor, and retardation spectra
Bradley (1998) [45]	Derakane 411	Flexural	RT	Up to 10,000 h	1	Curing conditions effect on creep responses
Stahlberg et al. (2005) [46]	Derakane 411-C50	Compressive and tensile	RT	1 h with 4 h creep recovery	1	Specimen geometry effect on creep responses
Plaseied and Fatemi (2009) [47]	Hetron 942/35	Tensile	RT and 50°C-100°C	100 hour	1	Creep behavior of neat resin and composite materials at various temperatures
Almagableh et al. (2010) [48]	Derakane 411-350	Flexural DMA	RT and 28°C-100°C	30 minutes	2	Temperature effect

DMA = dynamic mechanical analysis
RT = room temperature
T_g = glass transition temperature. T_g of Derkane 470-36 is 153°C. T_g of Derakane 411-C50 is 112°C

Table 2.2 Tensile properties of neat vinyl ester (VE) resins from Table 2.1.

Material	Tensile properties of clear casting† at 25°C		
	Strength (MPa)	**Modulus (GPa)**	**Elongation at yield (%)**
Derkane 470-36 (Ashland Co.)	90	3.6	3-4
Derakane 411-C-50 (Dow Chemical)	Not available	Not available	Not available
Hetron 942/35 (Ashland Co.)	92	3.6	5.5
Derakane 411-350 (Ashland Co.)	86	3.2	5-6
Derakane 441-400* (Ashland Co.)	90	3.4	5-6

†Cured at 24 hours at RT and 2 hours at 120°C
*Selected material in this study

CHAPTER III

EXPERIMENTAL DETERMINATION OF A VINYL ESTER POLYMER'S VISCOELASTIC RESPONSES

In this section, the experimental program for the determination of viscoelastic properties of a thermoset polymer is presented. Quasi-static tension and short-term (two-hour) tensile creep tests were conducted at four temperatures (24°C, 40°C, 60°C, 80°C) below the resin's glass transition temperature (T_g = 135°C). A digital image correlation (DIC) technique was used obtain strain measurements in the longitudinal (x_1) and transverse (x_2) directions, simultaneously.

3.1 Material and Specimen Fabrication

The thermoset VE resin Derakane 441-400, Ashland Co. with a styrene content of 33 wt% was selected for this study. The resin mixture was formulated locally to include a catalyst promoter (Cobalt naphthenate 6% solution, North American Composite Co.), two air release agents (BYK-A 515 and BYK-A 55, BYK USA, Inc.), and a free radical polymerization initiator (methyl ethyl ketone peroxide (MEKP), U.S. Composites, Inc.). Table 3.1 lists the ingredients used in the fabrication of the VE specimens, which was based on 100 g of resin. Upon curing, this formulation gives a solid highly cross-linked thermoset.

Table 3.1 Vinyl ester (VE) specimen ingredients.

Ingredient	Weight (g)
Derakane 441-400 (vinyl ester resin)	100
Cobalt naphthenate 6% (curing promoter)	0.20
BYK-A 515 (air release agent)	0.20
BYK-A 555 (air release agent)	0.20
MEKP (initiator)	1.00

The ingredients in Table 3.1 were combined and thoroughly mixed in the order listed. The mixture was degassed in a vacuum and carefully poured into a seven-specimen open-face mold with the dog-bone configuration based on ASTM D638-10 standard test method for tensile properties of plastics [49]. The dimensions of the reduced section specimens used in this study are shown in Fig. 3.1 and Table 3.2. The VE specimens were cured for five hours at 60°C and post cured for two hours at 120°C under a nitrogen atmosphere. The specimens were cooled to room temperature, polished to remove any air pockets and surface flaws, and stored in a climate-controlled environment (cool-dry) until testing. All specimens were speckle-painted with a high temperature (650°C) paint in preparation for quasi-static testing using the DIC technique.

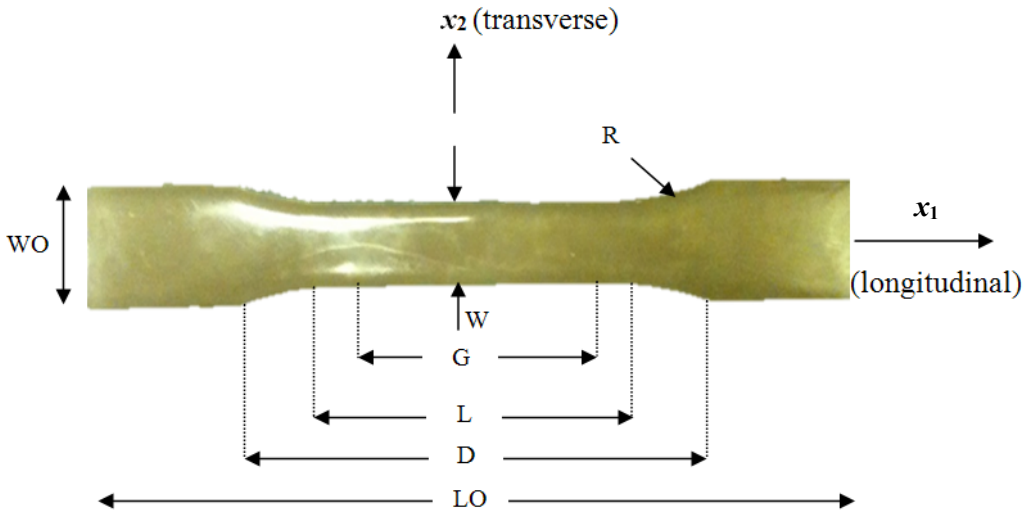

Figure 3.1 ASTM D638-10 test specimen configuration [49].

Table 3.2 Specimen dimensions.

	Dimension (mm)	Tolerance
W—Width of narrow section	13	± 0.5
L—Length of narrow section	57	± 0.5
LO—Length overall, min	165	no max
G—Gage length	50	± 0.25
D—Distance between grips	115	± 5
WO—Width overall	19	+ 6.4
R-Radius of fillet	76	± 1
Thickness	3.2	± 0.4

3.2 Mechanical Tensile Testing

Figure 3.2 shows the room temperature tensile test setup. An Instron model 5869 compression/tension electromechanical testing system was used to conduct the quasi-static tensile and tensile creep tests. A 50-kN load cell was mounted to the load

frame in series with the test specimen to measure the applied load. Friction grips were used with 80 grit sandpaper to maintain pressure and prevent damage to and slippage of the specimens during testing.

Strain measurements in the longitudinal x_1 and transverse x_2 directions (Fig. 3.1) were obtained through the LaVision® StrainMaster® DIC system (LaVision, Germany). The two-dimensional DIC system consists of a charge-coupled device (CCD) camera, imaging software for data acquisition and processing, and an analog to digital (A/D) converter for measuring the load cell signal from the test frame. The selected camera is a high resolution 14-bit Image ProX CCD digital camera. The camera has up to 16 million pixels of spatial resolution with a maximum recording capacity of 25 frames/sec. The DIC analyses were performed using the Davis Image Correlation software.

In addition to the DIC system, an Epsilon extensometer, with a gage length of 25.4 mm and travel distance of 6.35 mm was used to verify the measured strain in the longitudinal direction x_1. For elevated temperature experiments, the tests were performed inside an environmental chamber with an optical quality viewing window that was mounted to an electromechanical test system. The temperature was monitored using a programmable controller with an accuracy of ± 0.5%.

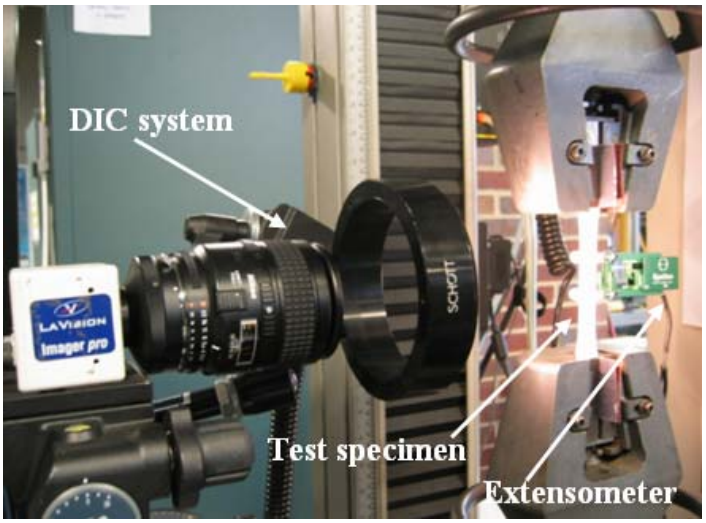

Figure 3.2 Room temperature tensile test setup.

3.2.1 Quasi-static Tensile Tests

As discussed in the previous chapter, a polymer can be considered as a linear or non-linear viscoelastic material depending on various factors such as temperature and stress level. Temperatures that are lower than the glass transition temperature T_g (135°C) of the cured VE Derakane 441-400 were chosen in this study. The T_g was obtained from dynamic mechanical analysis performed in a previous study [50]. Four temperatures (24°C, 40°C, 60°C, 80°C) ranging from room temperature (24°C) to 80°C were selected as the test temperatures to examine the linear viscoelastic behavior of the VE polymer in this study.

Quasi-static tensile tests in the x_1 loading direction were performed to obtain the ultimate tensile stresses σ_u, which were later used to establish the test matrix for the short-term tensile creep tests. These tests were conducted according to ASTM D638-10 [49] at a constant strain rate of 0.001/s to failure. Stress and strain

responses are shown in Fig. 3.3; the corresponding ultimate tensile stress σ_u, and percent of elongation are given in Table 3.3. As expected, the stress-strain responses are shown to be temperature-dependent. At constant strain rate, the percent of elongation increases and σ_u of the VE polymer decreases with increasing temperature. The percent of elongation of the VE polymer increases by 57% as the test temperature changes from 24°C to 80°C. The σ_u of the VE polymer decreases from 75 MPa to 46.4 MPa (40% decrease) as the temperature changes from 24°C to 80°C.

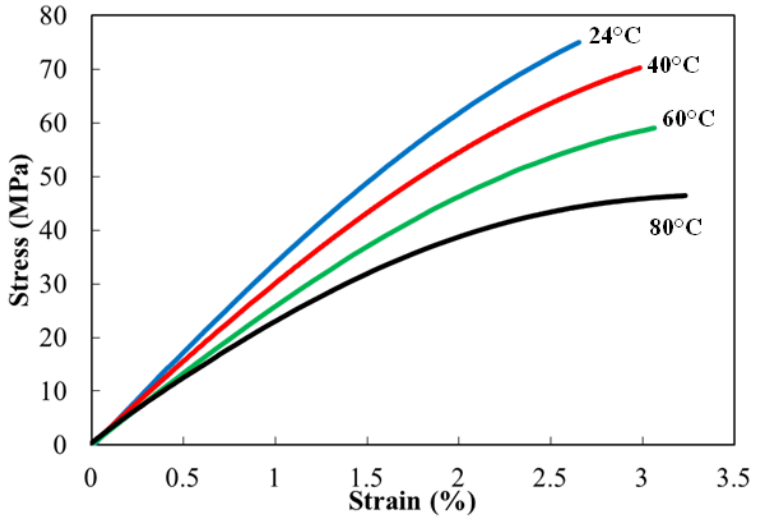

Figure 3.3 Experimental stress versus strain plots from quasi-static tensile tests of cured Derakane 441-400 at T = 24°C, 40°C, 60°C, and 80°C.

Table 3.3 Quasi-static tensile test results for cured Derakane 441-400.

Temperature (°C)	**Ultimate tensile stress, σ_u (MPa)**	**Elongation (%)**
24	75	2.6
40	70.2	2.8
60	59	3.0
80	46.4	4.1

3.2.2 Short-term Creep/Creep Recovery Tests

Following the determination of σ_u of the VE polymer, constant-stress creep tests were performed in accordance with ASTM D2990-77 Standard Test Methods for Tensile, Compressive, and Flexure Creep and Creep-Rupture of Plastics [51] at two stress levels (60% and 70% σ_u) and four temperatures (24°C, 40°C, 60°C, 80°C). Table 3.4 shows the test matrix used for the short-term creep tests, in which constant stress was applied for two hours, followed by one hour of recovery.

3.2.2.1 Determining the Number of Samples for the Creep/Creep Recovery Tests

A 95% confidence interval of the mean was used to determine the minimum number of specimens for the creep/creep recovery tests. If the sample data (creep strain) is assumed to be distributed normally (symmetric, bell shape curve), the minimum sample size required for an interval estimate of the mean is calculated using the following equation [52].

$$N_0 = \left(\frac{z_{\alpha/2} \cdot s}{K} \right)^2 \tag{3.1}$$

where N_0 is the sample size (number of specimens), s is the standard deviation of the data (creep strain), and K is half the width of the confidence interval. The $z_{\alpha/2}$ in Eq. (3.1) represents a number obtained from the Standard Normal Z-Table, which corresponds to the selected confidence interval. For a 95% confidence interval, $z_{\alpha/2}$ is 1.96 [53]. Hence, the minimum number of specimens for finding a 95% confidence interval on the mean is obtained by

$$N_0 = \left(\frac{1.96 \cdot s}{K} \right)^2 \tag{3.2}$$

The width of the confidence interval of 1.4s is commonly used to determine sample sizes in fatigue tests in polymers and PMCs [54] and, therefore, was selected in this study. By using Eq. (3.2) and a confidence interval width of 1.4s (K= 0.7s), the minimum number of test samples was calculated to be eight. Therefore, ten specimens, which exceeds the minimum number of sample sizes required, were tested at each test configuration and a total of 80 short-term tensile creep/creep recovery tests were conducted in this study.

Table 3.4 Test matrix for tensile creep/creep recovery tests for cured Derakane 441-400.

Temperature (°C)	**Stress level**	
	60% σ_u (MPa)	**70% σ_u (MPa)**
24	45	52.5
40	42.1	49.1
60	35.4	41.3
80	27.8	32.5

A series of load-controlled tests were performed on cured Derakane 441-400 to obtain the loading rate for the creep tests. An example of the tests conducted to achieve a constant stress level of 45 MPa at 24°C is illustrated in Fig. 3.4. As shown, the system reaches the specified stress level fastest at the stress rate of 113 MPa/s but it also produces the largest overshoot, which introduces an undesirable stress history in the specimen. This overshoot was minimized in the tests with reduced loading rates of 90 MPa/s and 45 MPa/s.

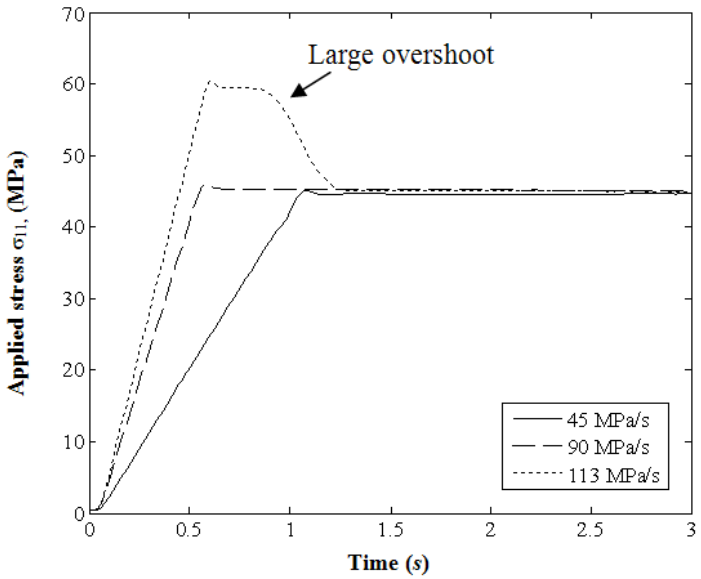

Figure 3.4 Comparing loading rates for cured Derakane 441-400 to achieve a constant stress level of 45 MPa at 24°C.

The loading cycle was determined and a typical loading profile for the creep/creep recovery tests is illustrated in Fig. 3.5. The initial load (stage I) was applied at a loading rate of 2025 MPa/min followed by an immediate reduction of the loading rate (stage II) to 1012 MPa/min. The constant creep load was applied for two hours (stage III). The load

was then removed (stages IV and stage V) and the creep-recovery responses were recorded for one hour (stage VI).

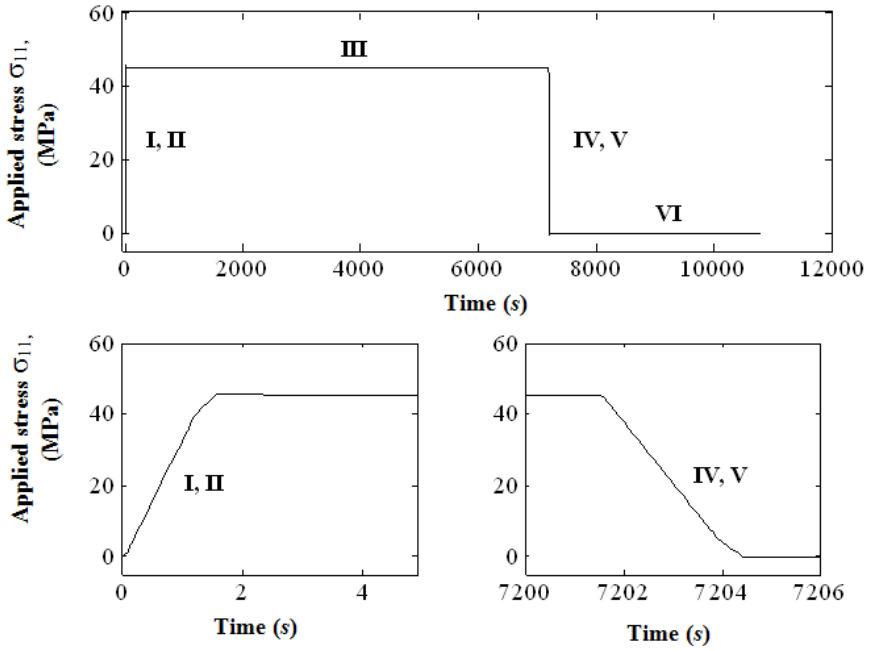

Figure 3.5 Six stages of creep loading for the tensile creep/creep recovery tests of cured Derakane 441-400.

3.3 Experimental Results

The measured longitudinal and transverse strains as functions of time for all short-term creep-creep recovery test configurations are presented in this section. Viscoelastic material linearity was determined by developing the isochronous stress-strain curves at all tested temperatures and applied stress levels.

3.3.1 Creep Strain versus Time Responses of Cured Derakane 441-400

Tensile creep tests were performed on the cured Derakane 441-400 samples and the strain versus time responses in both longitudinal and transverse directions were

obtained through a non-contact DIC technique. The measured creep strain versus time responses of ten specimens in the longitudinal direction for all test temperatures at stress levels of 60% σ_u and 70% σ_u are shown in Figs. 3.6 and 3.7, respectively. There is significant variation in the longitudinal creep strain data for the same test conditions. The creep deformation in the loading direction appears to monotonically increase with time, stress level, and temperature, particularly during the steady state creep phase ($t \geq 1000\ s$). For the 40°C, 42.1 MPa (60% σ_u) data (Fig. 3.6b), the magnitudes of longitudinal creep strain at each time for specimens #1 and #3 are greater than those of all other specimens, including specimens at 24°C and 60°C. Considerable variability in the longitudinal creep strains, ranging from 1%-5.5%, was observed at 80°C, 27.8 MPa (60% σ_u) in Fig. 3.6d. At the highest stress and temperature levels, 80ºC, 3.28 MPa (70% σ_u), seven specimens failed early during creep and specimen #4 developed significant strain levels (up to 13%) as seen in Fig. 3.7d. Some specimens, such as specimen #2 in Fig. 3.6b, exhibit significantly more scatter in the creep-versus time history than all other test articles. This data scatter is attributed to the quality of the speckle pattern, the resolution of the camera, or a high sampling rate used in the implementation of the DIC technique.

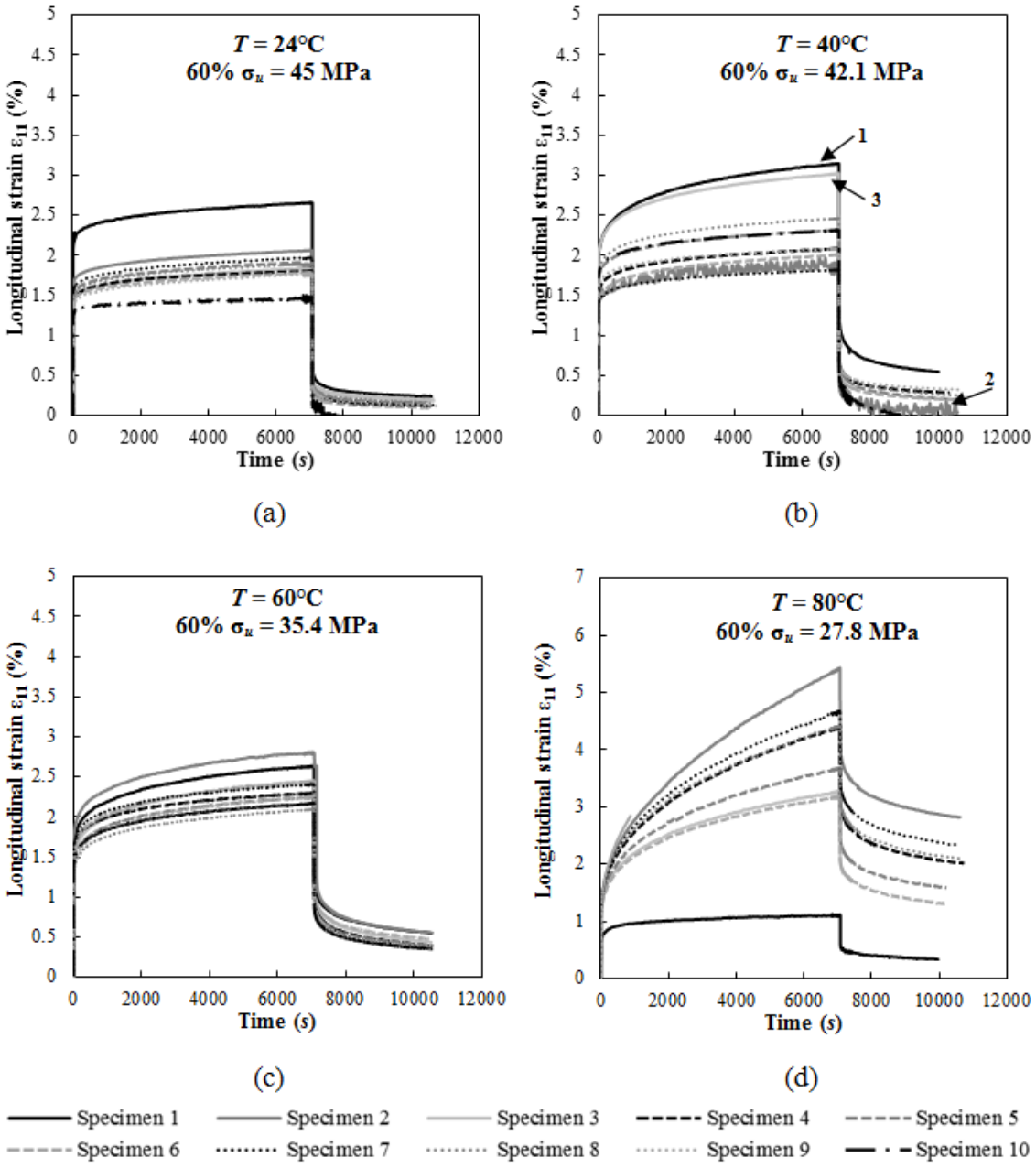

Figure 3.6 Longitudinal creep strain versus time responses $\varepsilon_{11}(t)$ of cured Derakane 441-400 at 60% σ_u at T = (a) 23.8°C, (b) 40°C, (c) 60°C, (d) 80°C.

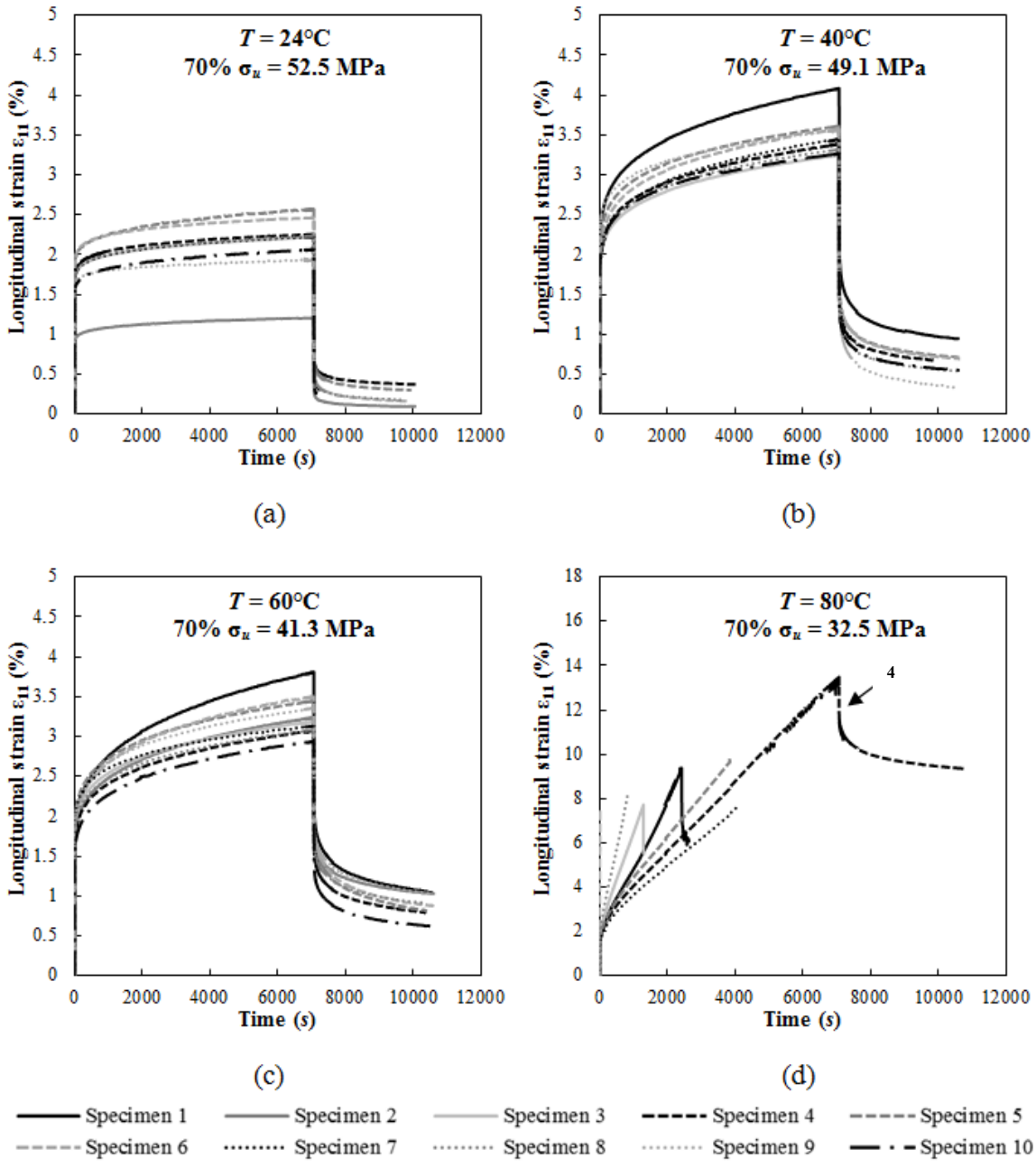

Figure 3.7 Longitudinal creep strain versus time responses $\varepsilon_{11}(t)$ of cured Derakane 441-400 at 70% σ_u at T = (a) 23.8°C, (b) 40°C, (c) 60°C, (d) 80°C.

The measured transverse creep strains as a function of time for all test temperatures at 60% σ_u and 70% σ_u stress levels are shown in Figs. 3.8 and 3.9, respectively. A considerable variability in the strains, ranging from -0.1% to -0.7%, was observed at 24°C, 60% σ_u (Fig. 3.8a). The transverse strains of approximately -0.4% to -0.9% were obtained at 24°C, 70% σ_u (Fig. 3.9a). Significant variations of transverse creep strains were observed in all creep/creep recovery tests. As expected, at a constant holding stress (at 60% σ_u or 70% σ_u), creep strains in the transverse direction increased as the temperature increased. Overall, the magnitudes of creep deformation in the longitudinal direction are greater than those in the transverse direction for all test configurations. For example, at 24°C, 60% σ_u, creep strains of approximately 1.3-2.5% were observed in the longitudinal direction (Fig. 3.6a) whereas creep strains in the transverse direction were about 0.2-0.9% (Fig. 3.8a). Additionally, the variation in the creep strains in the transverse direction is more pronounced than those in the longitudinal direction, especially at 24°C, 60% σ_u and 40°C, 60% σ_u. Again, this may be due to factors involved in the DIC technique that were used for strain measurement, such as the interrogation cell size, speckle size and pattern, and lighting. These factors appear to have more effect on the measured creep strain data in the transverse direction than the data in the loading direction.

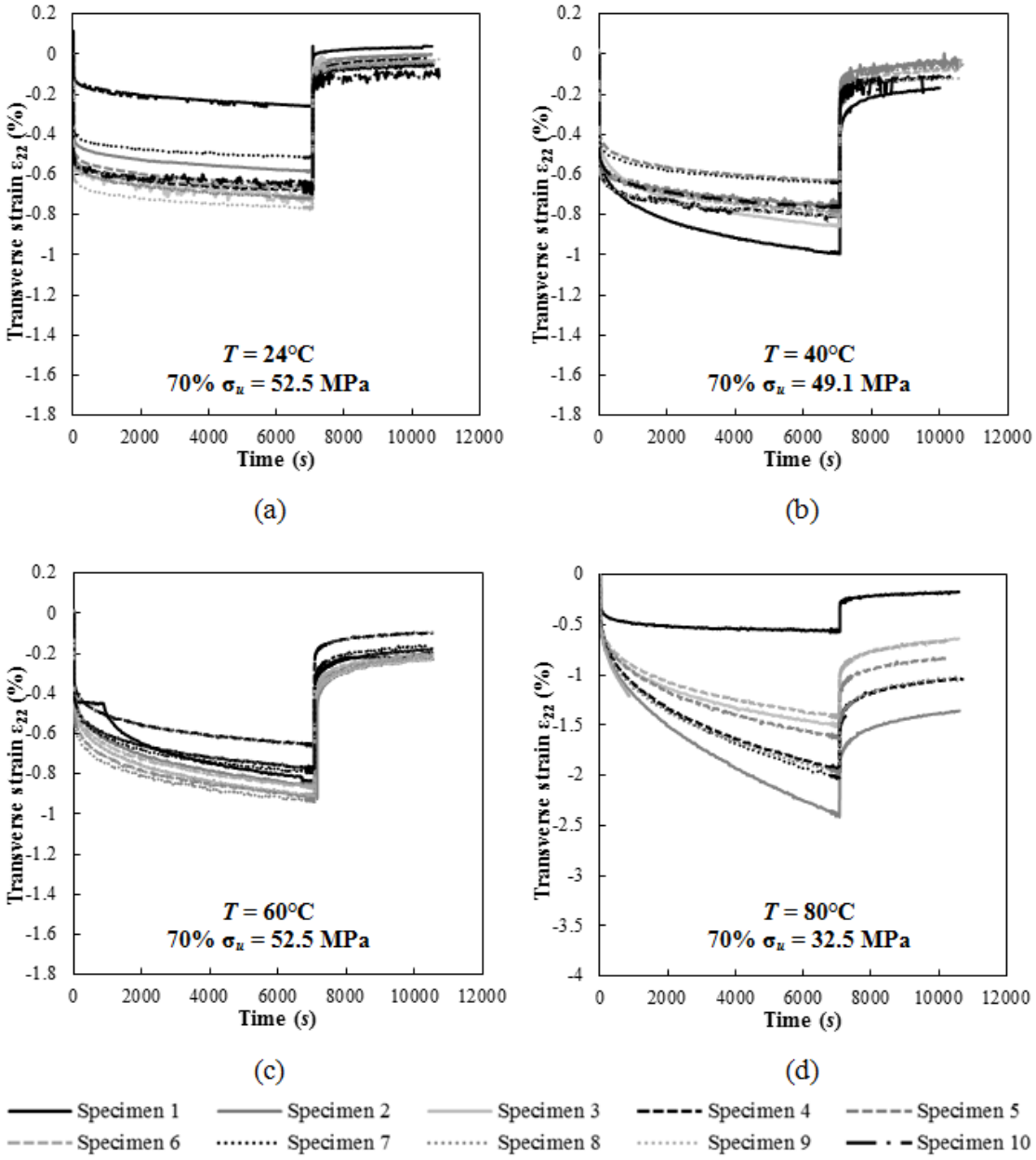

Figure 3.8 Transverse creep strain versus time responses $\varepsilon_{22}(t)$ of cured Derakane 441- 400 at 60% σ_u at T = (a) 23.8°C, (b) 40°C, (c) 60°C, (d) 80°C.

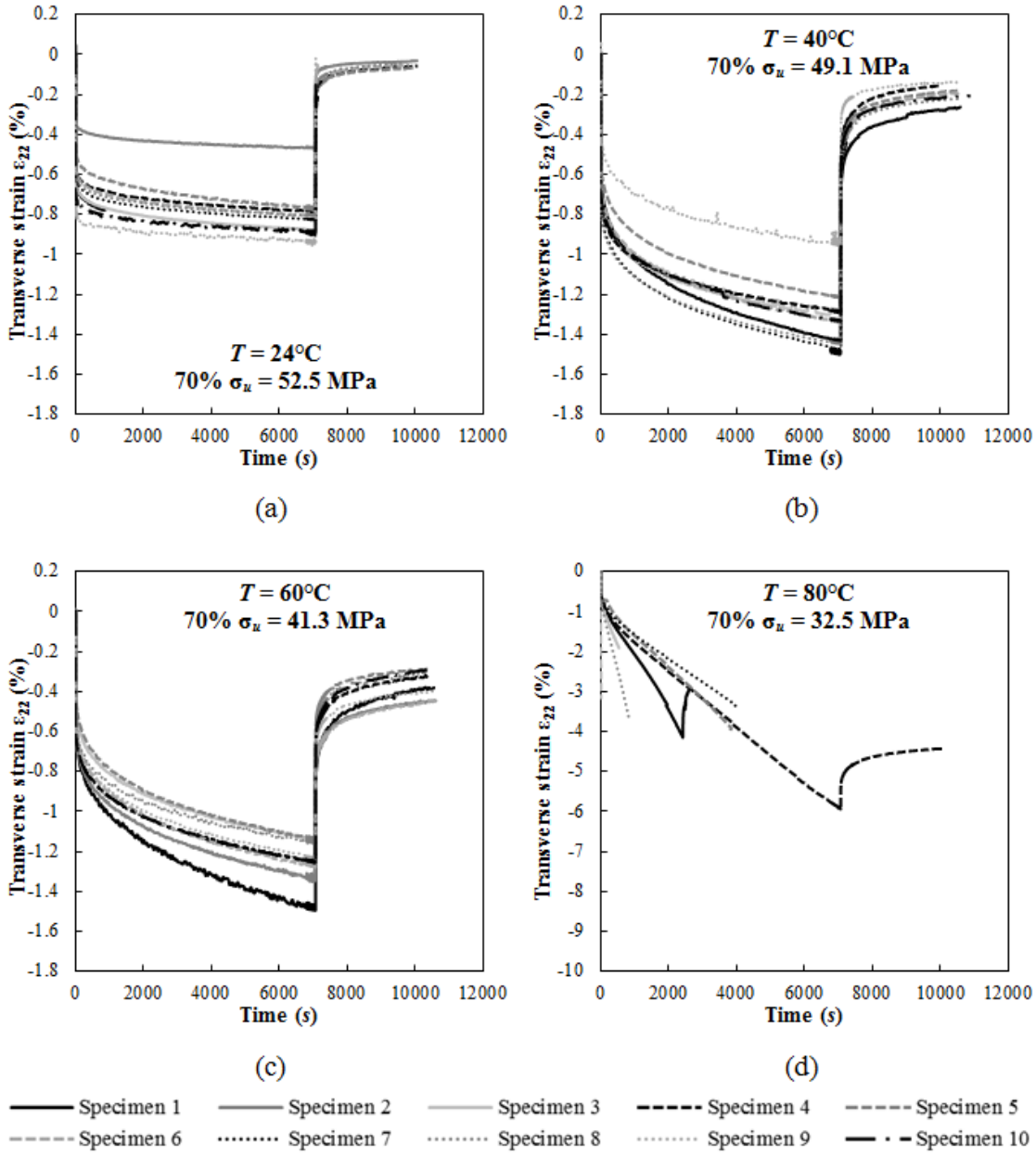

Figure 3.9 Transverse creep strain versus time responses $\varepsilon_{22}(t)$ of cured Derakane 441-400 at 70% σ_u at T = (a) 23.8°C, (b) 40°C, (c) 60°C, (d) 80°C.

3.3.2 Isochronous Stress-strain Relationships of Cured Derakane 441-400

The isochronous plots were constructed to determine the viscoelastic linearity of cured Derakane 441-400. Figure 3.10a shows the longitudinal creep strain versus time responses at 60°C for the holding stresses of 50% σ_u (27.8 MPa), 60% σ_u (35.4 MPa), and 70% σ_u (41.3 MPa). The experimental stress and the corresponding creep strain data obtained at 1000 *s*, 2000 *s*, 3000 *s*, 4000 *s*, 5000 *s*, and 6000 *s* were used to establish the material linearity for the complete duration of the creep tests. All isochronous stress-strain curves are approximately linear as seen in Fig. 3.10b. Thus, the material is regarded as linearly viscoelastic for all stresses in the test configuration.

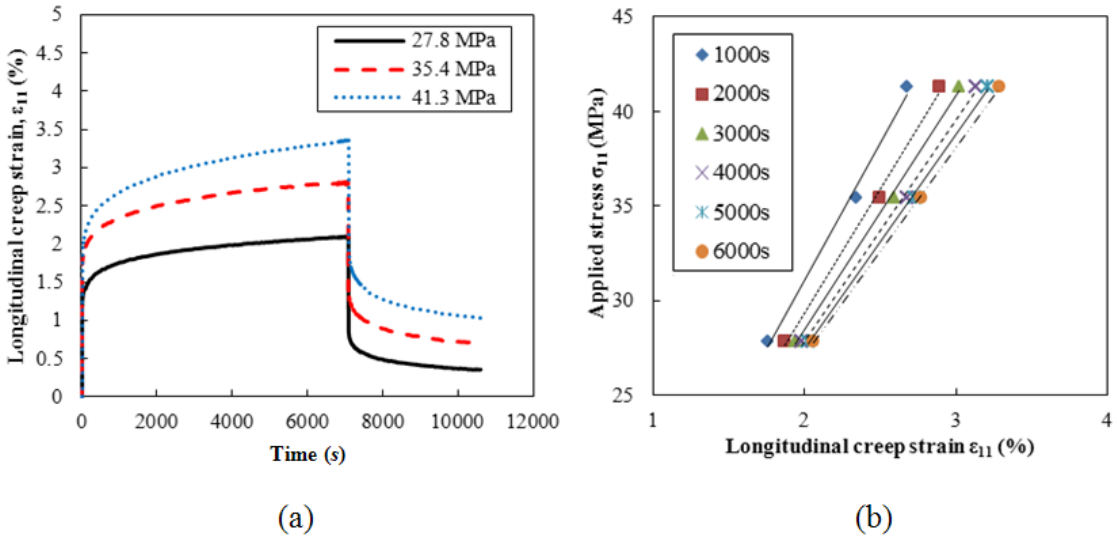

Figure 3.10 Isochronous stress versus longitudinal creep strain curves of cured Derakane 441-400 from tensile creep tests at 60°C.

(a) Longitudinal creep strain versus time responses $\varepsilon_{11}(t)$ at 60°C and 27.8 MPa, 34.5 MPa, 41.3 MPa, and (b) the corresponding isochronous stress-strain curves at selected times.

Isochronous stress-strain plots were also developed for creep tests at the other temperatures (24°C, 40°C, and 80°C) and can be found in Appendix A. Linear isochronous stress-strain curves at selected times were observed for the tensile creep tests at 24°C and 40°C, whereas non-linear curves were observed at 80ºC. The isochronous stress-strain curves at 80ºC begin to deviate from linearity at approximately 28 MPa (Fig. A.3). This indicates that cured Derakane 441-400 exhibits a non-linear viscoelastic behavior at 60% σ_u (27.8 MPa) and 70% σ_u (32.5 MPa) at 80ºC. Therefore, creep responses from tests at 80ºC were not included in this study.

CHAPTER IV

VISCOELASTIC CREEP COMPLIANCE REPRESENTATION USING A PRONY SERIES

Many theoretical and empirical models have been suggested for representing viscoelastic behavior and properties. In this study, the isothermal linear viscoelastic creep compliance functions of cured Derakane 441-400 were obtained using the generalized viscoelastic constitutive equation with a Prony series representation that includes the start-up transient response.

4.1 Creep Compliance Analysis Using a Prony Series Representation with a Start-up Transient Response

4.1.1 Prony Series Representation of Viscoelastic Behavior

The creep strain versus time responses of different viscoelastic materials can be simulated by models comprised of a variety of arrangements of linear spring (Hookean) elements for elastic behavior and damper (Newtonian) elements for viscous behavior. For example, the Kelvin model is a combination of a spring (with spring modulus k) and a damper (with viscosity μ) connected in parallel. The stress-strain relationship for an elastic spring element can be expressed by

$$\varepsilon = \frac{\sigma}{k} \tag{4.1}$$

where k is the spring modulus. The constitutive equation for a viscous damper element can be written as

$$\frac{d\varepsilon}{dt} = \frac{\sigma}{\mu} \tag{4.2}$$

where μ is the damper viscosity. Because the spring and the damper is connected in parallel, the total stress in the Kelvin model must equal the sum of the stresses in the spring and the damper as

$$\sigma = \sigma_s + \sigma_d \tag{4.3}$$

where σ is the applied stress, σ_s is the stress in the spring, and σ_d is the stress in the damper. Moreover, when the stress σ is simulated in the Kelvin model, both the spring and damper experience the same deformation as

$$\varepsilon = \varepsilon_s = \varepsilon_d \tag{4.4}$$

where ε is the total strain in the Kelvin element, ε_s is the strain in the spring, and ε_d is the strain in the damper. Substituting Eqs. (4.1), (4.2), and (4.4) into Eq. (4.3), the differential equation of the Kelvin Model can be obtained as

$$\sigma = k\varepsilon + \mu\frac{d\varepsilon}{dt} \ . \tag{4.5}$$

Equation (4.5) is a differential equation that can be solved for particular cases, such as constant stress or constant strain. For creep loading ($\sigma = \sigma_0$), the solution of Eq. (4.5) is given by [23, 24, 55, 56]

$$\varepsilon(t) = \frac{\sigma_0}{E}\left[1 - \exp\left(-\frac{t}{\tau}\right)\right] \tag{4.6}$$

where E is the modulus of elasticity or Young's modulus and $\tau = \mu/k$ is the retardation time. The creep strain $\varepsilon(t)$ is expressed in Eq. (2.1) as a product of the constant stress σ_0 and the creep compliance $C(t)$. Hence, the creep compliance $C(t)$ for the Kelvin model is obtained from Eq. (4.6) and given by [23, 24, 55, 56]

$$C(t) = \frac{1}{E}\left[1 - \exp\left(-\frac{t}{\tau}\right)\right] \tag{4.7}$$

A schematic of the idealized creep strain versus time under constant loading according to Eq. (4.6) is shown in Fig. 4.1. The constant creep loading σ_0 applied to a tensile specimen and its longitudinal creep strain response from the Kelvin model are illustrated in Figs. 4.1a and 4.1b, respectively. As seen in Fig. 4.1b, the longitudinal creep strain from the Kelvin model increases with time, which portrays the creep response. However, there is no initial creep strain due to an applied instantaneous loading (see Fig. 2.1). This is due to the damper element, which prevents the sudden increase in strain and allows the spring element to move slowly with time [33].

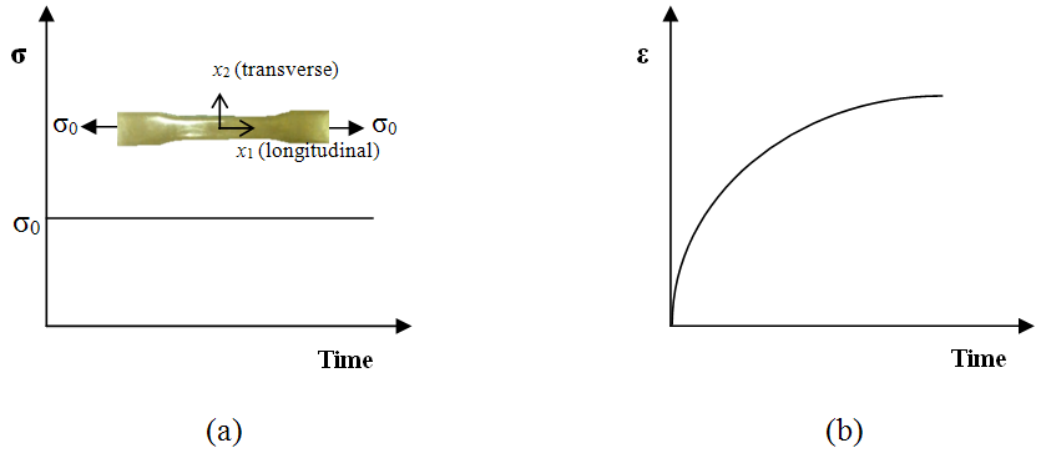

(a) (b)

Figure 4.1 Applied constant stress for a tensile creep test and its corresponding creep strain versus time responses obtained from the Kelvin model.

(a) Creep loading history applied to a tensile creep specimen and (b) its longitudinal creep strain response from the Kelvin model.

Although the simple Kelvin model is generally not adequate for representing real viscoelastic material behavior, these models can be used as elements in more complicated models such as the generalized Kelvin-Voigt (KV) model. The KV model is comprised of a finite number (N_{pr}) of Kelvin elements in series with a spring and is often used to represent the creep strain versus time history of polymers. The free spring is included in series in the KV model to include the instantaneous elastic response [24]. The KV model is shown in Fig. 4.2.

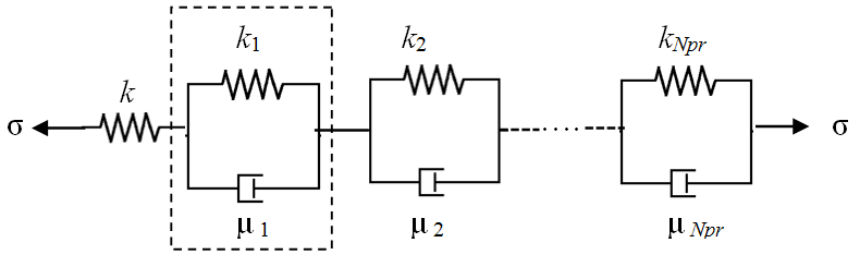

Figure 4.2 The generalized Kelvin-Voigt (KV) model comprised of a series of Kelvin elements in series with a spring.

The governing differential equation for the generalized KV model can be obtained using a procedure similar to that used for obtaining the differential equation for the single Kelvin element. For the case of creep at a constant hold stress, the solution of the differential equation is given by [24]

$$\varepsilon(t) = \sigma_0 \left\{ C^0 + \sum_{n=1}^{N_{pr}} C^n \left[1 - \exp\left(-\frac{t}{\tau_n} \right) \right] \right\} \tag{4.8}$$

where C^0 denotes the instantaneous creep compliance in the loading direction and N_{pr} is the total number of Kelvin elements. The Prony series coefficients and retardation times are C^n and τ_n , respectively. The creep compliance of the generalized KV model can be expressed using a Prony Series representation as [23]

$$C(t) = C^0 + \sum_{n=1}^{N_{pr}} C^n \left[1 - \exp\left(-\frac{t}{\tau_n} \right) \right] \tag{4.9}$$

where

$$C^0 = C^\infty - \sum_{n=1}^{N_{pr}} C^n \tag{4.10}$$

and C^{∞} is the experimentally measured creep compliance in the direction of loading at time $t = \infty$ or a time at which the experiment ends. To obtain creep compliances $C(t)$ in Eq. (4.9), the Prony coefficients C^n and the retardation times τ_n can be determined from curve fitting procedures. Several techniques are found in the literature to fit a Prony series to a linear viscoelastic constitutive response from the experimental creep data in the time domain (quasi-static tests) or the frequency domain (dynamic tests).

The Collocation method [57, 58], proposed by Schapery, and its extensions, such as the Multidata method developed by Cost and Becker [59], presents a straightforward technique from which Prony series coefficients C^n are determined by minimizing the mean square error in the Prony series representation (Eq. (4.9)). In these methods, the time constants (retardation times τ_n for creep tests or relaxation times for stress relaxation tests) are pre-selected. However, the Prony coefficients C^n obtained from these methods can be positive or negative values. The negative Prony coefficients create oscillations in the reconstructed curve of the material function. A number of methods have been proposed to eliminate the negative Prony coefficients. Emri and Tschoegl [60-62] developed the Windowing method to fit the creep compliance data in the time domain using a recursive computer algorithm that enforces non-negative coefficients. Park and Kim [64] used a power law series to pre-smooth experimental creep compliance data that contained significant variance. The pre-smoothing technique was applied to a Prony series representation of the creep compliance and relaxation modulus of asphalt concrete. Pre-smoothing was found to improve the quality of the Prony series fit.

Based on the Multidata method by Cost and Becker [59], the Sign Control method by Bradshaw and Brinson [65] incorporates an iterative approach in which the constraints

(positive values for the creep compliance) for all Prony coefficients C^n can be included in the analysis. The Sign Control method allows the user to select retardation times τ_n in the evenly spaced log time over the range of experimental time data. It was noted that the number of retardation times τ_n affect the smoothness of the reconstructed stress or strain curve. Once the retardation times are chosen, the Prony coefficients C^n are obtained to optimally match the experimental data by the least-squares method (LSQ) [65]. The LSQ method can also fit frequency domain data, such as storage and loss moduli, obtained from a dynamic mechanical analysis (DMA). In this study, the Sign Control method was employed [65], using the linear LSQ technique to determine the time-dependent creep compliances. The previously mentioned techniques to obtain Prony series coefficients C^n are referenced in Table 4.1.

Table 4.1 Techniques to obtain Prony series coefficients.

Technique	**Reference**
Collocation	Schapery (1961) [57, 58]
Multidata	Cost and Becker (1970) [59]
Windowing	Emri and Tschoegl (1992-1993) [60-62]
Power law pre-smoothing function	Park and Kim (2001) [64]
Sign Control	Bradshaw and Brinson (1997) [65]

4.1.2 Numerical Approach for Creep Compliance Characterization Using a Prony Series Representation

The constitutive relation for an isothermal isotropic linear viscoelastic material for creep tests with x_1 as the loading direction using a Prony series representation can be stated as [66]

$$\varepsilon_{\underline{ii}}(t) = \underbrace{C^0_{11\underline{ii}}\sigma_{11}(t)}_{\text{Instantaneous elastic response}} + \underbrace{\sum_{n=1}^{Npr}\left[C^n_{11\underline{ii}}\int_0^t e^{-\frac{t-\xi}{\tau_n}}\frac{\partial\sigma_{11}(\xi)}{\partial\xi}d\xi\right]}_{\text{Viscoelastic response}} + \underbrace{C^{Npr+1}_{11\underline{ii}}\int_0^t\frac{\partial\sigma_{11}(\xi)}{\partial\xi}d\xi}_{\text{Long time response}} \tag{4.11}$$

where $\varepsilon_{\underline{ii}}$ are the experimental strains, σ_{11} is the applied tensile stress, $C^0_{11\underline{ii}}$ are the instantaneous creep compliances, $C^n_{11\underline{ii}}$ are the Prony coefficients, and N_{pr} is the total number of Kelvin elements (length of Prony series). The underscored indices indicate no summations. The indices i = 1, 2 indicates the Cartesian longitudinal (and loading) and transverse directions, respectively. For example, C^0_{1111} is the instantaneous creep compliance in the longitudinal direction, whereas C^0_{1122} is the instantaneous creep compliance in the transverse direction. The first term on the right side of Eq. (4.11) describes the instantaneous elastic response, the second term represents the secondary viscoelastic creep, and the long-time response is described by the last term. Since only the short-term (two-hour) creep response was considered for this study, the long-time response (the last term on the right side of Eq. (4.11)) was neglected. The creep strains in the longitudinal and transverse directions, $\varepsilon_{11}(t)$ and $\varepsilon_{22}(t)$, were measured for all tensile creep tests.

The complete viscoelastic creep description should include the start-up transient response in the loading phase as well as the response to the loading in the transient steady-state phase because the stress history has a significant effect on the creep responses of viscoelastic materials [66, 67]. The constitutive response expressed in Eq. (4.11) was defined for a material that is subjected to an instantaneous constant load at zero time ($t = 0$). Therefore, for a creep test, the applied stress in the x_1 direction can be written as

$$\sigma_{11}(t) = \sigma_0 H(t) \tag{4.12}$$

where σ_0 is the applied constant stress for creep loading and $H(t)$ is the Heaviside unit step function, which is defined as

$$H(t) = \begin{cases} 1 & \text{for } t \geq 0 \\ 0 & \text{for } t < 0 \end{cases} \tag{4.13}$$

However, in laboratory testing, a specimen actually undergoes a transient loading phase over a short period of time ($0 \leq t \leq t_1$) prior to reaching the steady-state applied stress, as illustrated in Fig. 4.3.

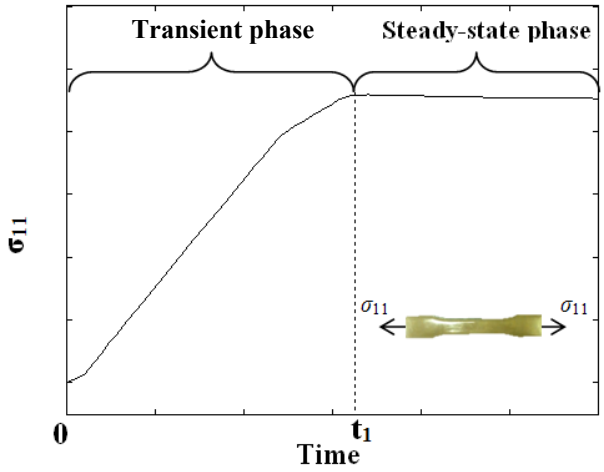

Figure 4.3 Transient phase and steady-state phase during the start-up of a creep test.

Hence, the applied stress in Eq. (4.12) is defined to include the initial and subsequent steady-state creep loading. This can be expressed as [66]

$$\sigma_{11}(t)=\begin{cases} f_\sigma(t) & 0\le t\le t_1 \quad \text{(transient phase)} \\ \sigma_0 H(t-t_1) & t>t_1 \quad \text{(steady-state phase)} \end{cases} \tag{4.14}$$

where $f_\sigma(t)$ is the loading function to be selected and $f_\sigma(t_1)=\sigma_0$ when the rise time t_1 corresponds to the end of the initial loading phase. By incorporating the starting transients (Eq. (4.14)) into the viscoelastic response term (second term in Eq. (4.11), the viscoelastic creep response can be defined as [66]

$$\sum_{n=1}^{N_{pr}}\left[C^n_{11\underline{ii}}\int_0^t e^{-\frac{t-\xi}{\tau_n}}\frac{\partial\sigma_{11}(\xi)}{\partial\xi}d\xi\right]=\begin{cases} \displaystyle\sum_{n=1}^{N_{pr}}\int_0^t e^{-\frac{t-\xi}{\tau_n}}\frac{\partial f_\sigma(\xi)}{\partial\xi}d\xi & 0\le t\le t_1 \\ \left[\displaystyle\sum_{n=1}^{N_{pr}}C^n_{11\underline{ii}}\int_0^{t_1} e^{-\frac{t_1-\xi}{\tau_n}}\frac{\partial f_\sigma(\xi)}{\partial\xi}d\xi + \sum_{n=1}^{N_{pr}}C^n_{11\underline{ii}}\int_{t_1}^{t} e^{-\frac{t-\xi}{\tau_n}}\frac{\partial\sigma_{11}(\xi)}{\partial\xi}d\xi\right] & t>t_1 \end{cases} \tag{4.15}$$

where $C^n_{11\underline{ii}} \geq 0$ and $\sigma_{11} \geq 0$. Therefore the viscoelastic constitutive equation that includes the start-up transient response for an isothermal isotropic linear viscoelastic material for creep tests with x_1 as the loading direction is obtained by substituting Eq. (4.15) into Eq. (4.11) as

$$\varepsilon_{\underline{ii}}(t) = \begin{cases} C^0_{11\underline{ii}}\sigma_{11}(t) + \sum_{n=1}^{N_{pr}} \left[C^n_{11\underline{ii}} \int_0^t e^{-\frac{t-\xi}{\tau_n}} \frac{\partial f_\sigma(\xi)}{\partial \xi} d\xi \right] & 0 \leq t \leq t_1 \\ C^0_{11\underline{ii}}\sigma_{11}(t) + \left[\begin{array}{l} \sum_{n=1}^{N_{pr}} C^n_{11\underline{ii}} \int_0^{t_1} e^{-\frac{t_1-\xi}{\tau_n}} \frac{\partial f_\sigma(\xi)}{\partial \xi} d\xi \\ + \sum_{n=1}^{N_{pr}} C^n_{11\underline{ii}} \int_{t_1}^t e^{-\frac{t-\xi}{\tau_n}} \frac{\partial \sigma_{11}(\xi)}{\partial \xi} d\xi \end{array} \right] & t > t_1 \end{cases} \tag{4.16}$$

An alternate form of Eq. (4.16) is obtained by integrating Eq. (4.16) by parts, which yields

$$\varepsilon_{\underline{ii}}(t) = \begin{cases} C^0_{11\underline{ii}}\sigma_{11}(t) + \sum_{n=1}^{N_{pr}} \left[C^{*n}_{11\underline{ii}} \int_0^t e^{-\frac{t-\xi}{\tau_n}} f_\sigma(\xi)\, d\xi \right] & 0 \leq t \leq t_1 \\ C^0_{11\underline{ii}}\sigma_{11}(t) + \left[\begin{array}{l} \sum_{n=1}^{N_{pr}} C^{*n}_{11\underline{ii}} \int_0^{t_1} e^{-\frac{t_1-\xi}{\tau_n}} f_\sigma(\xi)\, d\xi \\ + \sum_{n=1}^{N_{pr}} C^{*n}_{11\underline{ii}} \int_{t_1}^t e^{-\frac{t-\xi}{\tau_n}} \sigma_{11}(\xi)\, d\xi \end{array} \right] & t > t_1 \end{cases} \tag{4.17}$$

where

$$C^{*n}_{11\underline{ii}} = \frac{C^n_{11\underline{ii}}}{\tau_n} \tag{4.18}$$

Defining t_m as the discrete times at which the stress and strain data are obtained and M to be the total number of sampling points, the stress versus strain relation at t_m can be written as

$$\varepsilon_{\underline{ii}}(t_m)=\begin{cases} C^0_{11\underline{ii}}\sigma_{11}(t_m)+\sum_{n=1}^{N_{pr}}\left[C^{*n}_{11\underline{ii}}\int_0^{t_m} e^{-\frac{t-\xi}{\tau_n}} f_\sigma(\xi)\,d\xi\right] & 0\le t\le t_1 \\ C^0_{11\underline{ii}}\sigma_{11}(t_m)+\left[\begin{array}{l}\sum_{n=1}^{N_{pr}} C^{*n}_{11\underline{ii}}\int_0^{t_1} e^{-\frac{t_1-\xi}{\tau_n}} f_\sigma(\xi)\,d\xi \\ +\sum_{n=1}^{N_{pr}} C^{*n}_{11\underline{ii}}\int_{t_1}^{t_m} e^{-\frac{t-\xi}{\tau_n}} \sigma_{11}(\xi)\,d\xi\end{array}\right] & t>t_1 \end{cases} \tag{4.19}$$

In Eq. (4.19), $C^{*n}_{11\underline{ii}}$ and τ_n are the unknown coefficients and retardation times and $m = 1, \ldots, M$.

In the Prony series representation, the retardation times τ_n with $n = 1,\ldots, N_{pr}$ are typically prescribed, which reduces the problem to a linear system of equations rather than a system of nonlinear equations [63] . The collocation or LSQ methods can be used to avoid the calculation of the parameters $C^{*n}_{11\underline{ii}}$ and τ_n simultaneously through the non-linear relations. For the LSQ method, the time constants are taken to be the times in equidistant intervals on the log t axis, which yield the larger interval of τ_n compared to τ_m obtained from the collocation method. The time constants can be prescribed using Schapery's approximation [57, 58] as

$$\tau_n \cong 10^n \tag{4.20}$$

However, the time constants obtained using Eq. (4.20) may be outside the range of the real times for the large values of N_{pr}. Therefore, a modification of Eq. (4.20) is typically used for approximating the time constants as [4]

$$\begin{gathered}\log(\tau_n)=\frac{n\left(\log(t_\infty)-\log(t_0)\right)}{N_{pr}+1} \\ \log(t_0)-1\le\log(\tau_n)\le\log(t_\infty)+1\end{gathered} \tag{4.21}$$

and t_0 is the initial time and t_∞ is the time at the end of the experiment.

Eq. (4.19) reduces to a linear system of equations by prescribing the retardation times τ_n over the range of the sampling time data. The LSQ technique is employed to obtain the $C^{*n}_{11\underline{ii}}$ in Eq. (4.19) and the residual sum of squares (total square of errors) of Eq. (4.19) is given by [66]

$$S_{\underline{ii}}(C^{*n}_{11\underline{ii}}) = \sum_{m=1}^{M}\left[\varepsilon^{m}_{\underline{ii}} - \varepsilon_{\underline{ii}}(t_m)\right]^2 = \sum_{m=1}^{M}\left[\varepsilon^{m}_{\underline{ii}} - \left(C^{0}_{11\underline{ii}}\sigma_{11}(t_m) + \sum_{n=1}^{N_{pr}} C^{*n}_{11\underline{ii}}\Lambda_{mn}\right)\right]^2 \tag{4.22}$$

where

$$\Lambda_{mn} = \begin{cases} \int_0^{t_m} e^{-\frac{t-\xi}{\tau_n}} f_\sigma(\xi)\, d\xi \quad \text{for } 0 \le t_m \le t_1 \\ \int_0^{t_1} e^{-\frac{t_1-\xi}{\tau_n}} f_\sigma(\xi)\, d\xi + \int_0^{t_m} e^{-\frac{t-\xi}{\tau_n}} \sigma_{11}(\xi)\, d\xi \quad \text{for } t_m \ge t_1 \end{cases} . \tag{4.23}$$

Λ is a short-hand notation for the matrix of the time integrals in Eq. (4.22). The minimum values of the residual sum of squares in Eq. (4.22) are calculated by

$$\frac{\partial S_{\underline{ii}}}{\partial C^{*n}_{11\underline{ii}}} = 0 \tag{4.24}$$

Thus, obtaining

$$\sum_{m=1}^{M}\left[\sum_{n=1}^{N_{pr}} C^{*n}_{11\underline{ii}}\Lambda_{mn}\Lambda_{mn} - \varepsilon^{m}_{\underline{ii}}\Lambda_{mn} + C^{0}_{11\underline{ii}}\sigma^{m}_{11}\Lambda_{mn}\right] = 0 \tag{4.25}$$

The matrix form of Eq. (4.25) is formulated as

$$[A]\{c\} = \{B\} \tag{4.26}$$

where

$$[A] = \sum_{m=1}^{M} \sum_{n=1}^{N_{pr}} \Lambda_{mn} \Lambda_{mn}$$
$$\{c\} = C_{11\underline{ii}}^{*n} \qquad . \tag{4.27}$$
$$\{B\} = \sum_{m=1}^{M} \varepsilon_{\underline{ii}}^{m} \Lambda_{mn} - \sum_{m=1}^{M} C_{11\underline{ii}}^{0} \sigma_{11}^{m} \Lambda_{mn}$$

The values of $C_{11\underline{ii}}^{*n}$ can be determined by solving for $\{c\}$ in Eq. (4.27). Figure 4.4 shows a flow chart summarizing the LSQ optimization scheme used to obtain the Prony coefficients from one-dimensional tensile creep experiments.

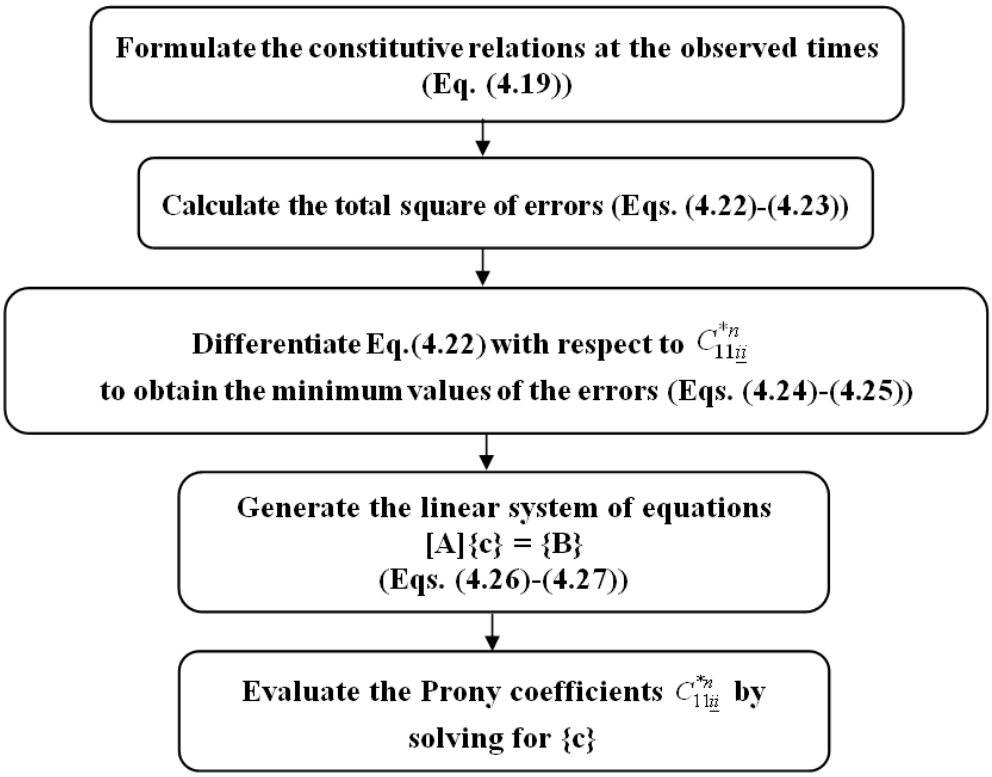

Figure 4.4 Procedure to calculate the Prony coefficients using the LSQ method.

In summary, the creep compliances of the uni-directional tensile creep test using a Prony series representation are obtained using the following steps. The loading function is determined from the experimental stress and strain data. Using the LSQ technique, the linear system of equations is solved and the Prony coefficients are determined. The analytical creep strain is then calculated and compared to the experimental strain data. The procedure to obtain creep compliances using the Prony series method is summarized and shown in Fig. 4.5.

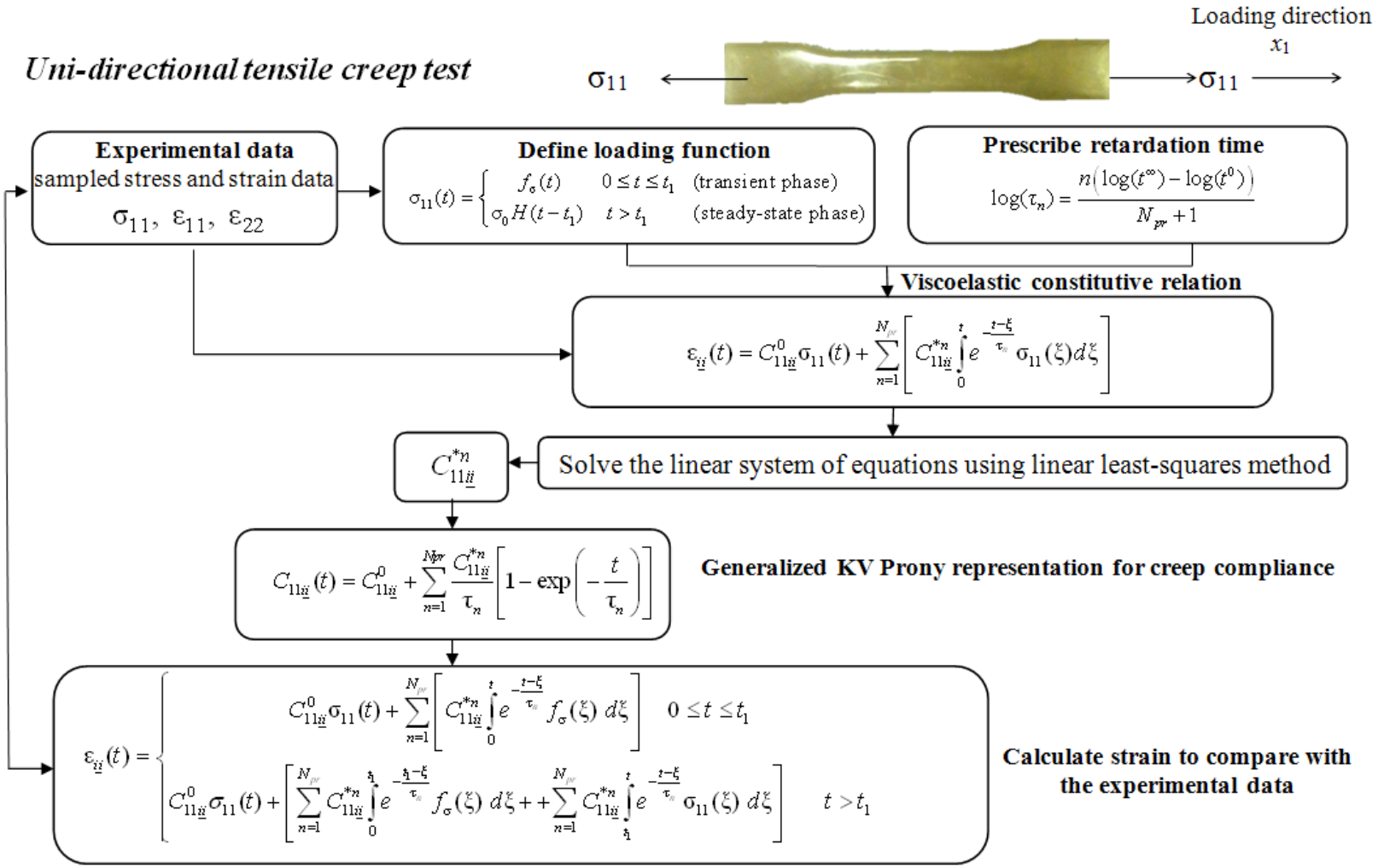

Figure 4.5 Procedure to calculate creep compliances using a Prony series representation.

4.1.3 Determination of the Tensile Loading Function

The tensile loading function $f_\sigma(t)$ was selected to simulate the applied stress during the transient phase for a tensile creep test. The function $f_\sigma(t)$ with $\left.\frac{df_\sigma(t)}{dt}\right|_{t=t_0} = \left.\frac{df_\sigma(t)}{dt}\right|_{t=t_\infty} = 0$ was chosen as

$$f_\sigma(t) = \sum_{q=0}^{Q} \phi_q t^q \qquad 0 \le t \le t_1 \tag{4.28}$$

where ϕ_q are the constants to be determined from curve-fitting each experimental creep stress versus time history using the LSQ method.

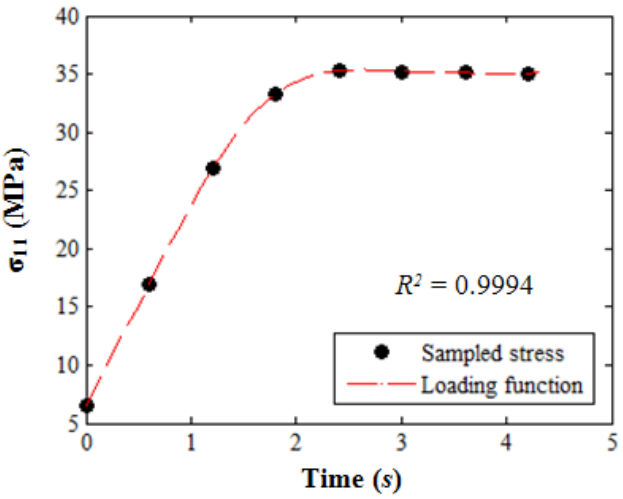

Figure 4.6 Creep loading function for 60°C and 35.4 MPa (60% σ_u = 34 MPa) obtained by the LSQ method.

Table 4.2 The constants ϕ_q obtained from curve-fitting the experimental data in Fig. 4.6.

q	t	ϕ_q
0	0	0.042
1	0.601	-0.656
2	1.202	3.894
3	1.804	-10.467
4	2.405	11.332
5	3.007	-4.706
6	3.608	17.708
7	4.210	6.568

Figure 4.6 shows the comparison of the tensile loading function (Eq. (4.28)) of the seventh order polynomial function ($Q = 7$) and the experimental creep stress versus time data at 60°C and 35.4 MPa (or 60% σ_u). The polynomial functions for $Q = 7$ shows excellent agreement (the correlation coefficient $R^2 = 0.9994$) with the experimental stress versus time data during the tensile transient phase ($0 \le t \le 4.2s$), as seen in Fig. 4.6. The constants ϕ_q obtained from the loading function in Fig. 4.6 are listed in Table 4.2.

4.1.4 Determination of the Number of Prony Series Elements

The mathematical constraints of the creep compliances and Prony coefficients were used in the calculation of the creep compliances to improve the quality of the LSQ fit of the experimental creep-strain responses. These constraints enforce positive values for the creep compliances and Prony coefficients in the loading direction x_1 and negative values for those in the transverse direction x_2. The constraints are given as

$$
\begin{aligned}
C_{1111}(t) &> 0 \\
C^{n}_{1111} &> 0 \\
C_{1122}(t) &< 0 \\
C^{n}_{1122} &< 0
\end{aligned}
\tag{4.29}
$$

Numerical convergence of the creep strain-time data was obtained by successively increasing the number of Prony series elements N_{pr}. Figure 4.7 contains the plots of the analytical and experimental creep strain versus time responses, ε_{11} at 60% σ_u and 24°C, 40°C, and 60°C. The analytical longitudinal creep strains were obtained using the number of Prony elements N_{pr} = 1, 5, 10, 30, 40. A goodness-of-fit test was conducted to determine the the number of Prony element N_{pr} for the analytical creep strain that best fits the experimental data. As seen in Fig. 4.7, the convergence of the LSQ fit of the analytical creep strain versus time data was improved by increasing the number of Prony elements N_{pr}. A good convergence of the LSQ fit was achieved with a 30-term (N_{pr} = 30) Prony series. No further improvement of the LSQ fits was obtained for Prony terms beyond 30.

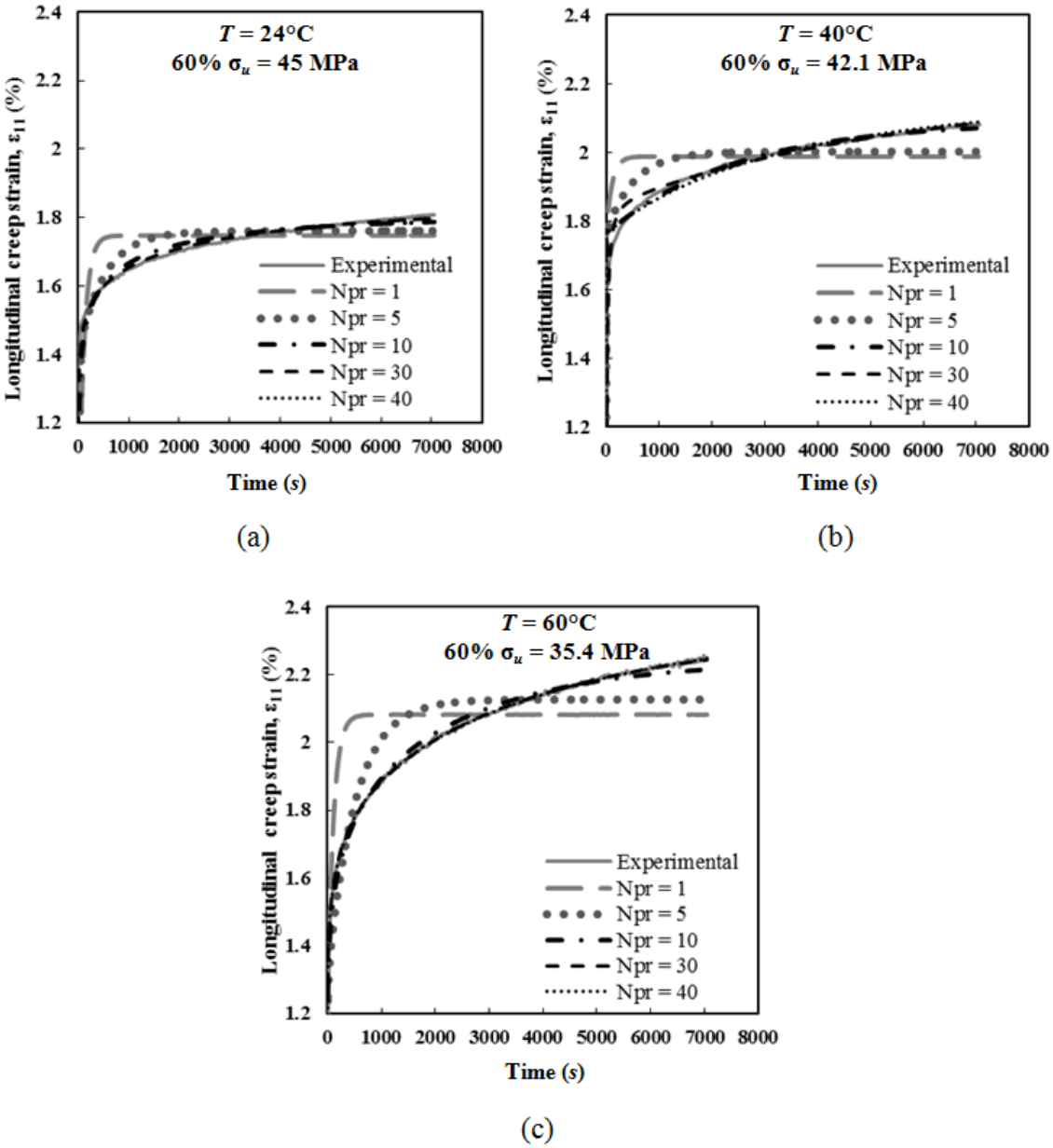

Figure 4.7 Comparison of the experimental and analytical longitudinal creep strain versus time responses $\varepsilon_{11}(t)$ of cured Derakane 441-400 at 60% σ_u at T = (a) 24°C, (b) 40ºC, and (c) 60ºC.

4.2 Creep Compliances of Cured Derakane 441-400

The creep compliance functions in longitudinal and transverse directions of cured Derakane 441-400 were obtained through the Prony series representation of the generalized KV model with the loading function in Eq. (4.11). The time-dependent longitudinal creep compliances $C_{1111}(t)$ for ten specimens at applied stresses of 60% σ_u are illustrated in Fig. 4.8. This figure shows the plots obtained at the applied constant stresses of 60% σ_u at 24°C, 40°C, and 60°C, which correspond to 45 MPa, 42.1 MPa, and 35.4 MPa, respectively. As seen, considerable variability in the longitudinal creep compliances is observed at all temperatures. A larger variation of longitudinal creep compliances is also observed as the temperature increases. For example, longitudinal creep compliances in the range of 0.025-0.04 MPa^{-1} are seen at 24°C (60% σ_u = 45 MPa), 0.35-0.62 MPa^{-1} at 40°C (60% σ_u = 42.1 MPa), and 0.45-0.75 MPa^{-1} at 60°C (60% σ_u = 35.4 MPa). In general, the longitudinal creep compliances of cured Derakane 441-400 monotonically increase with increasing temperature.

Figure 4.9 contains plots of the longitudinal creep compliances as a function of time of ten specimens at applied stresses of 70% σ_u. The applied stresses at 70% σ_u at 24°C, 40°C, and 60°C correspond to 52.5 MPa, 49.1 MPa, and 41.3 MPa, respectively. Again, a large variability in the longitudinal creep compliances are observed. Moreover, the longitudinal creep compliances increase with increasing temperature. This effect became more pronounced as the applied stress was increased. A significant increase in longitudinal creep compliances is seen at the highest temperature (Fig. 4.9c).

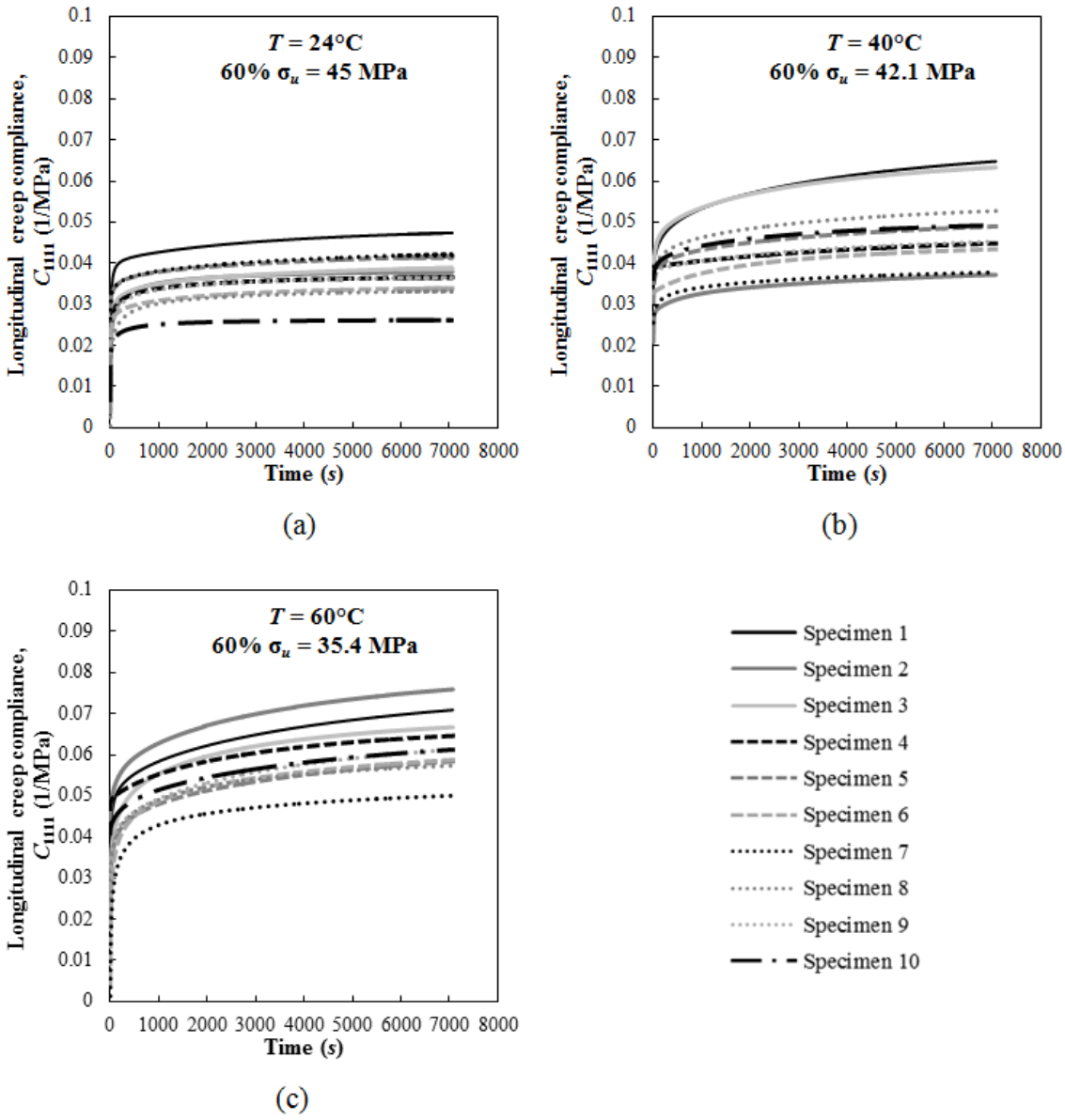

Figure 4.8 Longitudinal creep compliances $C_{1111}(t)$ of cured Derakane 441-400 at applied stresses of 60% σ_u at T = (a) 24°C, (b) 40°C and (c) 60°C.

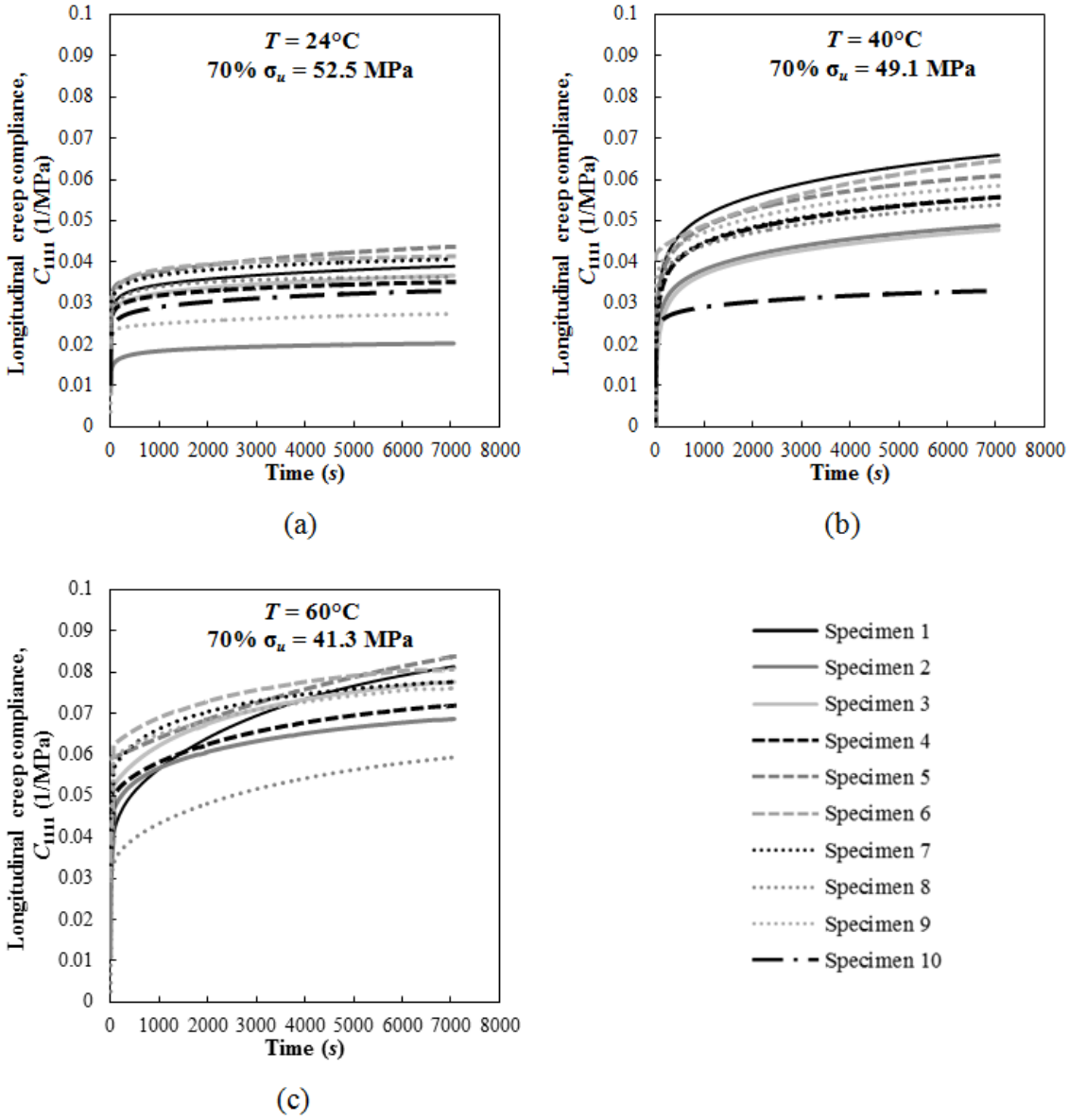

Figure 4.9 Longitudinal creep compliances $C_{1111}(t)$ of cured Derakane 441-400 at applied stresses of 70% σ_u at T = (a) 24°C, (b) 40°C, and (c) 60°C.

Figure 4.10 contains the plot of transverse creep compliances $C_{1122}(t)$ for ten cure Derakane 441-400 specimens at stress levels of 60% σ_u at 24°C (60% σ_u = 45 MPa), 40°C (60% σ_u = 42.1 MPa), and 60°C (60% σ_u = 35.4 MPa). The variation in the

transverse creep strains is observed at all temperatures. For example, the transverse creep compliances are approximately -0.005 to -0.015 MPa^{-1} at 24°C (60% σ_u = 45 MPa), as seen in Fig. 4.10a. As expected, at a constant holding stress, creep compliances in the transverse direction increased as the temperature increased. The creep compliances in the transverse direction at stress levels of 70% σ_u are presented in Fig. 4.11. Similar to those in the longitudinal direction, the transverse creep compliances are well-behaved during the steady state creep and appear to vary with the stress level. The transverse creep compliances decrease with increasing stress level. Overall, the magnitude of creep compliances in the transverse direction of cured Derakane 441-400 is smaller than those in the longitudinal direction for all temperatures and stress levels.

During steady-state creep ($t \geq 1000\ s$), the longitudinal creep compliances appear to be a monotonically increasing function of both temperature and stress level, whereas the transverse creep compliances appear to be a monotonically decreasing function of both temperature and stress level. This behavior enables the development of predictive models for the time and temperature dependent creep compliances.

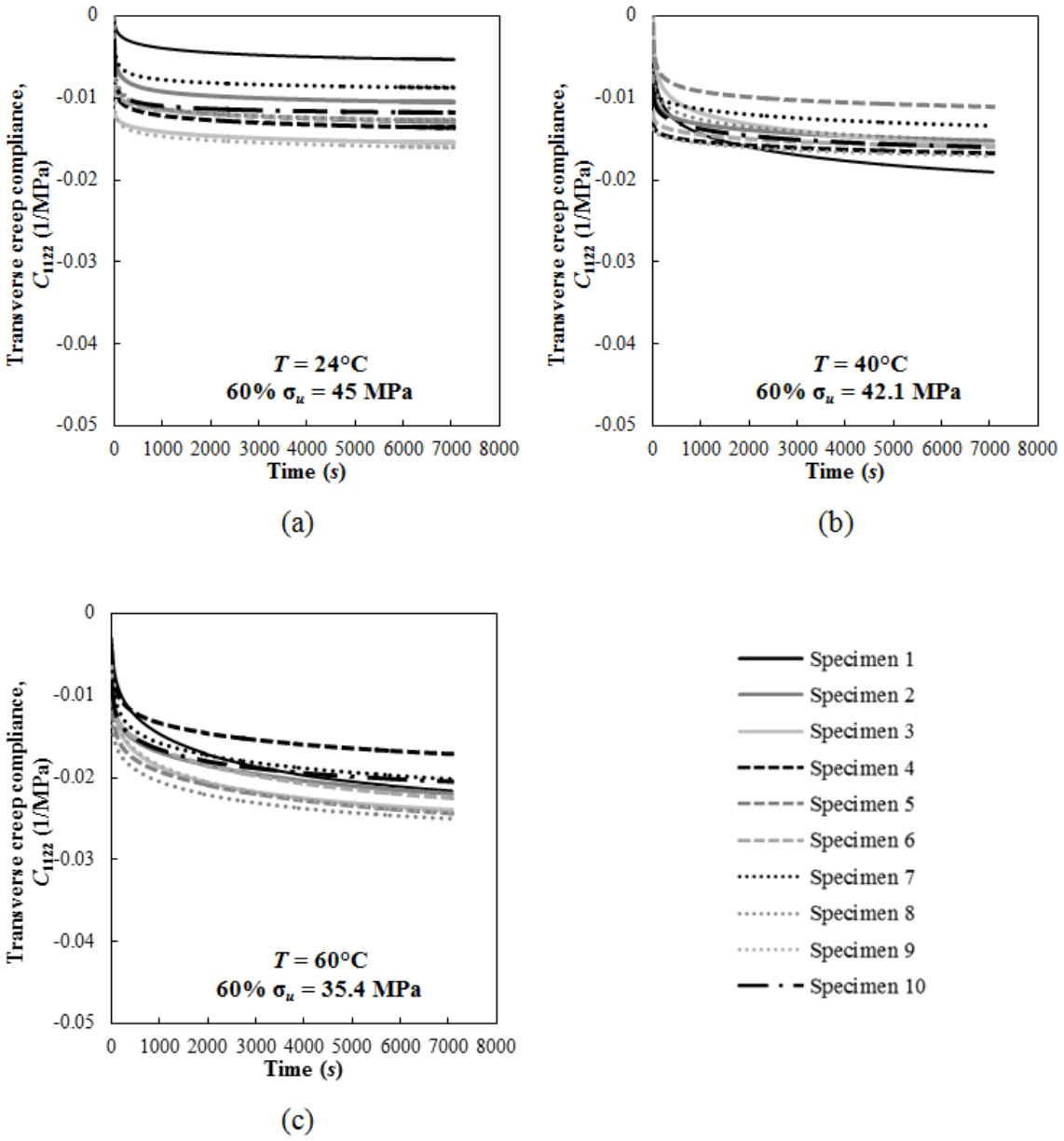

Figure 4.10 Transverse creep compliances $C_{1122}(t)$ of cured Derakane 441-400 at applied stresses of 60% σ_u at T = (a) 24°C, (b) 40°C, and (c) 60°C.

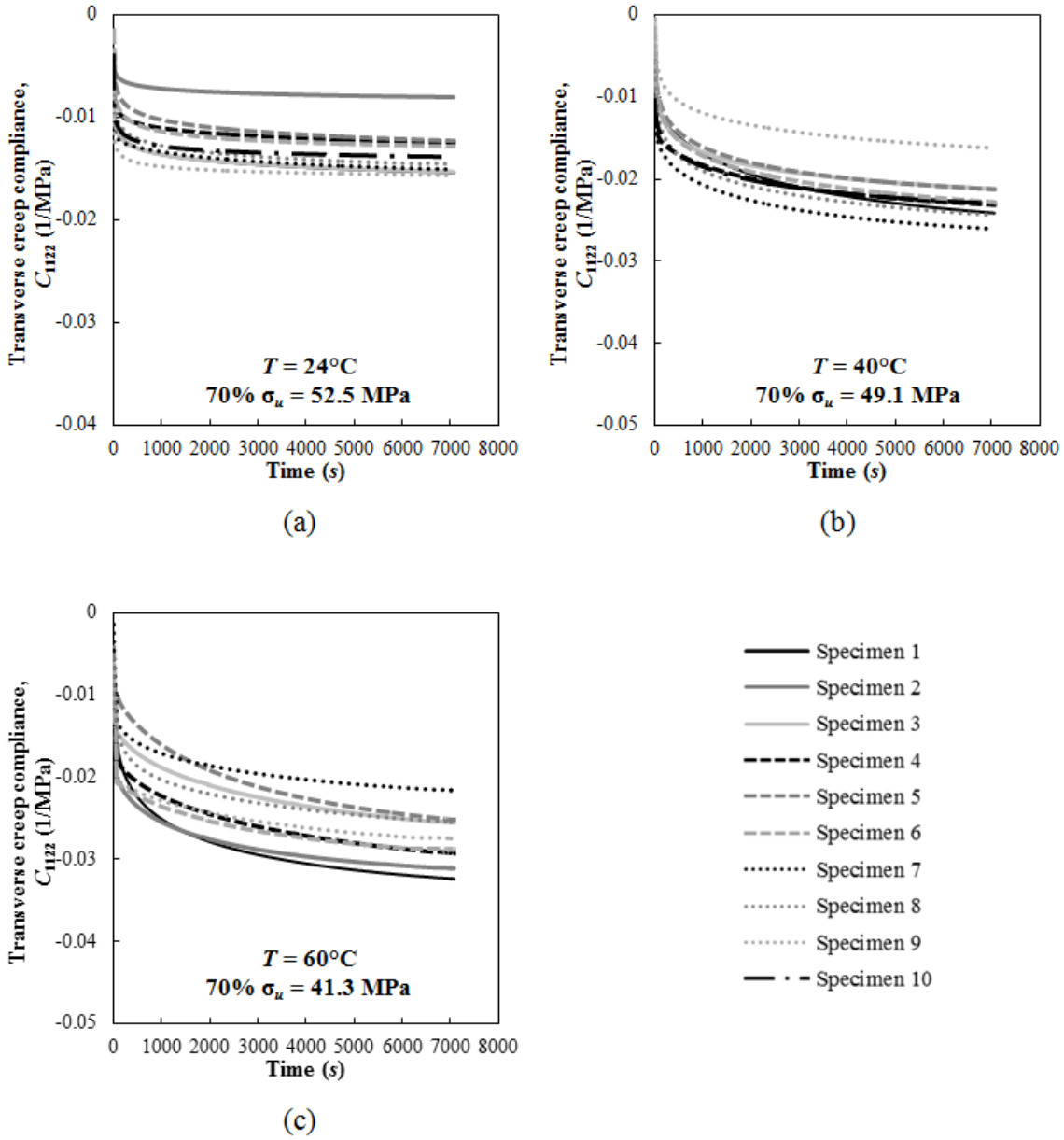

Figure 4.11 Transverse creep compliance $C_{1122}(t)$ of cured Derakane 441-400 at applied stresses of 70% σ_u at T = (a) 24°C, (b) 40°C, and (c) 60°C.

CHAPTER V

STATISTICAL MODELING OF CREEP COMPLIANCES OF A VINYL ESTER POLYMER

Two types of probability distributions were considered to analyze the variability of creep compliances of cured Derakane 441-400. Two-parameter Weibull and log-normal distributions were used to obtain the probability density functions (PDFs) and the corresponding cumulative distribution functions (CDFs) of the creep compliances for each tensile creep test configuration. The Weibull and log-normal distribution parameters were obtained using the method of maximum likelihood estimation (MLE). The Kolmogorov-Smirnov (K-S) hypothesis test was used to evaluate the goodness-of-fit of the Weibull and log-normal distribution models of the creep compliance data. A detailed description of the statistical analysis used in this study is given in this section.

5.1 Probability Distribution Function Selection

Weibull, Gaussian (normal), and log-normal distributions are commonly used in the statistical analysis of mechanical properties of polymers and composite materials [68-73]. Generally, the PDF, $f(x)$, describes the probability of a random variable (x) to fall within a range of values. The PDF describes how the observed data is distributed with respect to some scaled quantities [53]. Two or three parameters are typically used to characterize the distribution. The mean and variance of the Weibull

distribution are represented by the shape parameter (γ), scale parameter (β), and the gamma function[1] (Γ). The shape parameter (γ) represents the degree of scatter in the observed data (i.e., γ increases with the degree of scatter in the data). The scale parameter (β) represents the location of the 63.2 percentile of the distribution [74]. The Weibull PDF is the exponential PDF when the shape parameter γ = 1 and the Rayleigh PDF when the shape parameter γ = 2 [74].

The standard formulation of the Gaussian distribution is obtained by specifying its mean μ and standard deviation σ. This distribution can also be used to determine the log-normal distribution, which is essentially the Gaussian distribution with the log-transformed random variables log (*x*). The log-normal parameters consist of the location parameter (λ) and the scale parameter (ζ). The location parameter (λ) of the log-normal distribution is the mean of the log-transformed observed data vector *x*. The scale parameter (ζ) of the log-normal distribution represents the standard deviation of the logarithm of the data points [75]. Table 5.1 lists the PDF, mean, and variance of the two-parameter Weibull, log-normal, and Gaussian distributions.

[1]Γ is the gamma function defined as [94]

$$\Gamma(x) = \int^{\infty} e^{-t} t^{x-1} dt$$

Table 5.1 Probability density functions, means, and variances of Weibull, Gaussian, and log-normal distributions [75].

Distribution	Probability density function (PDF)	Mean	Variance
Weibull	$f(x\|\gamma,\beta)=\frac{\gamma}{\beta}\left(\frac{x}{\beta}\right)^{\gamma-1}e^{-\left(\frac{x}{\beta}\right)^{\gamma}}$ $0\le x\le\infty$, $\gamma>0,\beta>0$	$\beta^{\frac{1}{\gamma}}\Gamma\left(1+\frac{1}{\gamma}\right)$	$\beta^{\frac{2}{\gamma}}\left[\Gamma\left(1+\frac{2}{\gamma}\right)-\Gamma^2\left(1+\frac{1}{\gamma}\right)\right]$
Gaussian (Normal)	$f(x\|\mu,\sigma)=\frac{1}{\sqrt{2\pi}\sigma}\exp\left[-\frac{(x-\mu)^2}{2\sigma^2}\right]$ $-\infty<x<\infty$	μ	σ^2
Log-normal	$f(x\|\lambda,\zeta)=\frac{1}{x\zeta\sqrt{2\pi}}\exp\left[-\frac{(\log x-\lambda)^2}{2\zeta^2}\right]$ $0\le x<\infty$	$e^{\lambda+\frac{\zeta^2}{2}}$	$e^{2(\lambda+\zeta^2)}-e^{2\lambda+\zeta^2}$

The random variables x of the Weibull and log-normal distributions are strictly positive values ($0 \le x \le \infty$), whereas those for the Gaussian distribution can be any value ($-\infty \le x \le \infty$). The Gaussian distribution is the most widely used probability distribution; however, its PDF has an unbounded domain. The Gaussian distribution's PDF is a symmetrical bell-shaped curve that extends to a small infinite negative value. This negative domain is physically unrealistic for a random variable that is strictly positive such as the strength of a material [19]. Therefore, the Weibull and log-normal distributions with bounded domains ($0 \le x \le \infty$) were selected for the statistical analysis of cured Derakane 441-400's creep compliances. The PDFs of Weibull, Gaussian, and log normal distributions are illustrated in Fig. 5.1.

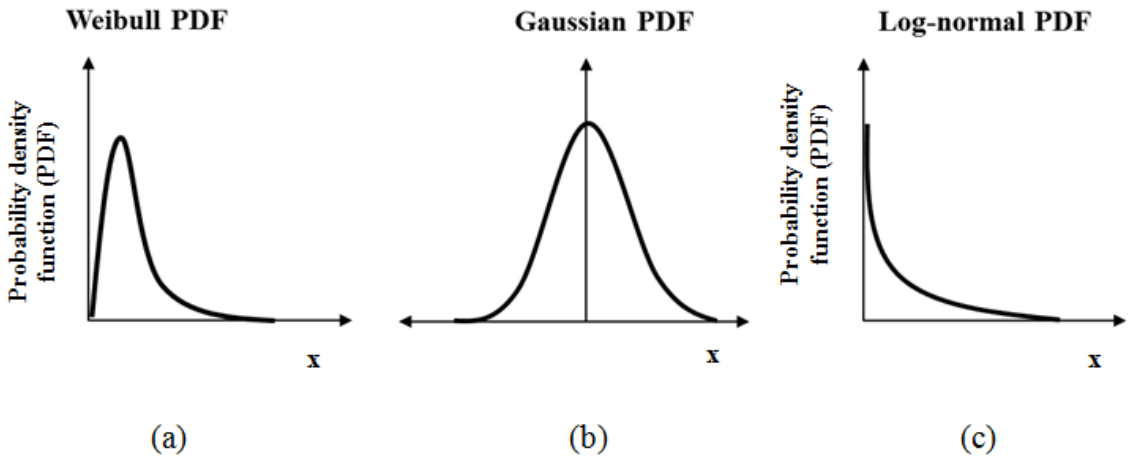

Figure 5.1 Probability density functions (PDFs) of Weibull, Gaussian, and log-normal distributions.

5.2 Protocol to Obtain Creep Compliance Distributions

The longitudinal and transverse creep strain versus time responses were obtained from short-term tensile creep tests using the experimental method described in Chapter 3. The creep compliances were subsequently determined using the generalized viscoelastic constitutive equation with a Prony series representation, which was presented in Chapter 4. Creep compliance values for ten specimens were obtained at each time ($0 \leq t \leq 7000\ s$) for each test configuration. The Weibull and log-normal parameters of these ten creep compliances were estimated at each time interval, using the MLE method. The corresponding PDFs were fitted to the creep compliance histograms. The Weibull and log-normal distributions were then evaluated for goodness-of-fit using the K-S test [76]. Figure 5.2 shows the flowchart for the determination of the creep compliance distributions of cured Derakane 441-400.

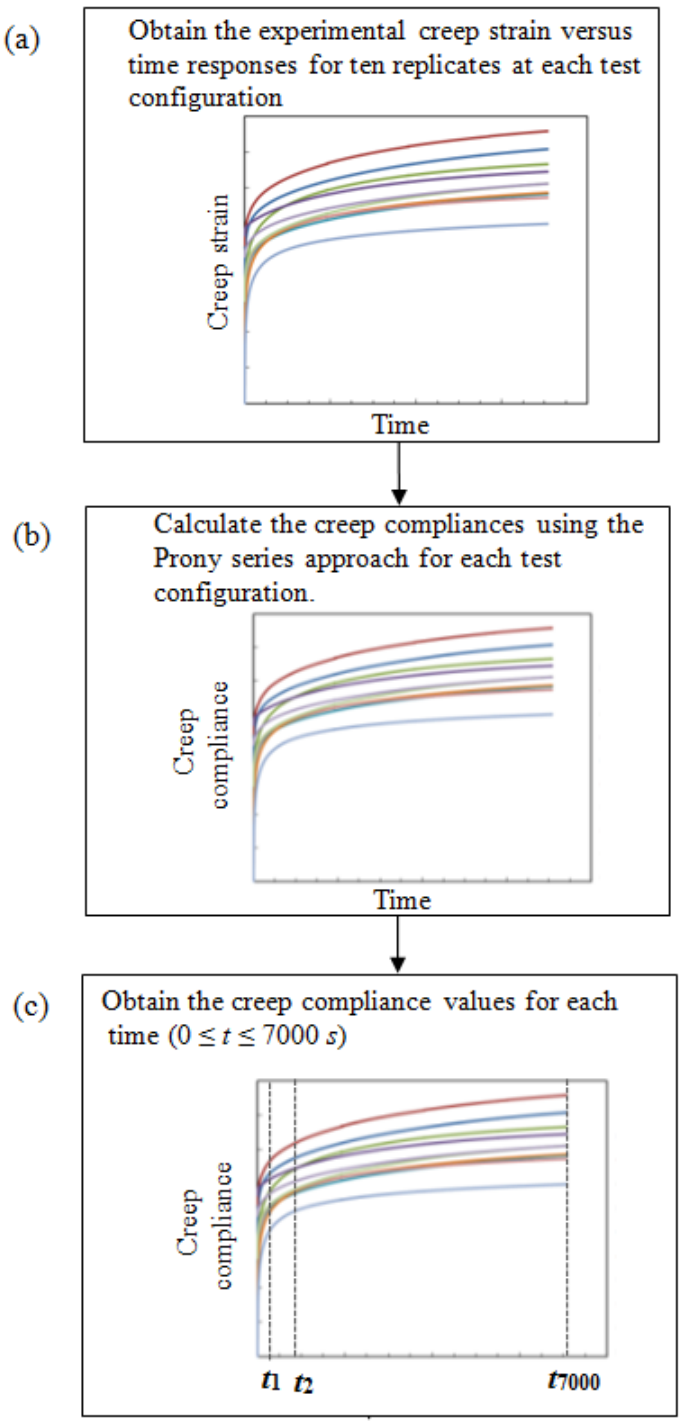

Figure 5.2 Protocol to obtain creep compliance distributions of cured Derakane 441-400 (continued on next page).

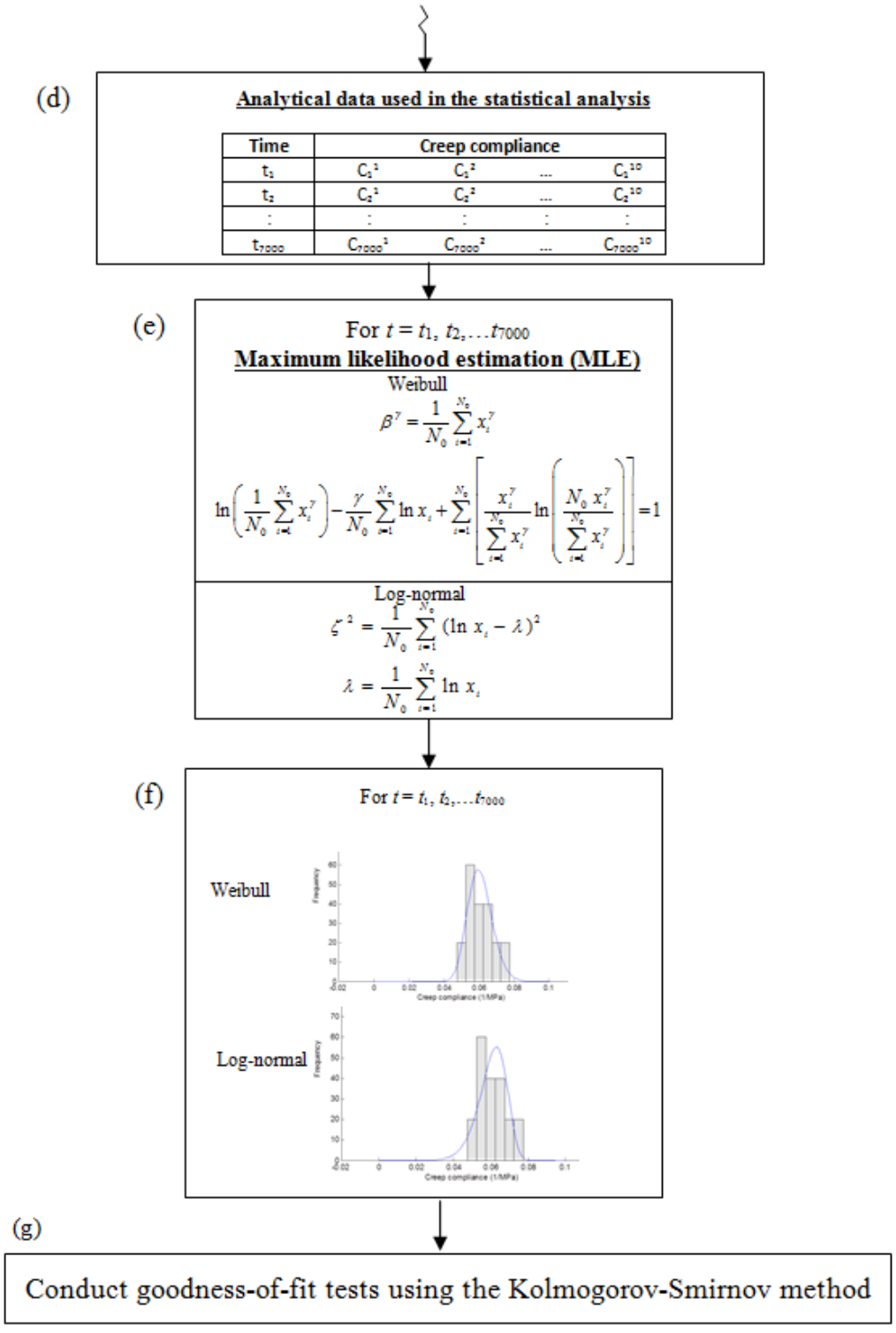

Figure 5.2 (Continued)

5.3 Statistical Analysis of the Creep Compliances of Cured Derakane 441-400

Two-parameter Weibull and log-normal functions were used to develop the probability distributions of the creep compliances for all tests at each time. The PDF $f(x|w)$ and CDF $F(x|w)$ of the Weibull distribution that identifies the probability of the observed data vector $x = (x_1, x_2, \ldots, x_{N_0})$, for N_0 samples, with the distribution parameters w are given by [75]

$$f(x|w) = \frac{\gamma}{\beta}\left(\frac{x}{\beta}\right)^{\gamma-1} \exp\left[-\left(\frac{x}{\beta}\right)^{\gamma}\right] \qquad 0 \le x \le \infty \tag{5.1}$$

$$F(x|w) = 1 - \exp\left[-\left(\frac{x}{\beta}\right)^{\gamma}\right] \qquad 0 \le x \le \infty \tag{5.2}$$

where γ and β are the Weibull shape and scale parameters, respectively.

The log-normal distribution is characterized by the log-transformed observation data vector x. The PDF and CDF of the two-parameter log-normal distribution are given by [75]

$$f(x|w) = \frac{1}{x\zeta\sqrt{2\pi}} \exp\left[-\frac{(\log x - \lambda)^2}{2\zeta^2}\right] \qquad 0 \le x \le \infty \tag{5.3}$$

$$F(x|w) = \frac{1}{2}\left[1 + \operatorname{erf}\left(\frac{\ln x - \lambda}{\zeta\sqrt{2}}\right)\right] \qquad 0 \le x \le \infty \tag{5.4}$$

where λ and ζ are the location and scale parameters, respectively. The function erf(x) in Eq. (5.4) is the error function that is defined by [77]

$$\operatorname{erf}(x) \equiv \frac{2}{\sqrt{\pi}} \int_0^x \exp\left[-z^2\right] dz \tag{5.5}$$

The ten creep compliance values at each time (Fig. 5.2c) were used to determine the Weibull parameters (γ , β) and the log-normal parameters (λ, ζ). The observation data vector x represents the ten creep compliance values ($N_0 = 10$) at each time ($0 \leq t \leq 7000\ s$).

5.3.1 Method of Maximum Likelihood

The Weibull and log-normal parameters were calculated using the method of maximum likelihood estimation (MLE), which maximizes the likelihood function or the probability of occurrence of the sample values. The likelihood function $L(x|w)$ of the observed data vector, $x = (x_1, x_2, \ldots, x_{N_0})$ with the distribution parameters w is defined as [76]

$$L(x_1, \ldots, x_{N_0} \mid w) = f(x_1 \mid w) f(x_2 \mid w) \ldots f(x_{N_0} \mid w) \tag{5.6}$$

The maximum likelihood estimators are obtained by differentiating the likelihood function $L(x|w)$ as [76]

$$\frac{\partial L(x_1, \ldots, x_{N_0} \mid w)}{\partial w} = 0 \tag{5.7}$$

The general expressions of the MLE for a Weibull distribution are determined from Eq. (5.7). The Weibull parameters (shape γ and scale β) are obtained by solving the following equation simultaneously, i.e.,

$$\beta^{\gamma} = \frac{1}{N_0}\sum_{i=1}^{N_0} x_i^{\gamma}$$

$$\ln\left(\frac{1}{N_0}\sum_{i=1}^{N_0} x_i^{\gamma}\right) - \frac{\gamma}{N_0}\sum_{i=1}^{N_0}\ln x_i + \sum_{i=1}^{N_0}\left[\frac{x_i^{\gamma}}{\sum_{i=1}^{N_0} x_i^{\gamma}}\ln\left(\frac{N_0\, x_i^{\gamma}}{\sum_{i=1}^{N_0} x_i^{\gamma}}\right)\right] = 1 \tag{5.8}$$

Similarly, the MLE for the log-normal distribution is obtained from

$$\lambda = \frac{1}{N_0}\sum_{i=1}^{N_0}\ln x_i$$

$$\zeta^2 = \frac{1}{N_0}\sum_{i=1}^{N_0}(\ln x_i - \lambda)^2 \tag{5.9}$$

Following the determination of the Weibull and log-normal parameters, the corresponding PDFs were obtained.

The following sections present the statistical analysis of the longitudinal creep compliances C_{1111} of cured Derakane 441-400 at 60% σ_u at three temperatures (24°C, 40°C, 60°C). The longitudinal creep compliances C_{1111} were used to construct the histograms at selected times at each temperature (24°C, 40°C, 60°C), as shown in Fig. 5.3. The times were selected in increments of 2000 *s* after the onset of the steady state creep. These are 1000 *s,* 3000 *s,* 5000 *s,* and 7000 *s*. It should be noted that at 40°C (Fig. (5.3b)), the creep compliance magnitudes from specimens #1 and #3 appear to deviate markedly from those of other specimens. Therefore, the creep compliance data from specimens #1 and #3 at 40°C was not considered in the statistical analyses.

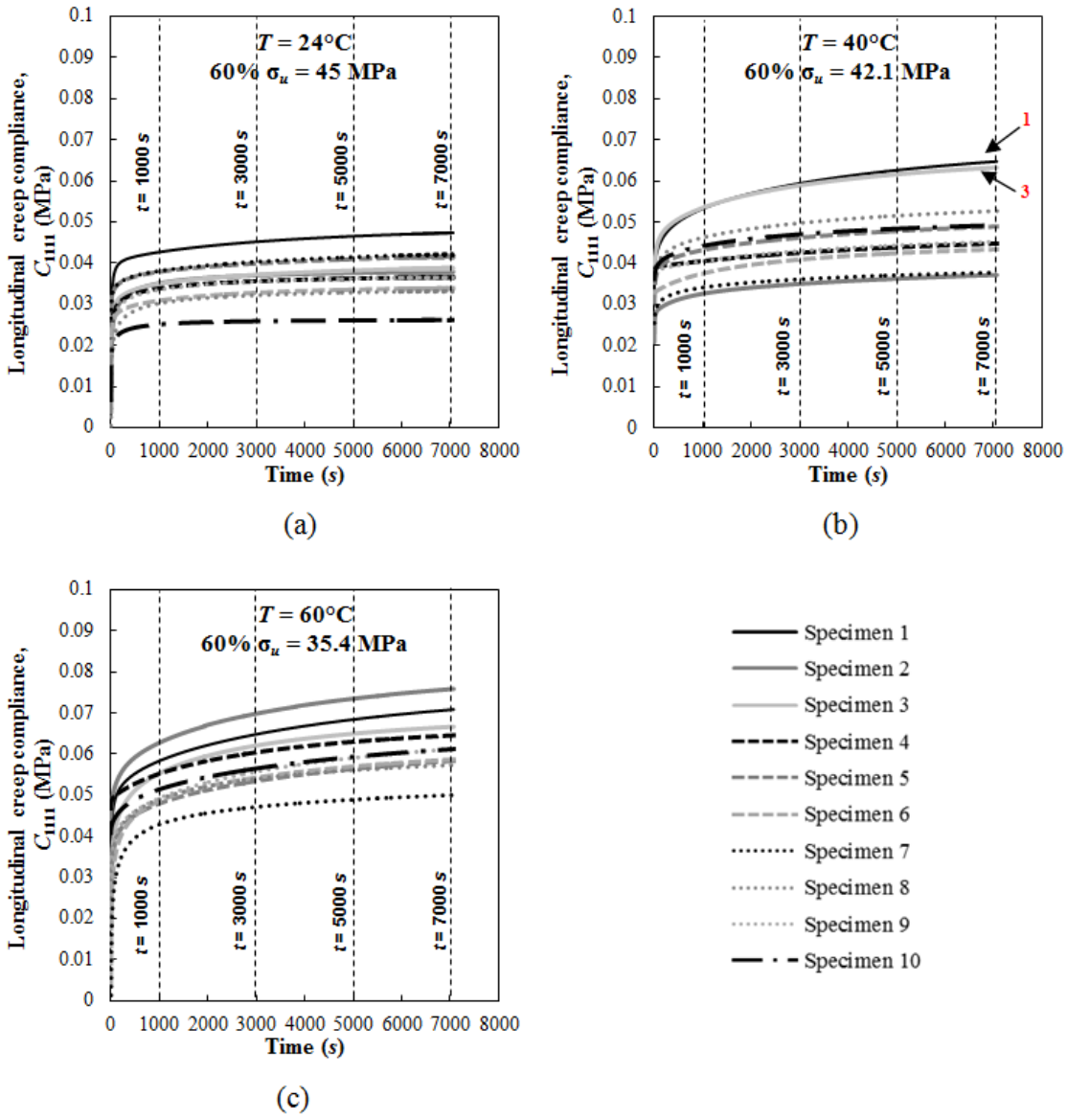

Figure 5.3 Longitudinal creep compliances $C_{1111}(t)$ of cured Derakane 441-400 at 60% $\sigma_{u,}$ at T = (a) 24°C, (b) 40°C, and (c) 60°C.

5.3.2 Time and Temperature Dependency of the Weibull and Log-normal Distribution Parameters of Cured Derakane 441-400

The Weibull shape (γ) and scale (β) parameters and the log-normal location (λ) and scale (ζ) parameters of cured Derakane 441-400 creep compliances are listed in

Table 5.2. Following the determination of the distribution parameters, the PDFs were obtained for the Weibull and log-normal distributions. The histograms of the creep compliances C_{1111} with the Weibull and log-normal PDFs for selected times at 24°C, 40°C, and 60°C are shown in Figs 5.4-5.6, respectively.

The magnitude of the distribution parameters give insight regarding the time and temperature dependency of their PDFs. Typically, the Weibull shape parameter (γ) is between 0.5 and 15 and governs the "shape" of the distribution. For example, a symmetric bell-shaped curve (similar to a Gaussian distribution) is obtained for $3 < \gamma < 4$ and the Weibull PDF curve becomes increasingly asymmetric for $\gamma > 5$ [74]. As seen in Table 5.2, the Weibull shape parameter values obtained in this study are $7 < \gamma < 10$ for all selected times, which indicates asymmetry in the Weibull PDF curves, i.e., the curves are skewed to the right. The right-skewed PDF curves indicate that the mean of the compliance data is higher than its median. For greater times, the Weibull shape parameter (γ) decreased, indicating that the C_{1111} data become slightly more symmetric. As stated previously, the Weibull scale parameter (β) generally represents the 63.2 percentile of the data [74]. For example, Table 5.2 shows the Weibull scale parameter $\beta = 0.00363$ at 1000 *s* at 24°C, 45 MPa (60% σ_u). This implies that 63.2% of the C_{1111} data has values below 0.0363 (MPa^{-1}) at 1000 *s*. Additionally, the Weibull scale parameter β increased for longer times, indicating the increasing values of the longitudinal creep compliance C_{1111}.

The location parameter (λ) of the log-normal distribution represents the mean of the log transformed observed data. The higher mean values of C_{1111} were observed for increasing times as seen in Fig. 5.4. Hence, the log-normal location parameter (λ) is also

expected to increase as time increases. The log-normal scale parameter (ζ) represents the standard deviation of the logarithm of majority of the data points. The standard deviation describes the variation or dispersion of the data points from the mean value. A low standard deviation indicates that the data points are very close to the mean, whereas a high standard deviation indicates that the data points are spread out over a large range of values [52]. In this study, as time increases, there is a larger variation (larger dispersion) of C_{1111} for longer times, which implies that the log-normal scale parameter (ζ) tends to slightly increase.

The Weibull and log-normal parameters were also found to be temperature-dependent. For higher temperatures, the Weibull PDF curve becomes more asymmetric (skewed to the right), which causes the increased shape parameter (γ). The larger creep compliance magnitudes lead to the increasing Weibull scale parameter (β). For the log-normal distribution, the increasing mean values of C_{1111} imply that the magnitude of the location parameter (λ) becomes larger for greater temperatures. Additionally, a reduced variation of the C_{1111} indicates the smaller scale parameter (β) for higher temperatures. As seen in Figs. 5.4-5.6, both Weibull and log-normal PDFs fit the creep compliances C_{1111} reasonably well at all times. A similar procedure was followed for the statistical characterization of the creep compliances obtained for creep tests conducted at 70% σ_u. These results can be found in Appendix B. Overall, both the Weibull and log-normal PDFs fit the creep compliances C_{1111} well at all selected times.

Table 5.2 Weibull and log-normal parameters of longitudinal creep compliances C_{1111} of cured Derakane 441-400 obtained at 60% σ_u at T = 24°C, 40°C, 60°C at selected times.

Parameters	**Test configuration**	**Time (*s*)**			
		1000 *s*	**3000 *s***	**5000 *s***	**7000 *s***
Weibull shape parameter γ	24°C, 60% σ_u = 45 MPa	8.2841	8.1956	7.9097	7.7048
	40°C, 60% σ_u = 42.1 MPa	9.1006	8.8757	8.7863	8.7634
	60°C, 60% σ_u = 35.4 MPa	9.8095	9.6958	9.5214	9.3804
Weibull scale parameter β	24°C, 60% σ_u = 45 MPa	0.0363	0.0383	0.0392	0.0398
	40°C, 60% σ_u = 42.1 MPa	0.0456	0.0496	0.0513	0.0525
	60°C, 60% σ_u = 35.4 MPa	0.0547	0.0607	0.0637	0.0656
Log-normal location parameter λ	24°C, 60% σ_u = 45 MPa	-3.3833	-3.3294	-3.3078	-3.2957
	40°C, 60% σ_u = 42.1 MPa	-3.2275	-3.1622	-3.1298	-3.1098
	60°C, 60% σ_u = 35.4 MPa	-2.9596	-2.8555	-2.8079	-2.7795
Log-normal scale parameter ζ	24°C, 60% σ_u = 45 MPa	0.1466	0.1516	0.1574	0.1617
	40°C, 60% σ_u = 42.1 MPa	0.1240	0.1241	0.1245	0.1243
	60°C, 60% σ_u = 35.4 MPa	0.1108	0.1125	0.1154	0.1176

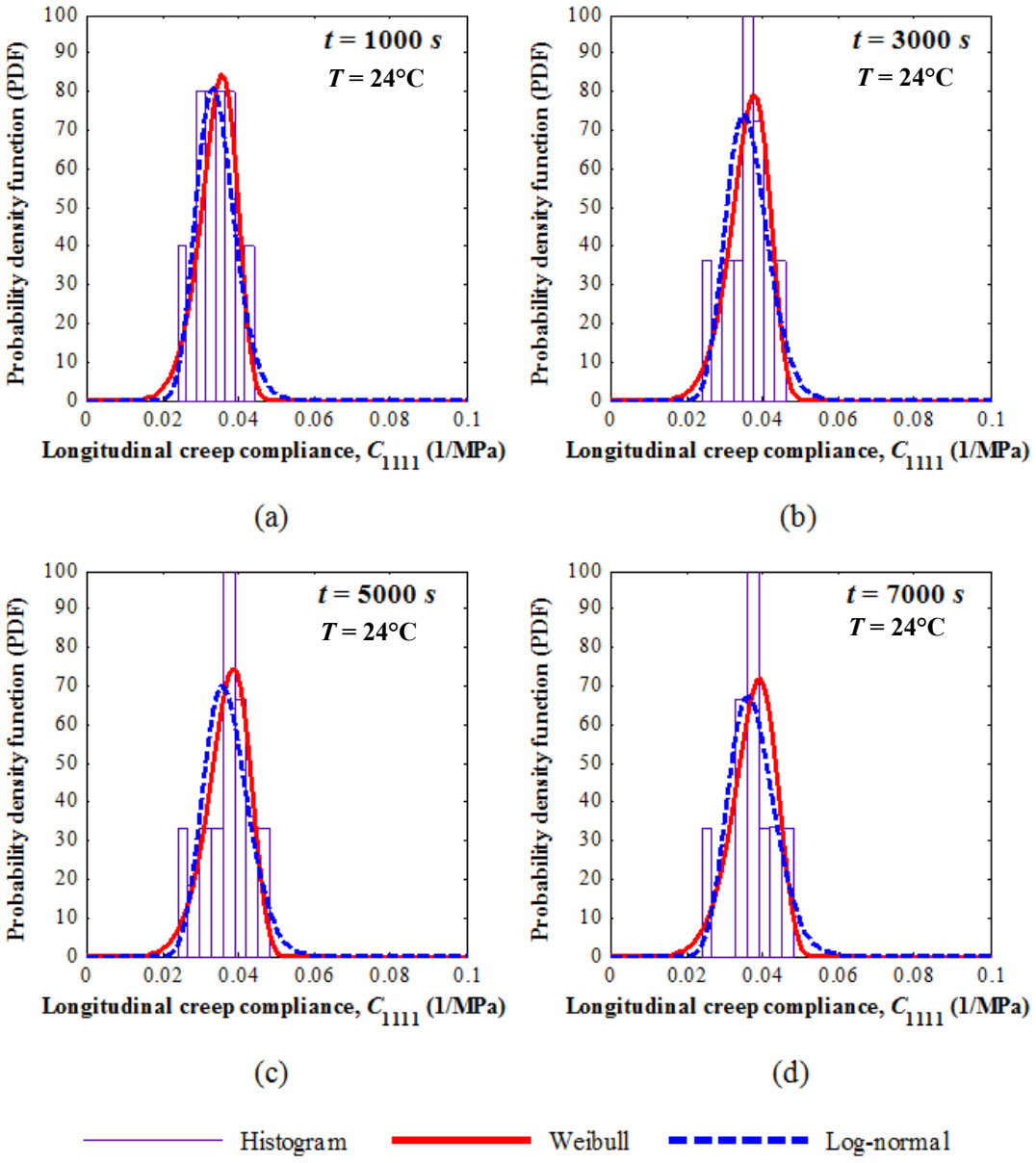

Figure 5.4 The longitudinal creep compliance C_{1111} histograms of cured Derakane 441-400 and the corresponding Weibull and log-normal probability density functions at 24°C, 45 MPa (60% σ_u) at t = (a) 1000 s, (b) 3000 s, (c) 5000 s, and (d) 7000 s.

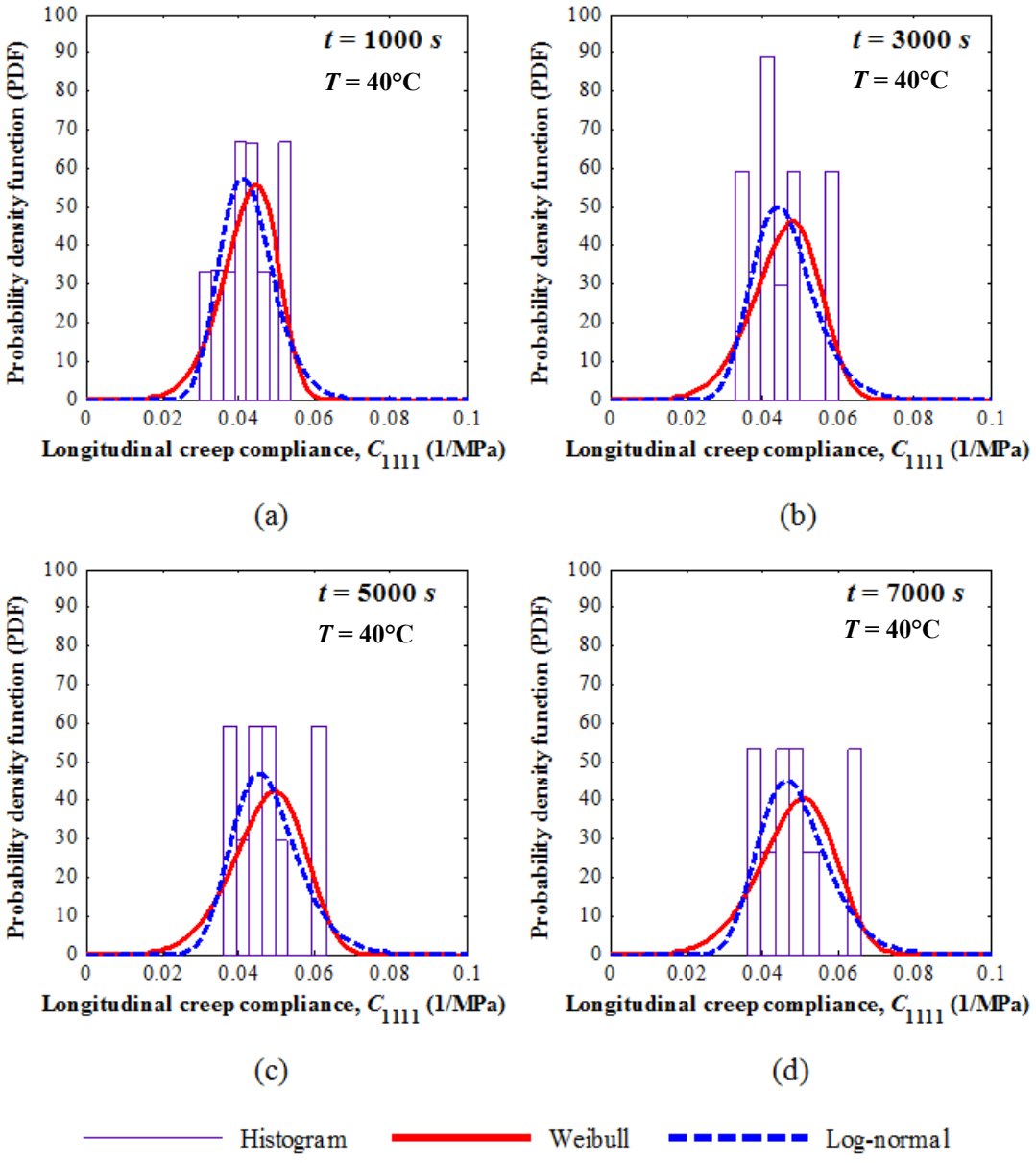

Figure 5.5 The longitudinal creep compliance C_{1111} histograms of cured Derakane 441-400 and the corresponding Weibull and log-normal probability density functions at 40°C, 42.1 MPa (60% σ_u) at t = (a) 1000 *s*, (b) 3000 *s*, (c) 5000 *s*, and (d) 7000 *s*.

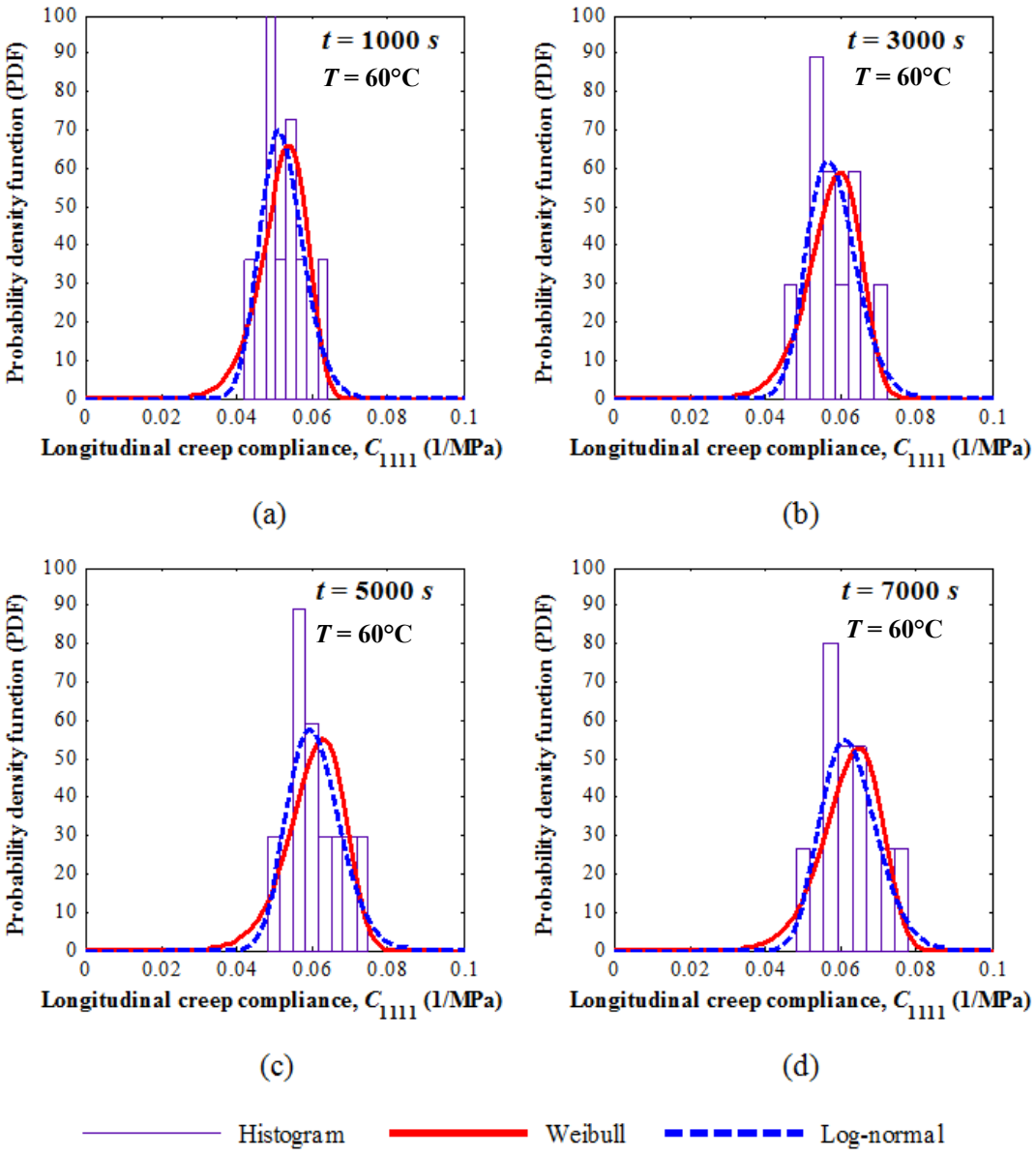

Figure 5.6 The longitudinal creep compliance C_{1111} histograms of cured Derakane 441-400 and the corresponding Weibull and log-normal probability density functions at 60°C, 35.4 MPa (60% σ_u) at t = (a) 1000 *s*, (b) 3000 *s*, (c) 5000 *s*, and (d) 7000 *s*.

The longitudinal creep compliance values of cured Derakane 441-400 for 60°C, 35.4 MPa (60% σ_u) at selected times were used to obtain the Weibull PDFs. Figure. 5.7a

shows the longitudinal creep compliance C_{1111} of cured Derakane 441-400 at 60°C, 35.4 MPa (60% σ_u) at 5 *s*, 500 *s*, 3000 *s* and 7000 *s*. The corresponding Weibull PDFs at selected times are illustrated in Fig. 5.7b. The probability distributions of the creep compliances are found to be highly time-dependent, with the peak of the PDF shifting toward the right, indicating the increasing magnitude of the creep compliances for increasing times.

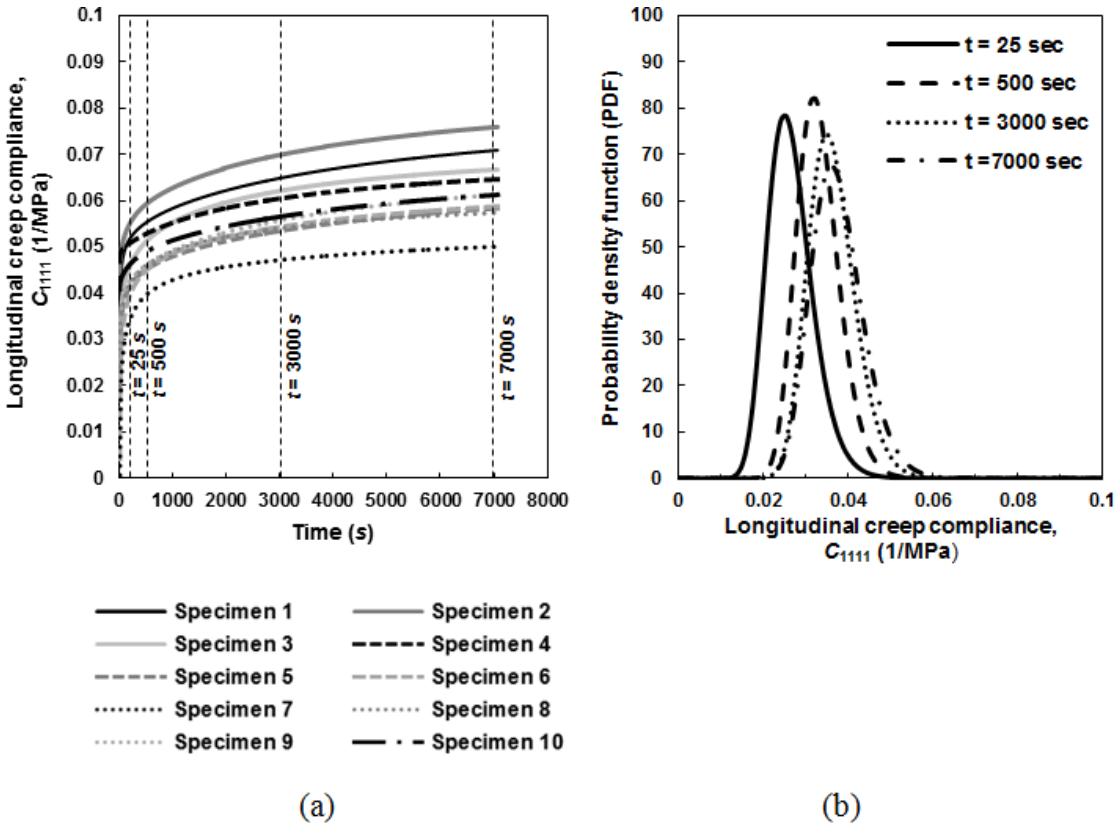

Figure 5.7 (a) Longitudinal creep compliance C_{1111} of cured Derakane 441-400 at 60°C, 35.4 MPa (60% σ_u)and (b) the corresponding Weibull PDFs at selected times.

The Weilbull PDFs and CDFs of cured Derakane 441-400 creep compliances were obtained at a single time for all temperatures (24°C, 40°C, and 60°C). The Weibull

PDFs and CDFs curves of longitudinal creep compliances at 60% σ_u and t = 3000 s are shown in Figs. 5.8a and 5.8b. As seen, both PDFs and CDFs are temperature dependent. The PDFs curve shifts toward the right and its peak decreases for increasing temperature. The decreasing magnitude of the PDF peak indicates that there is a greater variation of creep compliances for higher temperatures. The CDF curves for the three temperatures (24°C, 40°C, and 60°C) were found to have similar shapes and they also shift toward the right with increasing temperature. A similar trend of the PDF and CDF curves of the creep compliances for all times was observed.

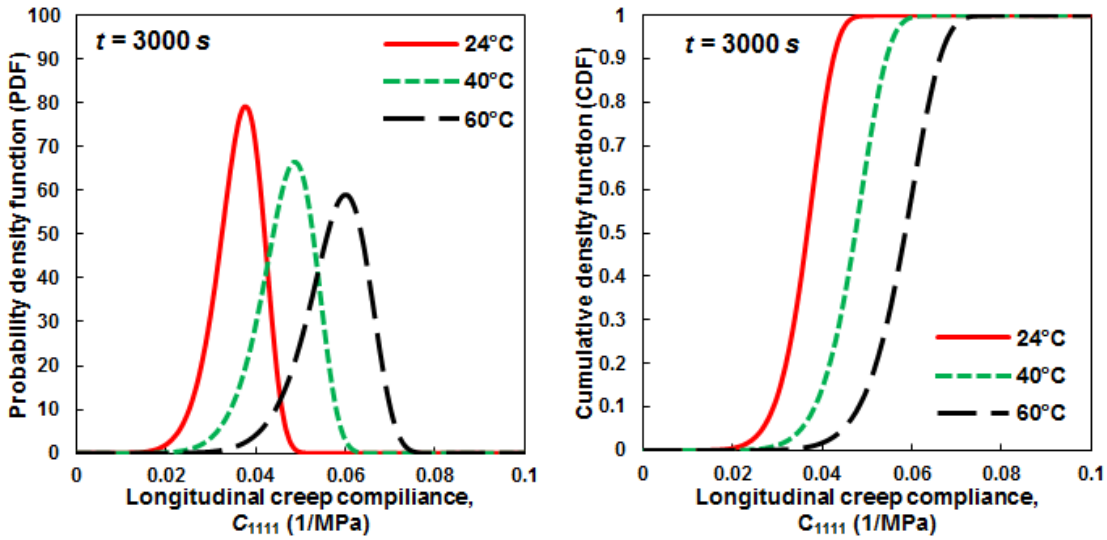

Figure 5.8 Weibull (a) PDFs and (b) CDFs of the longitudinal creep compliances C_{1111} of cured Derakane 441-400 at 60% σ_u and t = 3000 s.

Figure 5.9 shows the variation in the Weibull scale (β) and shape (γ) parameters of cured Derakane 441-400 longitudinal creep compliances C_{1111} at 60% σ_u and at 24°C,

40°C, and 60°C. The scale parameter (β) increases and the shape parameter (γ) decreases for increasing times and temperatures. The increasing scale parameter (β) indicates a wider distribution of compliance values and a decreasing peak value of the PDF. The decreasing shape parameter (γ) (Fig. 5.8a) is indicative of larger compliance values for increasing temperatures. Therefore, the PDF becomes more asymmetric with the peak shifting toward the right.

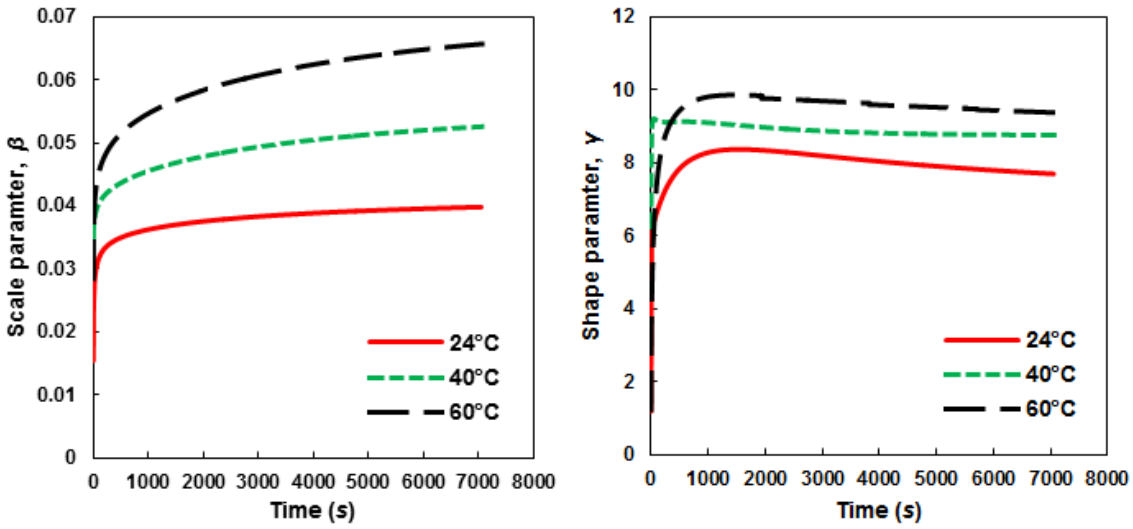

(a) (b)

Figure 5.9 Weibull distribution parameters, (a) β and (b) γ, of the longitudinal creep compliance C_{1111} of cured Derakane 441-400 at 60% σ_u.

5.3.3 Goodness-of-Fit Tests

In this study, the K-S hypothesis test was adopted to evaluate the goodness-of-fit of the Weibull and log-normal distribution models for creep compliances of cured

Derakane 441-400. The basic premise of the K-S test is to measure the maximum deviation D_{N_0} (in absolute value) between the theoretical cumulative distribution function *F(x)* and the experimental cumulative distribution function $F_{N_0}(x)$ at the same observation point. The maximum deviation D_{N_0} is given by [76]

$$D_{N_0} = \max \left| F_{N_0}(x) - F(x) \right| \tag{5.10}$$

If the maximum discrepancy D_{N_0} obtained from Eq. (5.10) is less than the normally expected value (critical value) $D_{N_0}^{\varsigma}$ for a given sample size at the prescribed significance level, the theoretical distribution is considered to be acceptable. Otherwise, it is rejected. The critical value $D_{N_0}^{\varsigma}$ is defined for a given sample size and significance level as [76]

$$P(D_{N_0} \le D_{N_0}^{\varsigma}) = 1 - \varsigma \tag{5.11}$$

where ζ is the significance level and typically taken to be 5% (ζ = 0.05). In this study, the critical value $D_{N_0}^{\varsigma}$ with 5% significance level (ζ = 0.05) for the sample size of ten (N_0 = 10) was determined to be 0.41.

The K-S test was performed to evaluate the maximum discrepancy D_{N_0} for the Weibull and log-normal distributions of creep compliances for all test configurations. The D_{N_0} values at selected times (1000 *s*, 2000 *s*, ..., 7000 *s*) for the 60% σ_u creep tests of cured Derakane 441-400 at 24°C, 40°C, 60°C are presented in Tables 5.3-5.5, respectively. Both Weibull and log-normal distributions are acceptable models for the 5% significance level because the maximum discrepancy D_{N_0} for all data shown in

Tables 5.3-5.5 is less than 0.41. The distribution with the lowest D_{N_0} values (shaded in Tables 5.3-5.5) indicates that the two-parameter Weibull distribution provides the best-fitted distribution at all selected times, except for the values at 1000 *s* at 40°C, 60% σ_u. The K-S test results for other test configurations can be found in Appendix C. Based on the results of the goodness-of-fit tests for all test configurations, the Weibull distribution was found to be the better distribution for creep compliances of cured Derakane 441-400 when compared to the log-normal distribution. Therefore, the Weibull distribution was selected for the creep compliance statistical analysis in this study.

Table 5.3 The maximum discrepancy D_{N_0} of the K-S tests for Weibull and log-normal distributions of longitudinal creep compliances C_{1111} of cured Derakane 441-400 at 24°C, 45 MPa (60% σ_u).

Time	Maximum Discrepancy, D_{N_0}	
	Weibull	Log-normal
1000 *s*	0.1615	0.1690
2000 *s*	0.1579	0.1791
3000 *s*	0.1560	0.1804
4000 *s*	0.1498	0.1786
5000 *s*	0.1442	0.1755
6000 *s*	0.1391	0.1717
7000 *s*	0.1346	0.1678

Table 5.4 The maximum discrepancy D_{N_0} of the K-S tests for Weibull and log-normal distributions of longitudinal creep compliances C_{1111} of cured Derakane 441-400 at 40°C, 42.1 MPa (60% σ_u).

Time	Maximum Discrepancy, D_{N_0}	
	Weibull	Log-normal
1000 *s*	0.1970	0.1467
2000 *s*	0.1582	0.1600
3000 *s*	0.1483	0.1724
4000 *s*	0.1551	0.1818
5000 *s*	0.1597	0.1893
6000 *s*	0.1613	0.1955
7000 *s*	0.1614	0.2005

Table 5.5 The maximum discrepancy D_{N_0} of the K-S tests for Weibull and log-normal distributions of longitudinal creep compliances C_{1111} of cured Derakane 441-400 at 60°C, 35.4 MPa (60% σ_u).

Time	**Maximum Discrepancy, D_{N_0}**	
	Weibull	**Log-normal**
1000 *s*	0.1733	0.1947
2000 *s*	0.1570	0.2012
3000 *s*	0.1616	0.2058
4000 *s*	0.1695	0.2046
5000 *s*	0.1656	0.2018
6000 *s*	0.1569	0.1987
7000 *s*	0.1496	0.1946

CHAPTER VI

PREDICTION OF CREEP COMPLIANCES OF A VINYL ESTER POLYMER (DERAKANE 441-400)

6.1 Prediction of Time and Temperature Dependent Creep Compliances

As noted in Chapter 5, the steady increase in the experimental creep strain and subsequently in the creep compliances was reflected in the creep compliances' PDFs and CDFs (Fig. 5.7) for increasing temperatures, particularly in the secondary or steady-state creep phase. Therefore, a procedure to determine the PDFs for the complete test temperature range ($24°C \leq T \leq 60°C$) during steady state creep ($t \geq 1000\ s$) was formulated.

In order to predict the PDFs of the creep compliance functions for any temperature in the range $24°C \leq T \leq 60°C$ and any time during steady state ($t \geq 1000\ s$), the Weibull shape (γ) and scale (β) parameters were expressed as functions of time and temperature. These functions were obtained using two-dimensional quadratic Lagrange interpolation functions consistent with those for an eight-node serendipity finite element [78]. The interpolation points at 24°C, 40°C, and 60°C and at three times (1000 *s*, 4000 *s*, 7000 *s*) are shown in Fig. 6.1. The center points β_C and γ_C were used for validation of the resulting PDF at 40°C and 4000 *s*.

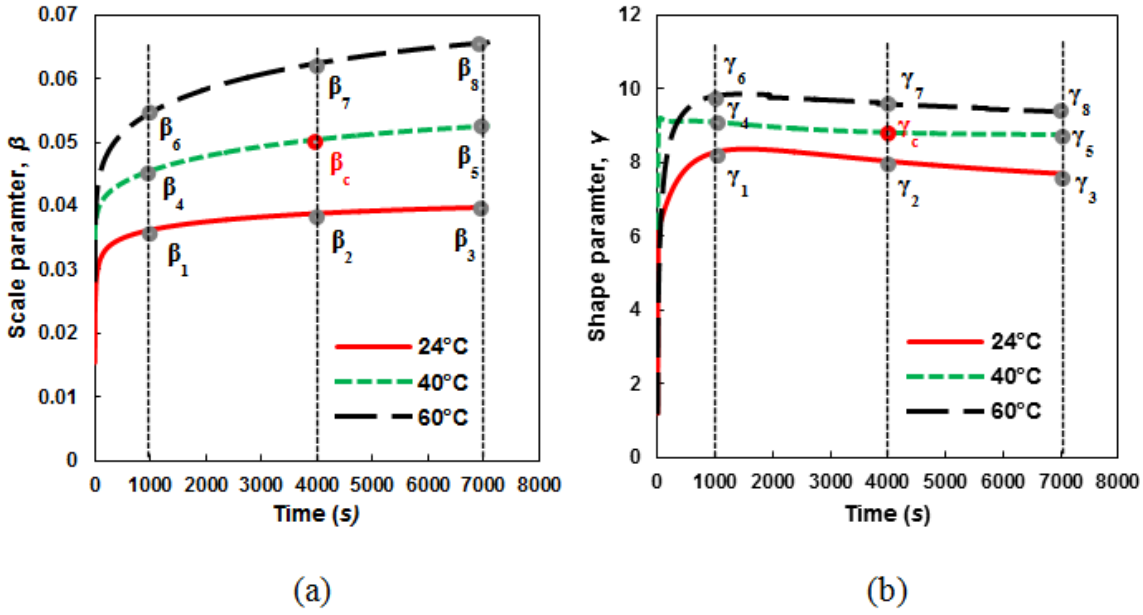

(a) (b)

Figure 6.1 Weibull distribution parameters, (a) scale β and (b) shape γ, of C_{1111} of cured Derakane 441-400 at 60% σ_u.

Consistent with a quadratic serendipity element, the two dimensional interpolation functions $\psi_1(t, T), \ldots, \psi_8(t, T)$ correspond to the interpolation points 1-8, respectively. They can be expressed as [78]

$$
\begin{aligned}
\psi_1(t,T) &= \frac{1}{4}(1-\omega)(1-\eta)(-1-\omega-\eta) \\
\psi_2(t,T) &= \frac{1}{2}(1-\omega^2)(1-\eta) \\
\psi_3(t,T) &= \frac{1}{4}(1+\omega)(1-\eta)(-1+\omega-\eta) \\
\psi_4(t,T) &= \frac{1}{2}(1-\omega)(1-\eta^2) \\
\psi_5(t,T) &= \frac{1}{2}(1+\omega)(1-\eta^2) \\
\psi_6(t,T) &= \frac{1}{4}(1-\omega)(1+\eta)(-1-\omega+\eta) \\
\psi_7(t,T) &= \frac{1}{2}(1-\omega^2)(1+\eta) \\
\psi_8(t,T) &= \frac{1}{4}(1+\omega)(1+\eta)(-1+\omega+\eta)
\end{aligned}
\tag{6.1}
$$

where $\omega(t)$ and $\eta(T)$ are expressed as

$$
\begin{aligned}
\omega(t) &= \frac{2(t-t^1)-(t^3-t^1)}{(t^3-t^1)} \\
\eta(T) &= \frac{2(T-T^1)-(T^3-T^1)}{(T^3-T^1)}
\end{aligned}
\tag{6.2}
$$

In this study, the times t^1 =1000 s , t^2 = 4000 s, and t^3 =7000 s ,whereas the temperatures T^1 = 24°C, T^2 = 40°C, and T^3 = 60°C. The time and temperature-dependent Weibull distribution parameters for the time range of 1000 $s \leq t \leq$ 7000 s and temperature range of 24°C ≤ T ≤ 60°C were characterized by the quadratic interpolation functions $\psi_i(t,T)$ as

$$
\begin{aligned}
\beta(t,T) &= \sum_{i=1}^{8} \beta_i \psi_i(t,T) \\
\gamma(t,T) &= \sum_{i=1}^{8} \gamma_i \psi_i(t,T)
\end{aligned}
\tag{6.3}
$$

The Weibull parameters, obtained from Eq. (6.3), were used to develop the creep compliance PDFs and CDFs. The approximations for the Weibull shape (γ) and scale (β) parameters, which are expressed in terms of the interpolation functions (Eq. (6.3)) are verified by comparison with the PDF and CDF obtained from the experimental data. As an example, Fig. 6.2 shows the distribution functions of the longitudinal creep compliance C_{1111} at $t = 3000\ s$ for all three temperatures (24°C, 40°C,60°C) at 60% σ_u. The predicted PDFs and CDFs obtained from using the interpolation functions agree well with the PDFs and CDFs obtained from the experimental data at all temperatures as shown. The PDFs and CDFs were formulated from the interpolation functions for all temperatures in the temperature design space $24°C \leq T \leq 60°C$ for steady state creep ($1000\ s \leq t \leq 7000\ s$).

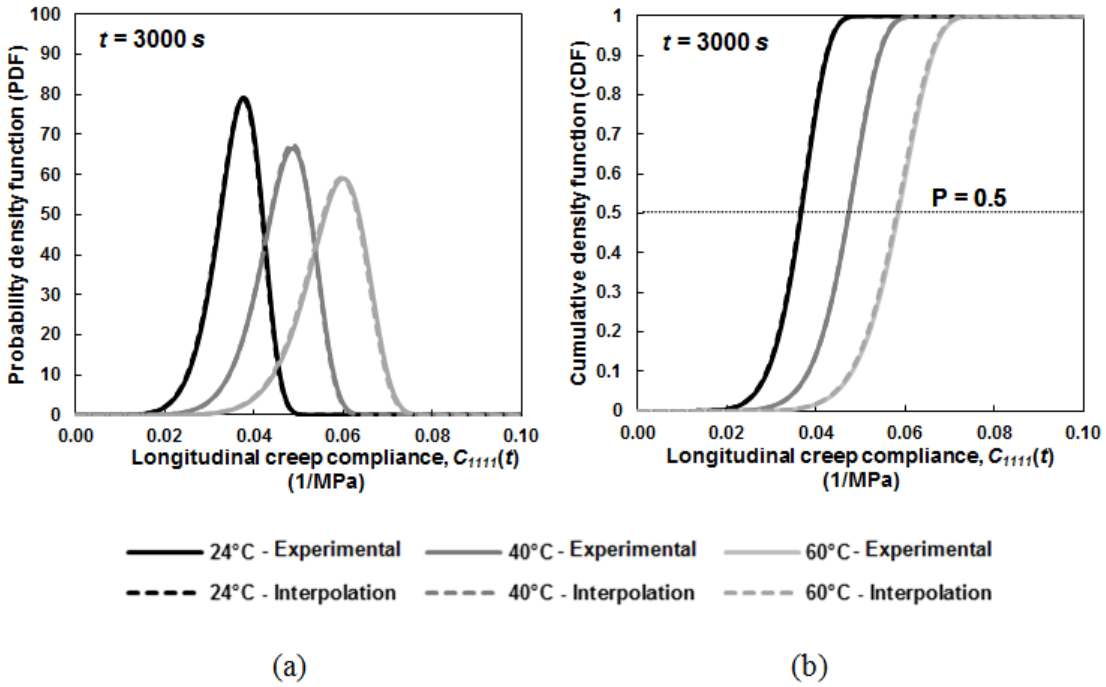

Figure 6.2 Comparison between the experimental and predicted (a) PDFs and (b) CDFs of C_{1111} of cured Derakane 441-400 at 60% σ_u and t = 3000 *s*.

6.2 Creep Compliance Curves at Constant Cumulative Distribution Function Values

The time-dependent creep compliance can be obtained for steady state creep for all temperatures in the design space for constant CDF values. For example, Fig. 6.3 shows a three-dimensional plot of the time- and temperature-dependent creep compliances for 0.5 CDF. This corresponds to the mean of the creep compliance data. The figure clearly shows that the creep compliance increases for increasing time and temperature at a constant applied stress. The creep compliances for 0.5 CDF can be obtained using this model for any temperature and time within the design space.

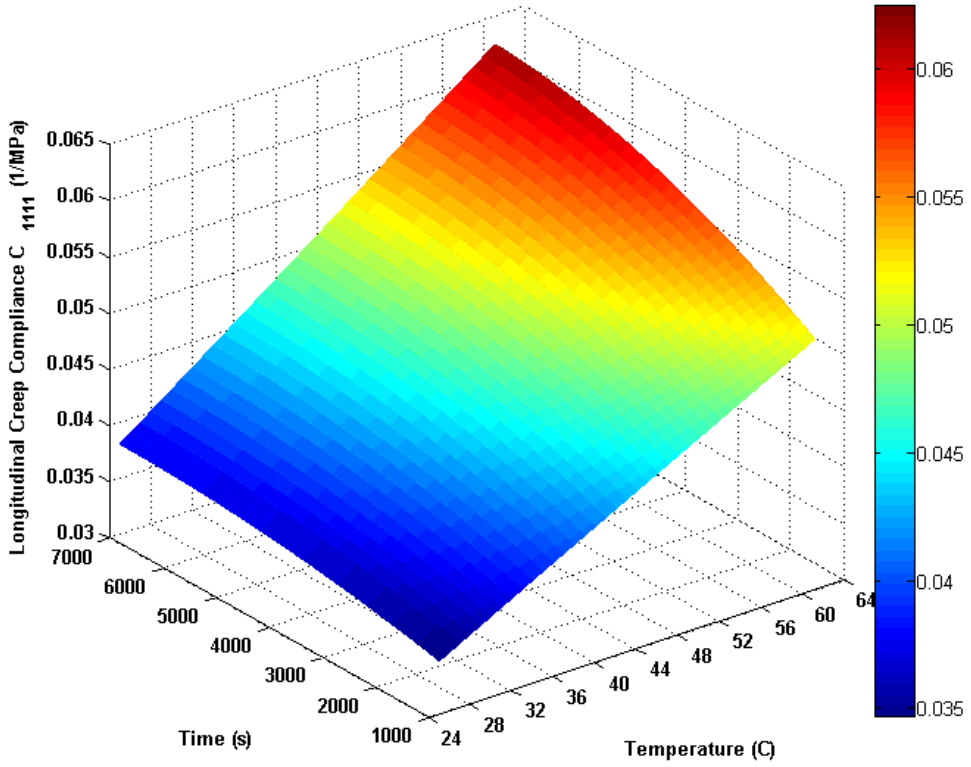

Figure 6.3 Three-dimensional plot of the predicted creep compliance C_{1111} of cured Derakane 441-400 at 60% σ_u at CDF = 0.5 as a function of time and temperature.

Figure 6.4 shows the comparison of the predicted longitudinal creep compliance of cured Derakane 441-400 at constant probabilities with the creep compliance obtained from the measured data. These plots show the creep compliances at 60% σ_u at T = 24°C (Fig. 6.4a), 40°C (Fig. 6.4b), and 60°C (Fig. 6.4c). In Fig. 6.4a, the longitudinal creep compliances obtained from CDF = 0.05 and 0.95 are compared with the longitudinal creep compliances for specimens #1 and #10, respectively. The creep compliances for specimens #1 and #10 correspond to the highest and lowest creep compliance curves at 60% σ_u at T = 24°C , respectively. The longitudinal creep compliances obtained from CDF = 0.5 are compared to the mean of the experimental data. Additionally, the 95%

confidence interval of the mean data for each temperature is shown. As seen in Fig. 6.4a, the lowest experimentally obtained creep compliance is within the 5% of the probability curve (CDF = 0.05), whereas those for CDF = 0.5 agree well with the mean of experimentally obtained longitudinal creep compliance data. However, the 95% probability curve (CDF = 0.95) slightly under-predicts the highest experimental creep compliance curve. Figure 6.4b contains the plots of the predicted creep compliance functions and the experimentally obtained lowest (specimen #7), mean, and highest (specimen #2) creep compliances at 60% σ_u at $T = 40°C$. The predicted creep compliances obtained from CDF = 0.05 agree well with the magnitudes of the lowest experimental data. The compliance predictions from the 0.5 and 0.95 CDFs satisfactorily represent the longitudinal creep compliance data at the earlier stage of steady state creep, but the difference between the prediction and the experimentally derived compliance values increases with increasing time after approximately 1500 *s*. This may be attributed to the small data set (8 specimens) used for the 40°C creep compliance curve. Figure 6.4c shows the comparison of the predicted creep compliance functions and the experimentally obtained lowest (specimen #2), mean, and highest (specimen #7) creep compliances at 60% σ_u at $T = 60°C$. The predicted compliance curves at 60°C capture the range of the experimental lowest and mean data fairly well but slightly under predict the experimentally obtained highest curve. Additionally, predictions of the creep compliances at 70% σ_u for the complete design temperature range ($24°C \leq T \leq 60°C$) during steady state creep ($1000\ s \leq t \leq 7000\ s$) were also obtained. The comparison of the predicted creep compliance at 70% σ_u at constant probabilities with the creep compliance obtained from the measured data for 24°C, 40°C and 60°C are presented in Appendix D.

Overall, the predicted compliance curves capture the experimental data fairly well for all three test temperatures (24°C, 40°C, and 60°C).

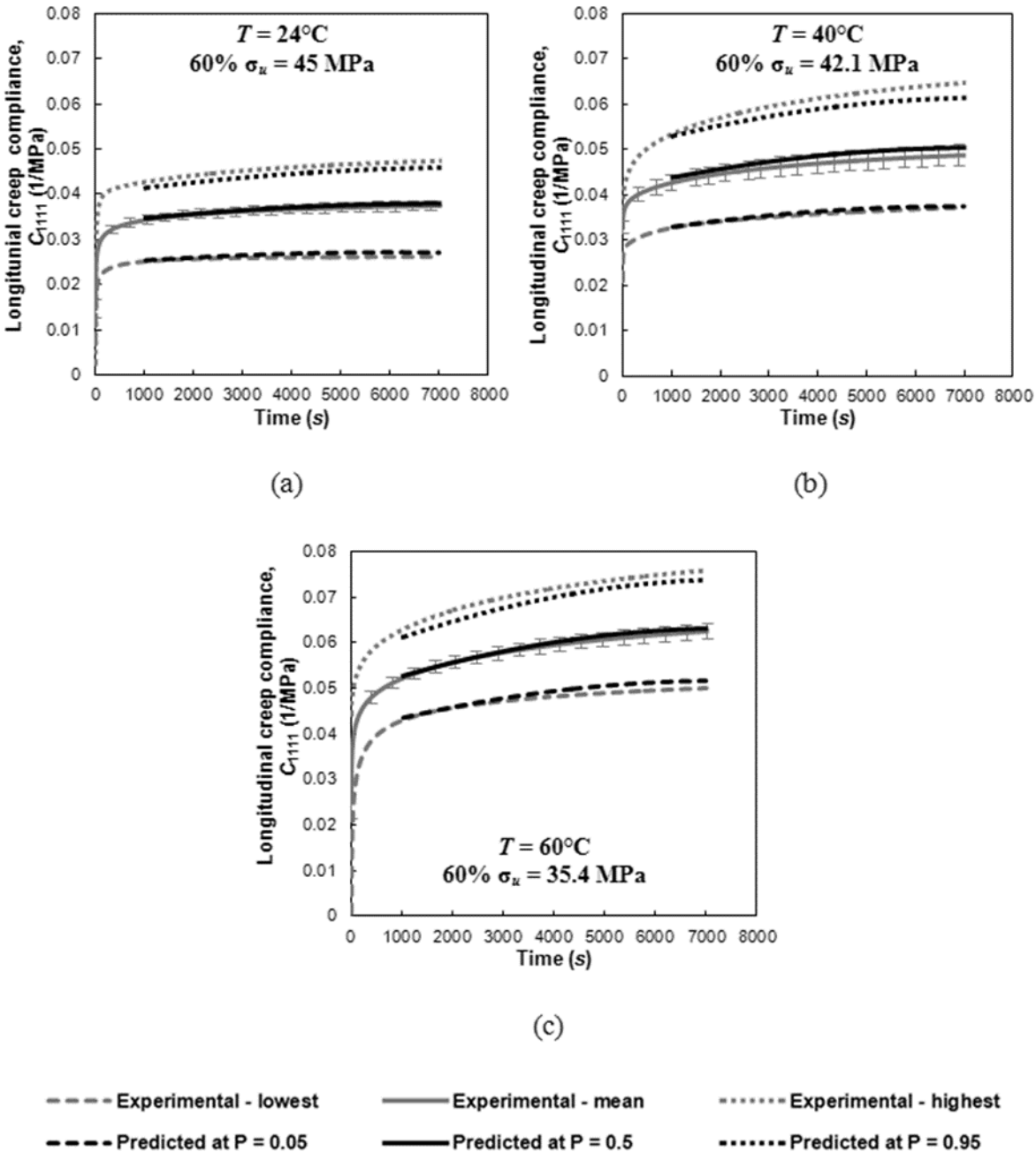

Figure 6.4 Predicted creep compliance functions at CDF = 0.05, 0.5, 0.95, and the experimentally obtained lowest, mean, and highest creep compliances C_{1111} of cured Derakane 441-400 at 60% σ_u at T = (a) 24°C, (b) 40°C, and (c) 60°C.

6.3 Viscoelastic Constitutive Relations with Material Property Variations

Ultimately, the aim of this research is to perform accurate stress-strain analysis of polymer matrix composite (PMC) structures. This requires an appropriate constitutive model that accurately captures the variability of the matrix material properties.

The variation in material properties can be represented by including the PDFs of the creep compliances in the constitutive law. Recalling Eqs. (2.6), the constitutive relation for an isotropic, homogeneous linearly viscoelastic material subjected to one-dimensional tensile creep tests can be expressed as

$$\varepsilon_{\underline{ii}}(t) = \int_0^t C_{11\underline{ii}}(t-\xi)\frac{d\sigma_{11}(\xi)}{d\xi}d\xi \tag{6.4}$$

The creep compliance $C_{11\underline{ii}}(t)$ in Eq. (6.4) can be represented by a Prony series (as discussed in Chapter 2) as

$$C_{11\underline{ii}}(t) = C^0_{11\underline{ii}} + \sum_{n=1}^{N_{pr}} C^n_{11\underline{ii}}\left[1-\exp\left(-\frac{t}{\tau_n}\right)\right] \tag{6.5}$$

The creep compliance distributions are time-dependent; therefore, their two-parameter Weibull PDFs (Eq. (5.1)) can be expressed as

$$f(t,Y) = \frac{\gamma(t)}{\beta(t)}\left(\frac{Y}{\beta(t)}\right)^{\gamma(t)-1}\exp\left[-\left(\frac{Y}{\beta(t)}\right)^{\gamma(t)}\right] \tag{6.6}$$

where Y is a non-dimensionalized creep compliance. In Eq. (6.6), β and γ are the time-dependent Weibull shape and scale parameters, respectively. These parameters can be obtained using the protocol described in Chapter 5.

Hilton et al. [19] developed a mathematical approach to obtain the stochastic stress and strain solutions for specific quasi-static problems such as beam flexure and

pressurized hollow cylinders. The material in these problems was assumed to be an isotropic, homogeneous linearly viscoelastic material. However, in [19], time-independent distribution parameters of the creep compliance PDFs were used as multipliers of the convolution integral in Eq. 6.4. Following this approach, one way to introduce the PDFs of the creep compliances into the viscoelastic constitutive relation is to multiply some form of the deterministic creep compliances $C_{11\underline{ii}}(t)$ by the PDFs of the non-dimensionalized creep compliances $f(t, Y)$. As a result, the probabilistic creep compliances $\tilde{C}_{11\underline{ii}}[t;Y]$ can be expressed as

$$\tilde{C}_{11\underline{ii}}[t;Y] = f(t,Y)C_{11\underline{ii}}(t) \tag{6.7}$$

where $f(Y,t)$ and $C_{11\underline{ii}}(t)$ are obtained by using Eqs. (6.6) and (6.5), respectively. As a result, Eq. (6.7) can be written as

$$\underbrace{\tilde{C}_{11\underline{ii}}[t;Y]}_{\substack{\textit{probabilistic}\\ \textit{creep}\\ \textit{compliances}}} = \underbrace{f(t,Y)}_{\substack{\textit{creep}\\ \textit{compliance}\\ \textit{PDF}}} \underbrace{\left\{ C^0_{11\underline{ii}} + \sum_{n=1}^{N_{pr}} C^n_{11\underline{ii}} \left[1 - \exp\left(-\frac{t}{\tau_n} \right) \right] \right\}}_{\substack{\textit{deterministic}\\ \textit{creep}\\ \textit{compliances}}} \tag{6.8}$$

Consequently, the constitutive stress-strain relation for an isothermal isotropic linear viscoelastic material (Eq. (6.4)) with variations in the creep compliance functions can be expressed as

$$\tilde{\varepsilon}_{\underline{ii}}[t;Y] = \int_0^t \tilde{C}_{11\underline{ii}}[(t-\xi);Y] \frac{d\tilde{\sigma}_{11}[\xi, Y(\xi)]}{d\xi} d\xi \tag{6.9}$$

where $\tilde{\varepsilon}_{\underline{ii}}[t;Y]$ and $\tilde{\sigma}_{11}[t;Y]$ are the probabilistic strain versus time responses and stresses, respectively. The mathematical techniques such as the Laplace or Fourier transforms can

no longer be used as Eq. (6.9) becomes a non-convolution type integral equation. Therefore, other numerical approaches must be considered when solving for the probabilistic stresses or strains.

CHAPTER VII

CONCLUSIONS AND RECOMMENDATIONS

The present research effort focused on developing a method to predict the creep compliances of a vinyl ester (VE) polymer (Derakane 441-400) with variation in its material properties under isothermal mechanical loading. The analytical and experimental framework to include the stochastic nature of viscoelastic material functions of a polymer matrix has been presented.

A two-parameter Weibull function was used to develop the probability density functions (PDFs) of the creep compliances of cured Derakane 441-400. The Weibull shape (γ) and scale (β) parameters were found to be strongly time- and temperature-dependent; therefore, it was concluded that a single probability distribution to effectively represent the creep compliances for all times was not acceptable. Despite the time and temperature dependency of the Weibull parameters, they were found to be well behaved during steady state ($t \geq 1000\ s$). Therefore, two-dimensional quadratic Lagrange interpolation functions were used to develop creep compliance predictions as functions of time ($t \geq 1000\ s$) and temperature ($24°C \leq T \leq 60°C$). For constant cumulative distribution function (CDF) values, the time-dependent creep compliance predictions were obtained for steady state creep for all temperatures in the design space and compared to the experimental data. It was shown that the predicted compliance curves capture the experimental data fairly well for all three test temperatures (24°C,

40°C, and 60°C). Overall, the method described in this study can be used to obtain creep compliances for any constant probability in the complete design temperature range for steady state creep.

To optimize the procedure for obtaining the best PDF for each time, an algorithm can be developed which identifies the best-fit probability distribution from the goodness-of-fit tests, then computes the corresponding parameters, and returns a value of the material function that includes the statistics for each time. This study presents a model that uses the time and temperature varying statistical parameters for obtaining the probabilistic range of values of the creep compliance of a VE polymer. It can also be extended to obtain master creep compliance curves [55], which can be used to describe long-term creep behavior. Creep compliances at any temperature within the design space ($24°C \leq T \leq 60°C$) can be obtained to construct a master creep compliance curve for selected CDF values. This significantly decreases the number of experimental tests that must be performed to obtain master creep compliance curves of cured Derakane 441-400 over a long time period.

The development of the predictive model establishes a general protocol that can be used to incorporate the variability in creep compliances of any isotropic, homogenous linearly viscoelastic material. Better predictions of creep compliances may be obtained with a larger data set. Furthermore, the creep compliance characterization model using a Prony series representation presented in this study can be applied to other isotropic, homogeneous linear viscoelastic materials.

Future work also includes investigation of mathematical and numerical techniques to obtain the stochastic viscoelastic stress and strain solutions for a VE polymer. As

discussed in Section 6.2, the constitutive viscoelastic relation that includes the PDFs of creep compliances is a non-convolution type integral equation; therefore, the integral transforms (Laplace or Fourier transforms) can no longer be used. Mathematical and numerical techniques to include the variation in viscoelastic material properties should be investigated for the development of accurate viscoelastic stress-strain analysis. Ultimately, the stochastic viscoelastic stress-strain solutions of a VE polymer will be included in the constitutive model for VE matrix composite materials.

REFERENCES

[1] S. Thomas, K. Joseph, S. K. Malhotra, K. Goda, and M. S. Sreekala, *Polymer Composites, Macro- and Microcomposites* vol. 1. Weinheim: Wiley-VCH Verlag & Co., 2012.

[2] K. D. Naumenko and H. Altenbach, *Modeling of creep for structural analysis*. New York: Springer-Verlag, 2007.

[3] A. B. Strong, *High performace and engineering thermoplastic composites*. Lancaster: CRC Press, 1993.

[4] C. E. Beldica and H. H. Hilton, "Analytical and computational simulations of experimental determinations of deterministic and random linear viscoelastic constitutive relations," in *the proceedings of Twelfth International Conference on Composite Materials* Paris, France, 1999.

[5] W. F. Smith and J. Hashemi, *Foundations of material science and engineering*. Boston: McGraw-Hill, 2006.

[6] J. L. Sullivan, "Creep and physical aging of composites," *Composites Science and Technology,* vol. 39, pp. 207-232, 1990.

[7] M. C. Cook, J. M. Henshaw, and D. Q. Houston, "Creep characterization of seven automotive composite materials," in *the proceedings of International SAMPE Technical Conference*, Memphis, TN, 2008.

[8] E. J. Barbero and M. J. Julius, "Time-temperature-age viscoelastic behavior of commercial polymer blends and felt filled polymers," *Mechanics of Advanced Materials and Structures,* vol. 11, pp. 287-300, 2004.

[9] I. Y. Gnip, S. Vaitkus, V. Kersulis, and S. Vejelis, "Experiments for the long-term prediction of creep strain of expanded polystyrene under compressive stress," *Polymer Testing,* vol. 29, pp. 693-700.

[10] I. Y. Gnip, S. Vaitkus, V. Keršulis, and S. Vejelis, "Long-term prediction of compressive creep development in expanded polystyrene," *Polymer Testing,* vol. 27, pp. 378-391, 2008.

[11] I. Y. Gnip, S. Vaitkus, V. Keršulis, and S. Vėjelis, "Analytical description of the creep of expanded polystyrene (EPS) under long-term compressive loading," *Polymer Testing,* vol. 30, pp. 493-500, 2011.

[12] F. R. Schwarzl and F. Zahradnik, "The time temperature position of the glass-rubber transition of amorphous polymers and the free volume," *Rheologica Acta,* vol. 19, pp. 137-152, 1980.

[13] C. Marston, B. Gabbitas, J. Adams, S. Nutt, P. Marshall, and C. Galiotis, "Failure characteristics in carbon/epoxy composite tows," *Composites Part A: Applied Science and Manufacturing,* vol. 27, pp. 1183-1194, 1996.

[14] P. W. M. Peters, J. Hemptenmacher, K. Weber, and H. Assler, "Fiber dominant tensile and creep strength at 600°C of SCS-6 fiber reinforced titanium alloys," *Journal of Composites Technology and Research,* vol. 24, pp. 246-253, 2002.

[15] F. M. Zhao, T. Okabe, and N. Takeda, "The estimation of statistical fiber strength by fragmentation tests of single-fiber composites," *Composites Science and Technology,* vol. 60, pp. 1965-1974, 2000.

[16] R. Bedi and R. Chandra, "Fatigue-life distributions and failure probability for glass-fiber reinforced polymeric composites," *Composites Science and Technology,* vol. 69, pp. 1381-1387, 2009.

[17] X. Diao, L. Ye, and Y.-W. Mai, "A statistical model of residual strength and fatigue life of composite laminates," *Composites Science and Technology,* vol. 54, pp. 329-336, 1995.

[18] X. Diao, L. B. Lessard, and M. M. Shokrieh, "Statistical model for multiaxial fatigue behavior of unidirectional plies," *Composites Science and Technology,* vol. 59, pp. 2025-2035, 1999.

[19] H. H. Hilton, J. Hsu, and J. S. Kirby, "Linear viscoelastic analysis with random material properties," *Probabilistic Engineering Mechanics,* vol. 6, pp. 57-69, 1991.

[20] R. F. Gibson, *Principles of composite material mechanics*, 3 ed. Boca Raton: CRC Press, 2011.

[21] R. S. Lakes, *Viscoelastic solids*. Boca Raton: CRC Press, 1998.

[22] W. N. Findley, J. S. Lai, and K. Onaran, *Creep and relaxation of nonlinear viscoelastic materials: with an introduction to linear viscoelasticity*: Dover Publications, 1989.

[23] W. Flügge, *Viscoelasticity*, 2nd ed. New York: Springer, 1975.

[24] H. F. Brinson and L. C. Brinson, *Polymer engineering science and viscoelasticity: an introduction*. New York: Springer Verlag, 2008.

[25] M. Michaeli, A. Shtark, H. Grosbein, E. Altus, and H. H. Hilton, "A unified real time approach to characterizations of isotropic linear viscoelastic media from 1-D experiments without use of poisson's ratios," in *the proceedings of 54th AIAA/ASME/ASCE/AHS/ASC Structures, Structural Dynamics, and Materials Conference*, Boston, Massachusetts, 2013.

[26] V. Shunmugasamy, D. Pinisetty, and N. Gupta, "Viscoelastic properties of hollow glass particle filled vinyl ester matrix syntactic foams: effect of temperature and loading frequency," *Journal of Materials Science,* vol. 48, pp. 1685-1701, 2013.

[27] S. Kumar, B. K. Satapathy, and A. Patnaik, "Viscoelastic interpretations of erosion performance of short aramid fibre reinforced vinyl ester resin composites," *Journal of Materials Science,* vol. 46, pp. 7489-7500, 2011.

[28] F. Vautard, S. Ozcan, and H. Meyer, "Properties of thermo-chemically surface treated carbon fibers and of their epoxy and vinyl ester composites," *Composites Part A: Applied Science and Manufacturing,* vol. 43, pp. 1120-1133, 2012.

[29] J. Lee, S. Nouranian, G. W. Torres, T. E. Lacy, H. Toghiani, C. U. Pittman Jr, and J. L. Dubien, "Characterization, prediction, and optimization of flexural properties of vapor-grown carbon nanofiber/vinyl ester nanocomposites by response surface modeling," *Journal of Applied Polymer Science,* vol. 130, pp. 2087-2099, 2013.

[30] G. W. Torres, S. Nouranian, T. E. Lacy, H. Toghiani, C. U. Pittman Jr, and J. L. Dubien, "Statistical characterization of the impact strengths of vapor-grown carbon nanofiber/vinyl ester nanocomposites using a central composite design," *Journal of Applied Polymer Science,* vol. 128, pp. 1070-1080, 2013.

[31] V. P. McConnell, "Vinyl esters get radical in composite markets," *Reinforced Plastics,* vol. 54, pp. 34-38, 2010.

[32] H. Y. Yeh and S. C. Yang, "Building of a composite transmission tower," *Journal of Reinforced Plastics and Composites,* vol. 16, p. 414, 1997.

[33] K. Liao, R. Altkorn, S. Milkovich, J. Fildes, J. Gomez, C. Schultheisz, D. Hunston, and L. Brinson, "Long-term durability of glass-fiber reinforced composites in infrastructure applications," *Journal of advanced materials,* vol. 28, pp. 54-63, 1997.

[34] C. A. Harper, *Handbook of plastics, elastomers, and composites*. New York, NY: McGraw-Hill Professional, 2002.

[35] W. K. Goertzen and M. R. Kessler, "Creep behavior of carbon fiber/epoxy matrix composites," *Materials Science and Engineering A,* vol. 421, pp. 217-225, 2006.

[36] M. Katouzian, O. S. Brueller, and A. Horoschenkoff, "Effect of temperature on the creep behavior of neat and carbon fiber reinforced PEEK and epoxy resin," *Journal of Composite Materials,* vol. 29, pp. 372-387, 1995.

[37] S. L. Phoenix, P. Schwartz, and H. H. Robinson, "Statistics for the strength and lifetime in creep-rupture of model carbon/epoxy composites," *Composites Science and Technology,* vol. 32, pp. 81-120, 1988.

[38] D. J. Plazek and I. C. Choy, "Physical properties of bisphenol-A-based epoxy resins during and after curing. II. Creep behavior above and below the glass transition temperature," *Journal of Polymer Science, Part B: Polymer Physics,* vol. 27, pp. 307-324, 1989.

[39] K. Aniskevich and J. Hristova, "Creep of Polyester Resin Filled with Minerals," *Journal of Applied Polymer Science,* vol. 77, pp. 45-52, 2000.

[40] H. N. Dhakal, Z. Y. Zhang, and M. O. W. Richardson, "Creep behaviour of natural fibre reinforced unsaturated polyester composites," *Journal of Biobased Materials and Bioenergy,* vol. 3, pp. 232-237, 2009.

[41] H. Y. Jeon, S. H. Kim, and H. K. Yoo, "Assessment of long-term performances of polyester geogrids by accelerated creep test," *Polymer Testing,* vol. 21, pp. 489-495, 2002.

[42] C. Oudet and A. R. Bunsell, "Effects of structure on the tensile, creep and fatigue properties of polyester fibres," *Journal of Materials Science,* vol. 22, pp. 4292-4298, 1987.

[43] J. L. Sullivan, E. J. Blais, and D. Houston, "Physical aging in the creep behavior of thermosetting and thermoplastic composites," *Composites Science and Technology,* vol. 47, pp. 389-403, 1993.

[44] J. L. Sullivan, Y. F. Wen, and R. F. Gibson, "Universal aspects of composite viscoelastic behavior," *Polymer Composites,* vol. 16, pp. 3-9, 1995.

[45] S. W. Bradley, P. M. Puckett, W. L. Bradley, and H. J. Sue, "Viscoelastic creep characteristics of neat thermosets and thermosets reinforced with E-glass," *Journal of Composites Technology and Research,* vol. 20, pp. 51-58, 1998.

[46] D. Ståhlberg, L. O. Nordin, J. Varna, and M. Johansson, "Mechanical response of thermoset polymers under high compressive loads, 1," *Macromolecular Materials and Engineering,* vol. 290, pp. 1063-1072, 2005.

[47] A. Plaseied and A. Fatemi, "Tensile creep and deformation modeling of vinyl ester polymer and its nanocomposite," *Journal of Reinforced Plastics and Composites,* vol. 28, pp. 1775-1788, 2009.

[48] A. Almagableh, P. R. Mantena, and A. Alostaz, "Creep and stress relaxation modeling of vinyl ester nanocomposites reinforced by nanoclay and graphite platelets," *Journal of Applied Polymer Science,* vol. 115, pp. 1635-1641, 2010.

[49] ASTM Standard D 638M-89, Standard Test Methods for Tensile Properties of Plastics, American Society of Testing and Materials, West Conshohocken, PA, Vol. 08.01, 1998.

[50] S. Nouranian, "Vapor-grown carbon nanofiber/vinyl ester nanocomposites: Designed experimental study of mechanical properties and molecular dynamics simulations," Ph.D. Dissertation, Department of Chemical Engineering, Mississippi State University, 2011.

[51] ASTM Standard D 2990-77, Standard Test Methods for Tensile, Compressive, and Flexural Creep and Creep-Rupture of Plastics, American Society of Testing and Materials, West Conshohocken, PA, Vol. 08.01, 1998.

[52] A. G. Bluman, *Elementary statistics*, 8th ed. New York: McGraw Hill, 2011.

[53] J. A. Collins, *Failure of materials in mechanical design: analysis, prediction, prevention*, 2nd ed. New York: John Wiley & Sons, Inc., 1993.

[54] A. Plaseied and A. Fatemi, "Fatigue Behavior of Vinyl Ester Polymer and Effects of Carbon Nanofiber Reinforcement," in *ICF12, Ottawa 2009*, 2013.

[55] R. M. Christensen, *Theory of viscoelasticity: an introduction*. Mineola, NY: Dover Publications, Inc., 1982.

[56] J. Ferry, *Viscoelasticity properties of polymers*. New York, NY: Wiley, 1980.

[57] R. A. Schapery, "A simple collocation method for fitting viscoelastic models to experimental data," in *Rep. GALCIT SM 61-23A* ed, 1961.

[58] R. A. Schapery, "Stress analysis of viscoelastic composite materials," *Journal of Composite Materials,* vol. 1, pp. 228-267, 1967.

[59] T. L. Cost and B. Becker, "Multidata method of approximate Laplace transform inversion," *International Journal for Numerical Methods in Engineering* vol. 2, pp. 207-219, 1970.

[60] N. W. Tschoegl and I. Emri, "Generating line spectra from experimental responses. Part III: Interconversion between relaxation and retardation behavior," *International Journal of Polymeric Materials.,* vol. 18, pp. 117-127, 1992.

[61] N. Tschoegl and I. Emri, "Generating line spectra from experimental responses. Part II: Storage and loss functions," *Rheologica Acta,* vol. 32, pp. 322-327, 1993.

[62] N. W. Tschoegl and I. Emri, "Generating line spectra from experimental responses. Part I: Relaxation modulus and creep compliance," *Rheologica Acta,* vol. 32, pp. 311-322, 1993.

[63] S. W. Park and R.A. Schapery, " Methods of interconversion between linear viscoelastic material functions. Part I: A numerical method based on Prony Series," *International Journal of Solids and Structures,,* vol. 36, p. 1653-1675, 1999.

[64] S. W. Park and Y. R. Kim, "Fitting prony-series viscoelastic models with power-law presmoothing," *Journal of Materials in Civil Engineering,* vol. 13, pp. 26-32, 2001.

[65] R. D. Bradshaw and L. C. Brinson, "A sign control method for fitting and interconverting material functions for linearly viscoelastic solids," *Mechanics of Time-Dependent Materials,* vol. 1, pp. 85-108, 1997.

[66] M. Michaeli, A. Shtark, H. Grosbein, A. J. Steevens, and H. H. Hilton, "Analytical, experimental and computational viscoelastic material characterizations absent Poisson's ratios," in *the proceedings of 52nd AIAA/ASME/ASCE/AHS/ASC Structures, Structural Dynamics, and Materials Conference*, Denver, CO, 2011.

[67] W. G. Knauss and J. Zhao, "Improved relaxation time coverage in ramp-strain histories," *Mechanics of Time-Dependent Materials,* vol. 11, pp. 199-216, 2007.

[68] Q.-D. Zeng, L. Ling, and Z.-L. Wang, "Statistical strength of unidirectional composites and the effect of the interfacial shear strength," *Composites Science and Technology,* vol. 56, pp. 1191-1200, 1996.

[69] T. P. Philippidis and D. J. Lekou, "Probabilistic failure prediction for FRP composites," *Composites Science and Technology,* vol. 58, pp. 1973-1982, 1998.

[70] S. W. Yang and W. K. Chin, "Mechanical properties of aligned long glass fiber reinforced polypropylene. I: tensile strength," *Polymer Composites,* vol. 20, pp. 200-206, 1999.

[71] M. R. Gurvich and R. B. Pipes, "Strength size effect of laminated composites," *Composites Science and Technology,* vol. 55, pp. 93-105, 1995.

[72] L. Ferry, D. Perreux, D. Varchon, and J. Le Bras, "Tensile failure of filament-wound pipes under long-term creep loading: A probabilistic analysis," *Composites Science and Technology,* vol. 57, pp. 1281-1288, 1997.

[73] S. Behzadi, P. T. Curtis, and F. R. Jones, "Improving the prediction of tensile failure in unidirectional fibre composites by introducing matrix shear yielding," *Composites Science and Technology,* vol. 69, pp. 2421-2427, 2009.

[74] B. Dodson, *The Weibull analysis handbook*, 2nd ed. Milwaukee: ASQ Quality Press, 2006.

[75] G. Casella and R. Berger, *Statistical inference*, 2nd ed. Pacific Grove: Duxbury, 2002.

[76] A. Ang and W. Tang, *Probability concepts in engineering planning and design, Volume 1: Basic principles*, 1st ed. New York, NY: John Wiley & Sons, 1975.

[77] A. Papoulis and S. U. Pillai, *Probability, random variables, and stochastic processes*, 4th ed.: Tata McGraw-Hill Education, 2002.

[78] J. N. Reddy, *An introduction to the finite element method*, 3 ed. New York: McGraw-Hill 2005.

APPENDIX A

ISOCHRONOUS STRESS-STRAIN CURVES FOR TENSILE CREEP TESTS OF CURED DERAKANE 441-400

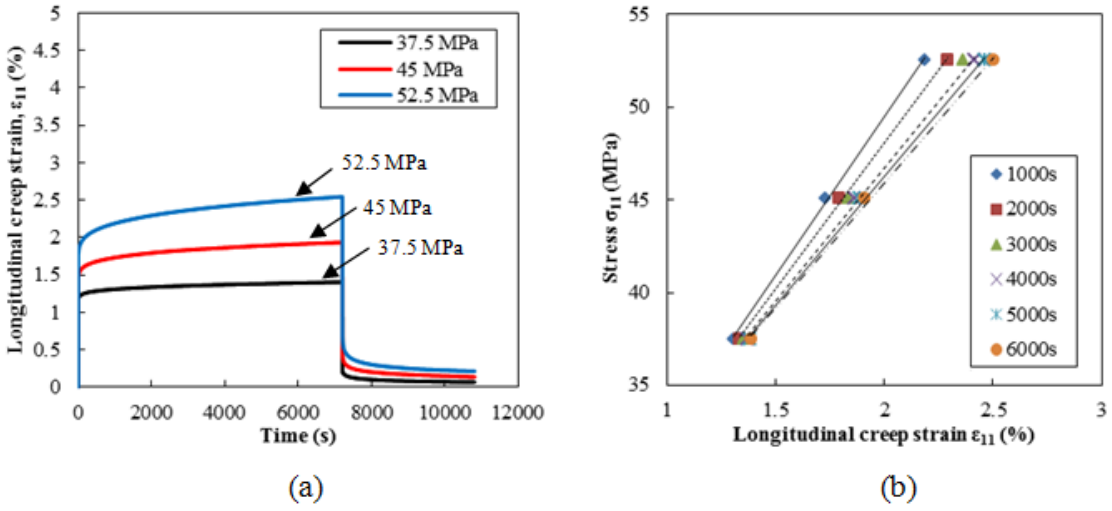

Figure A.1 (a) Longitudinal creep strain versus time responses $\varepsilon_{11}(t)$ of cured Derakane 441-400 at 24°C and 37.5 MPa, 45 MPa, 52.5 MPa, and (b) the corresponding isochronous stress-strain curves at selected times.

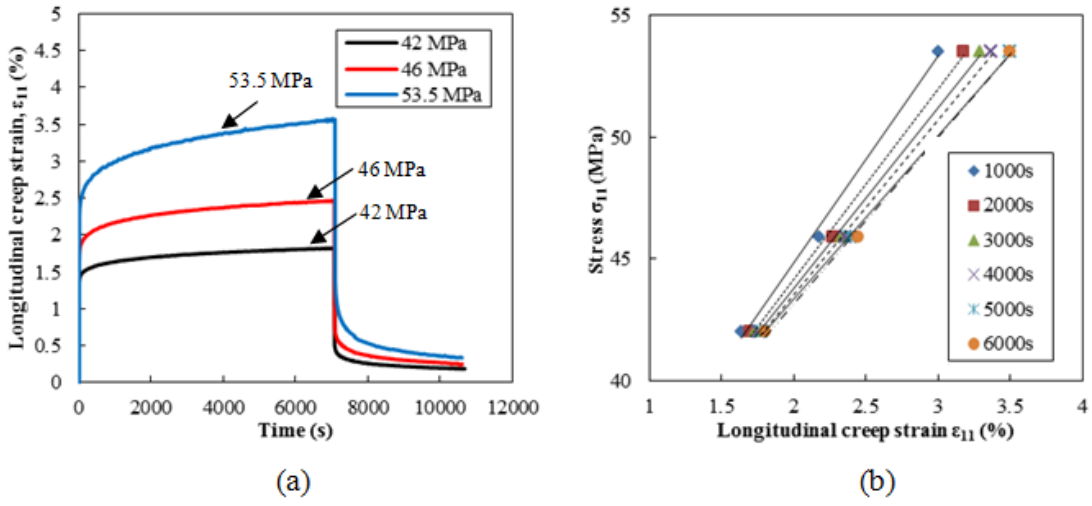

Figure A.2 (a) Longitudinal creep strain versus time responses $\varepsilon_{11}(t)$ of cured Derakane 441-400 at 40°C and 42 MPa, 46 MPa, 53.5 MPa, and (b) the corresponding isochronous stress-strain curves at selected times.

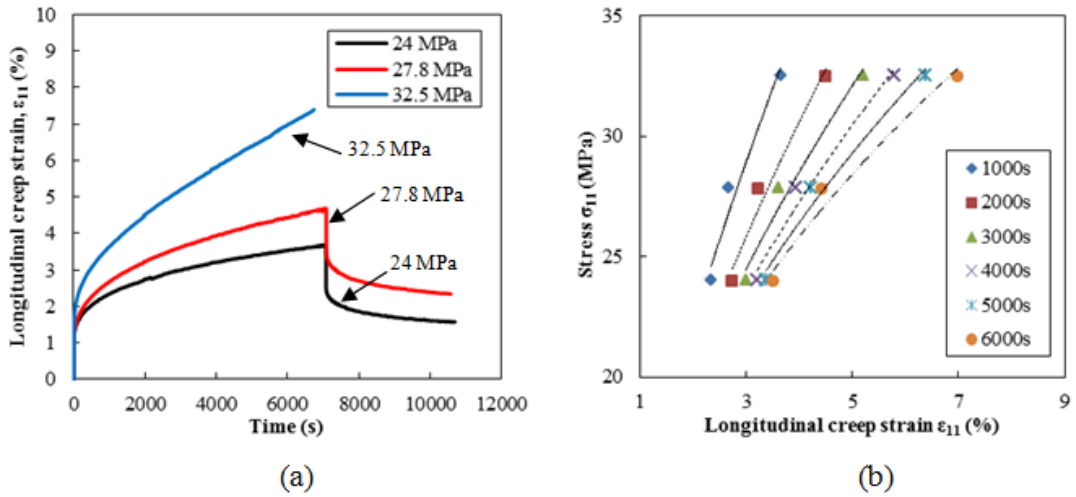

Figure A.3 (a) Longitudinal creep strain versus time responses $\varepsilon_{11}(t)$ of cured Derakane 441-400 at 80°C and 24 MPa, 27.8 MPa, 32.5 MPa, and (b) the corresponding isochronous stress-strain curves at selected times.

APPENDIX B

CREEP COMPLIANCE HISTOGRAMS OF CURED DERAKANE 441-400 AND THE CORRESPONDING WEIBULL AND LOG-NORMAL PROBABILITY DENSITY FUNCTIONS AT SELECTED TIMES

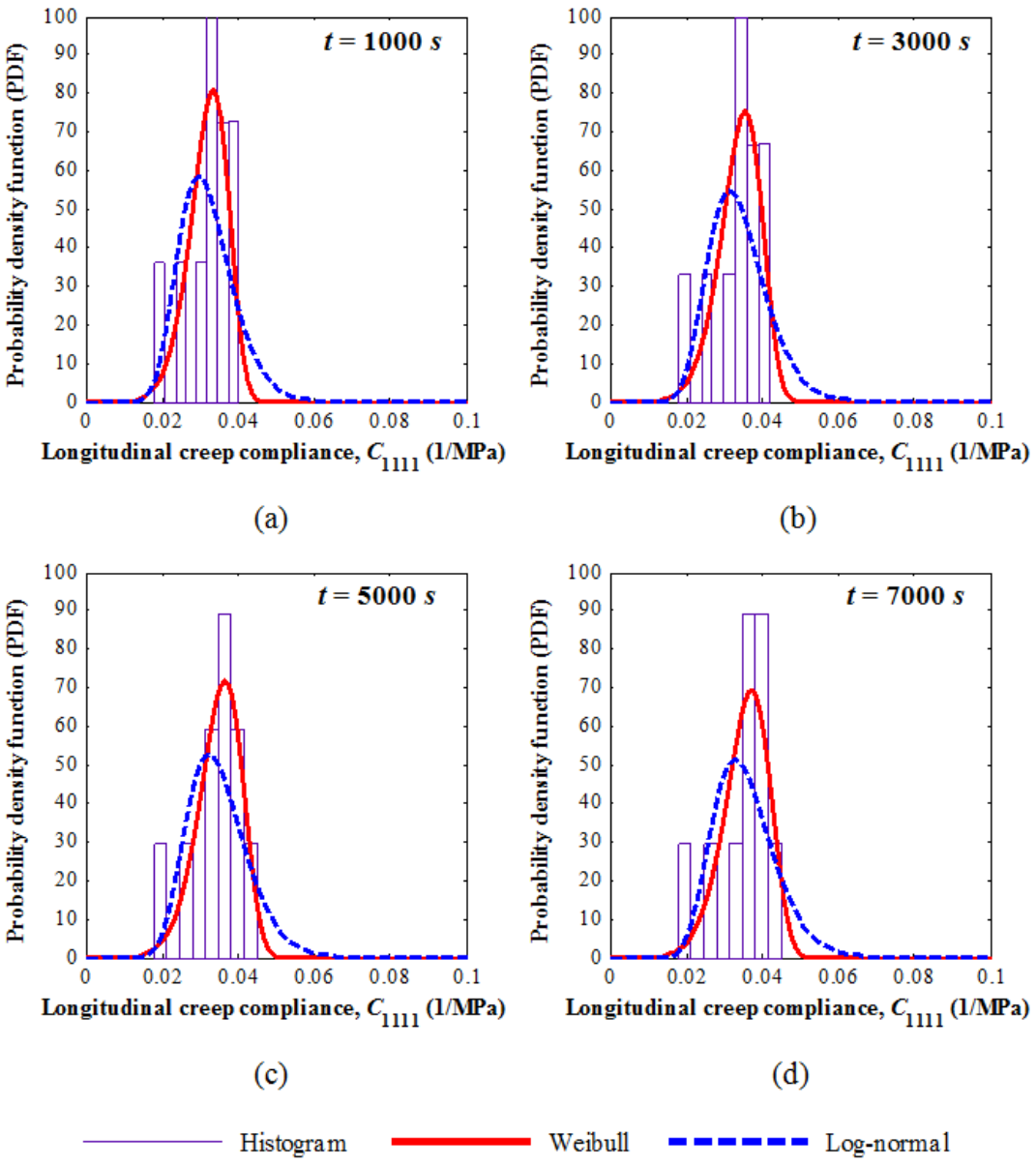

Figure B.1 The longitudinal creep compliance C_{1111} histograms of cured Derakane 441-400 and the corresponding Weibull and log-normal probability density functions at 24°C, 52.5 MPa (70% σ_u) at (a) t =1000 s, (b) t =3000 s, (c) t = 5000 s, and (d) t =7000 s

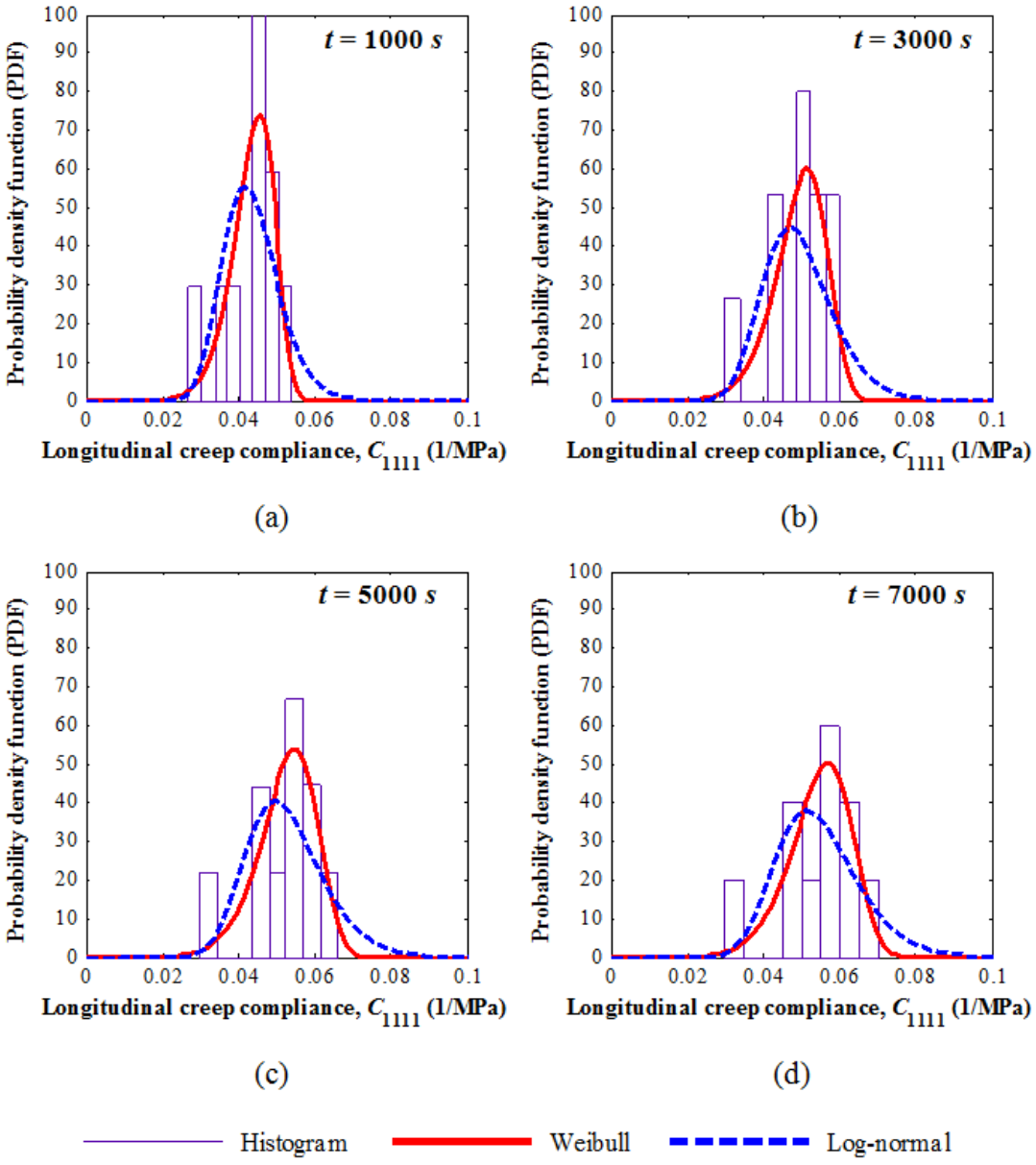

Figure B.2 The longitudinal creep compliance C_{1111} histograms of cured Derakane 441-400 and the corresponding Weibull and log-normal probability density functions at 60°C, 49.1 MPa (70% σ_u) at (a) t =1000 s, (b) t =3000 s, (c) t = 5000 s, and (d) t =7000 s.

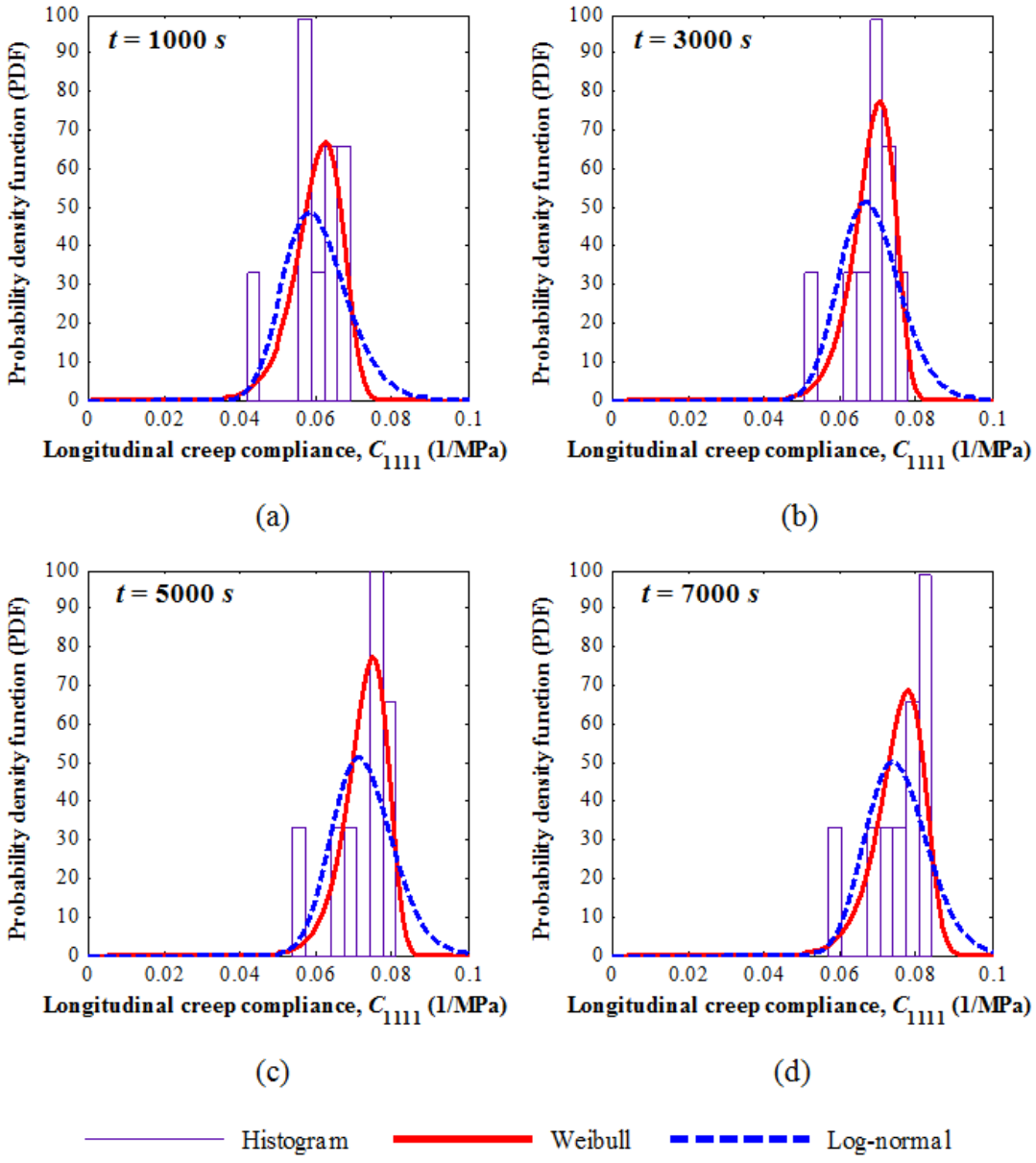

Figure B.3 The longitudinal creep compliance C_{1111} histograms of cured Derakane 441-400 and the corresponding Weibull and log-normal probability density functions at 60°C, 41.3MPa (70% σ_u) at (a) t =1000 s, (b) t =3000 s, (c) t = 5000 s, and (d) t =7000 s.

APPENDIX C

KOLMOGOROV-SMIRNOV TEST RESULTS

Table C.1 The maximum discrepancy D_{N_0} of the K-S tests for Weibull and log-normal distributions of longitudinal creep compliances C_{1111} of cured Derakane 441-400 at 24°C, 52.5 MPa (70% σ_u).

Time	Maximum Discrepancy, D_{N_0}	
	Weibull	**Log-normal**
1000 *s*	0.1599	0.2423
2000 *s*	0.1525	0.2371
3000 *s*	0.1481	0.2337
4000 *s*	0.1452	0.2312
5000 *s*	0.1432	0.2293
6000 *s*	0.1417	0.2277
7000 *s*	0.1599	0.2423

Table C.2 The maximum discrepancy D_{N_0} of the K-S tests for Weibull and log-normal distributions of longitudinal creep compliances C_{1111} of cured Derakane 441-400 at 40°C, 49.1 MPa (70% σ_u).

Time	Maximum Discrepancy, D_{N_0}	
	Weibull	**Log-normal**
1000 *s*	0.1971	0.2677
2000 *s*	0.1584	0.2380
3000 *s*	0.1430	0.2257
4000 *s*	0.1351	0.2191
5000 *s*	0.1305	0.2151
6000 *s*	0.1275	0.2123
7000 *s*	0.1971	0.2677

Table C.3 The maximum discrepancy D_{N_0} of the K-S tests for Weibull and log-normal distributions of longitudinal creep compliances C_{1111} of cured Derakane 441-400 at 60°C, 41.3 MPa (70% σ_u).

Time	Maximum Discrepancy, D_{N_0}	
	Weibull	**Log-normal**
1000 *s*	0.1601	0.2385
2000 *s*	0.2042	0.2258
3000 *s*	0.2380	0.2473
4000 *s*	0.2300	0.2433
5000 *s*	0.2274	0.2424
6000 *s*	0.2276	0.2432
7000 *s*	0.2165	0.2363

Table C.4 The maximum discrepancy D_{N_0} of the K-S tests for Weibull and log-normal distributions of transverse creep compliances C_{1122} of cured Derakane 441-400 at 24°C, 45 MPa (60% σ_u).

Time	Maximum Discrepancy, D_{N_0}	
	Weibull	**Log-normal**
1000 *s*	0.2231	0.2827
2000 *s*	0.1984	0.2665
3000 *s*	0.1819	0.2550
4000 *s*	0.1822	0.2463
5000 *s*	0.1815	0.2395
6000 *s*	0.1808	0.2341
7000 *s*	0.1804	0.2297

Table C.5 The maximum discrepancy D_{N_0} of the K-S tests for Weibull and log-normal distributions of transverse creep compliances C_{1122} of cured Derakane 441-400 at 40°C, 42.1 MPa (60% σ_u).

Time	Maximum Discrepancy, D_{N_0}	
	Weibull	**Log-normal**
1000 *s*	0.1223	0.1467
2000 *s*	0.1291	0.1600
3000 *s*	0.1303	0.1724
4000 *s*	0.1306	0.1818
5000 *s*	0.1309	0.1893
6000 *s*	0.1375	0.1954
7000 *s*	0.1431	0.2005

Table C.6 The maximum discrepancy D_{N_0} of the K-S tests for Weibull and log-normal distributions of transverse creep compliances C_{1122} of cured Derakane 441-400 at 60°C, 35.4 MPa (60% σ_u).

Time	Maximum Discrepancy, D_{N_0}	
	Weibull	**Log-normal**
1000 *s*	0.1556	0.1823
2000 *s*	0.1839	0.1962
3000 *s*	0.1846	0.1974
4000 *s*	0.1783	0.1946
5000 *s*	0.1721	0.1901
6000 *s*	0.1666	0.1851
7000 *s*	0.1618	0.1803

Table C.7 The maximum discrepancy D_{N_0} of the K-S tests for Weibull and log-normal distributions of transverse creep compliances C_{1122} of cured Derakane 441-400 at 24°C, 52.5 MPa (70% σ_u).

Time	Maximum Discrepancy, D_{N_0}	
	Weibull	**Log-normal**
1000 *s*	0.2000	0.2348
2000 *s*	0.1850	0.2234
3000 *s*	0.1624	0.2088
4000 *s*	0.1662	0.2106
5000 *s*	0.1742	0.2230
6000 *s*	0.1810	0.2331
7000 *s*	0.1840	0.2421

Table C.8 The maximum discrepancy D_{N_0} of the K-S tests for Weibull and log-normal distributions of transverse creep compliances C_{1122} of cured Derakane 441-400 at 40°C, 49.1 MPa (70% σ_u).

Time	Maximum Discrepancy, D_{N_0}	
	Weibull	**Log-normal**
1000 *s*	0.1546	0.2372
2000 *s*	0.1684	0.2569
3000 *s*	0.1706	0.2621
4000 *s*	0.1683	0.2617
5000 *s*	0.1628	0.2572
6000 *s*	0.1595	0.2509
7000 *s*	0.1690	0.2465

Table C.9 The maximum discrepancy D_{N_0} of the K-S tests for Weibull and log-normal distributions of transverse creep compliances C_{1122} of cured Derakane 441-400 at 60°C, 41.3 MPa (70% σ_u).

Time	**Maximum Discrepancy, D_{N_0}**	
	Weibull	**Log-normal**
1000 *s*	0.2283	0.1747
2000 *s*	0.1436	0.1294
3000 *s*	0.1536	0.1971
4000 *s*	0.1640	0.2037
5000 *s*	0.1702	0.2090
6000 *s*	0.1732	0.2124
7000 *s*	0.1802	0.2163

APPENDIX D

THE COMPARISON BETWEEN THE PREDICTED AND THE EXPERIMENTALLY OBTAINED CREEP COMPLIANCES OF CURED DERAKANE 441-400

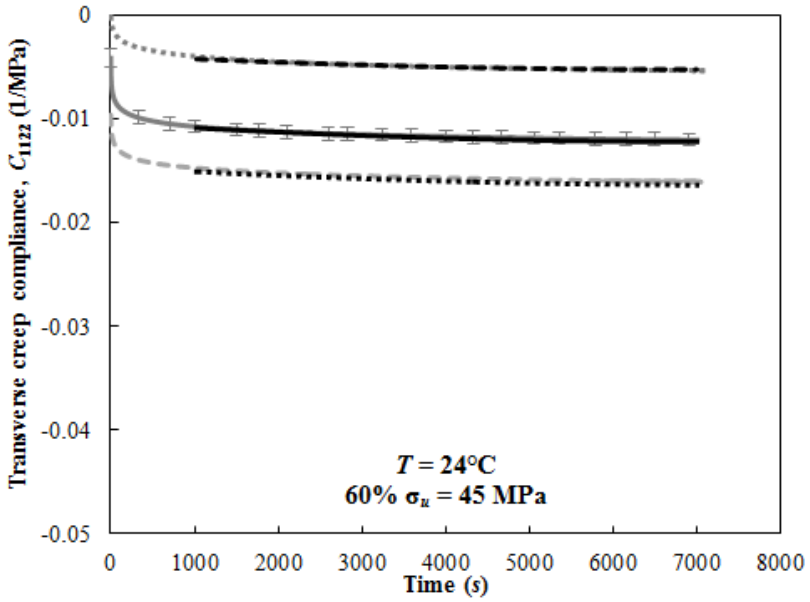

(a)

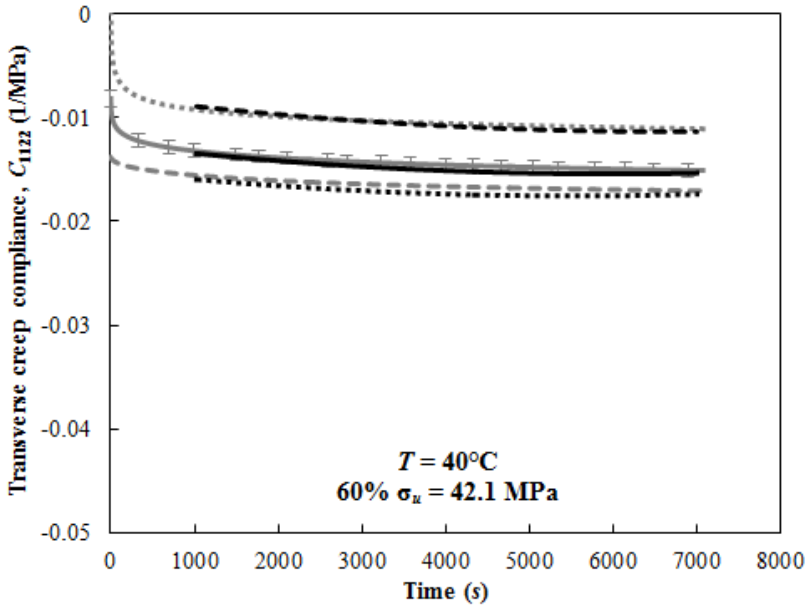

(b)

Figure D.1 Predicted creep compliance functions at CDF = 0.05, 0.5, 0.95, and the experimentally obtained lowest, mean, and highest creep compliances C_{1122} of cured Derakane 441-400 at 60% σ_u at T = (a) 24°C, (b) 40°C, and (c) 60°C.

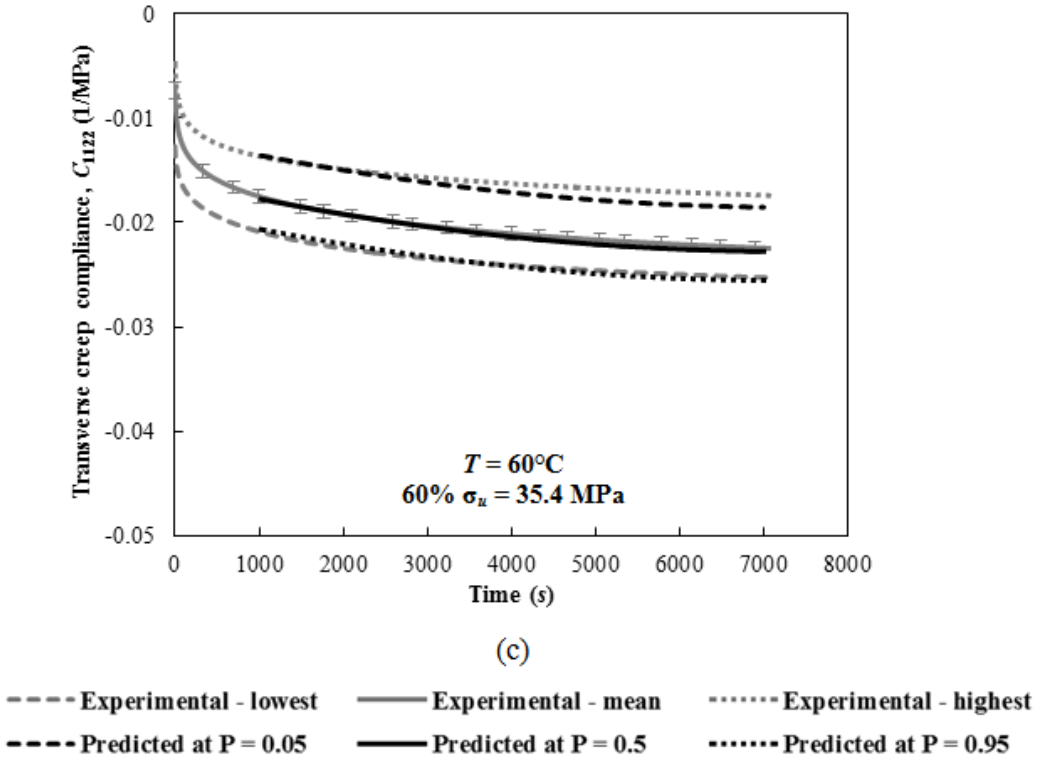

Figure D.1 (Continued)

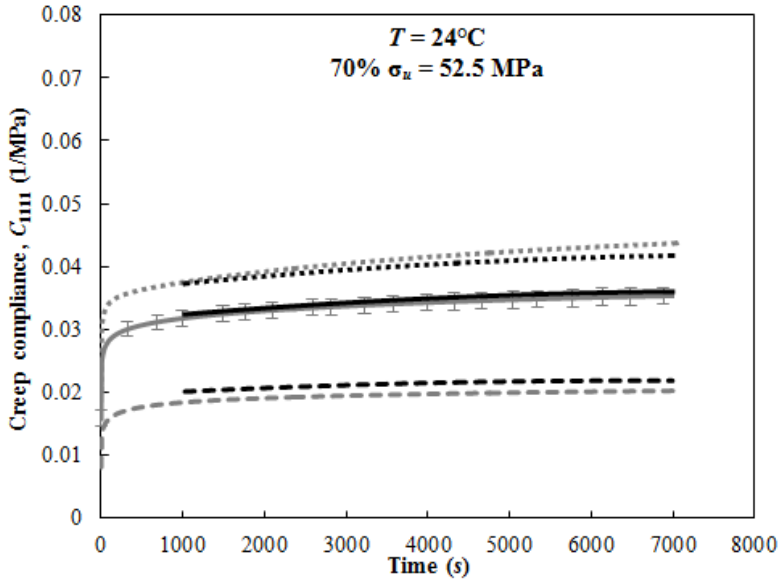

(a)

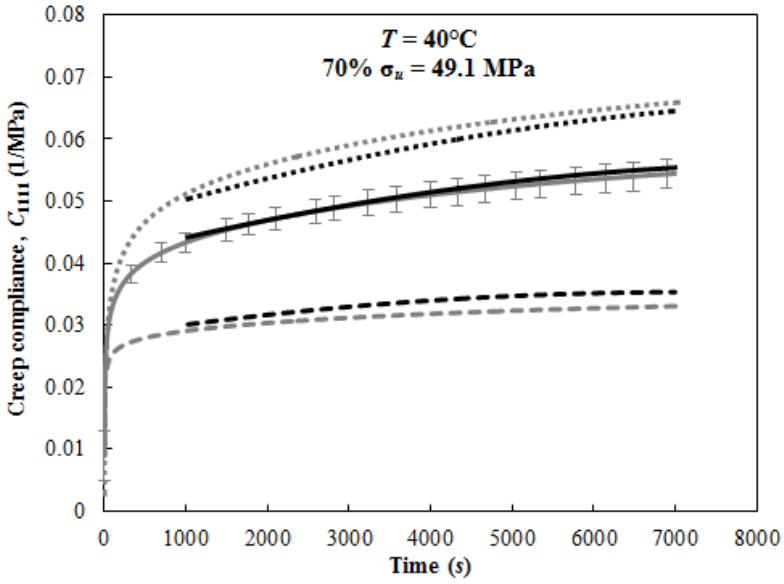

(b)

Figure D.2 Predicted creep compliance functions at CDF = 0.05, 0.5, 0.95, and the experimentally obtained lowest, mean, and highest creep compliances C_{1111} of cured Derakane 441-400 at 70% σ_u at T = (a) 24°C, (b) 40ºC, and (c) 60ºC.

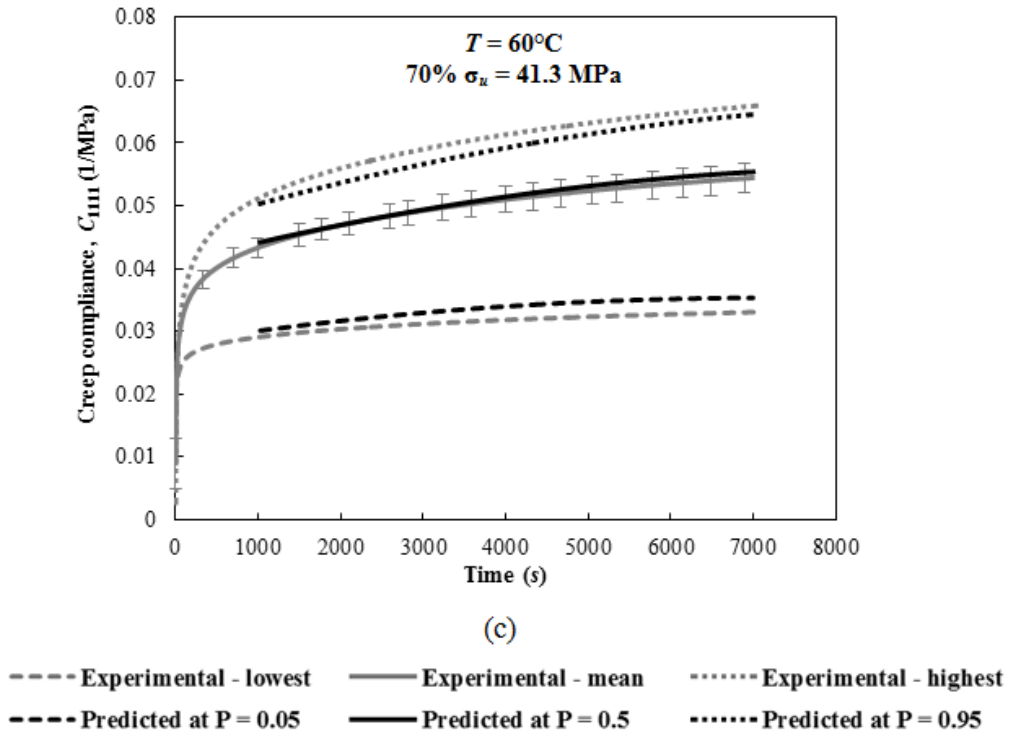

Figure D.2 (Continued)

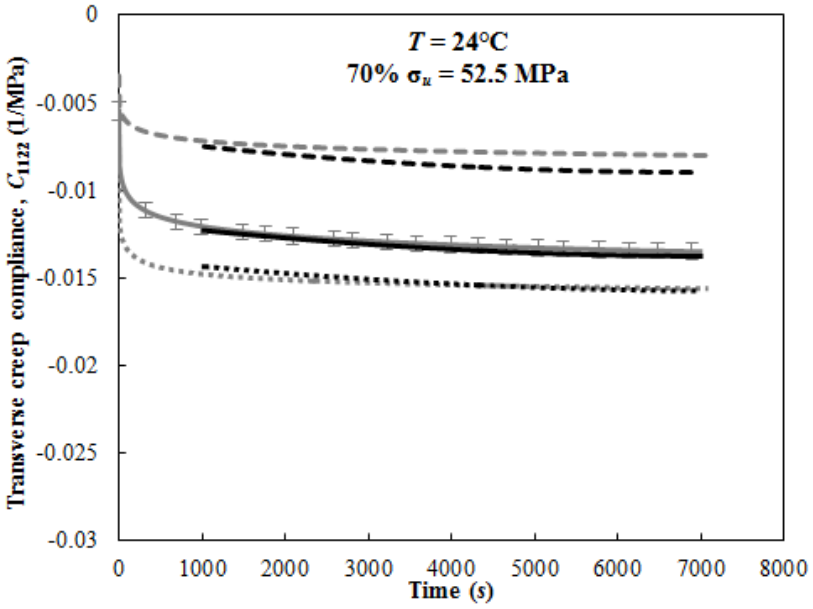

(a)

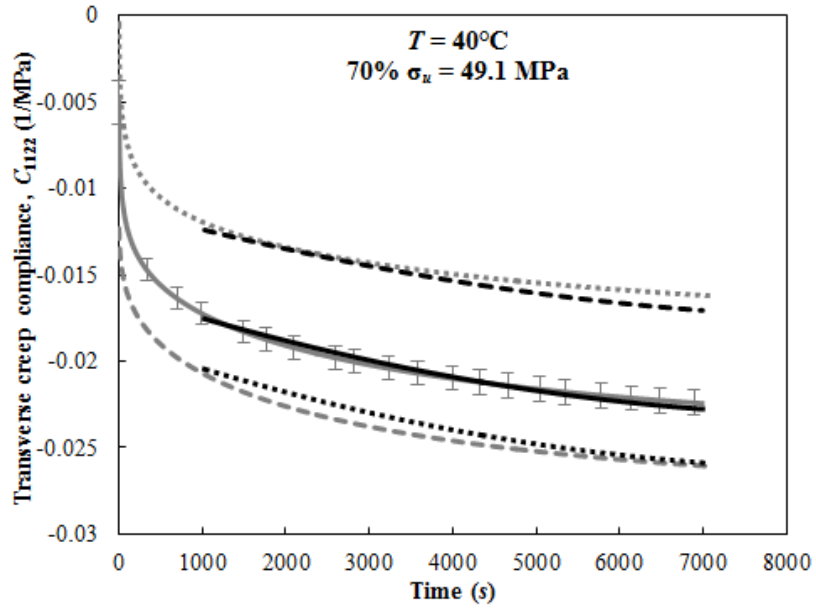

(b)

Figure D.3 Predicted creep compliance functions at CDF = 0.05, 0.5, 0.95, and the experimentally obtained lowest, mean, and highest creep compliances C_{1122} of cured Derakane 441-400 at 70% σ_u at T = (a) 24°C, (b) 40ºC, and (c) 60ºC.

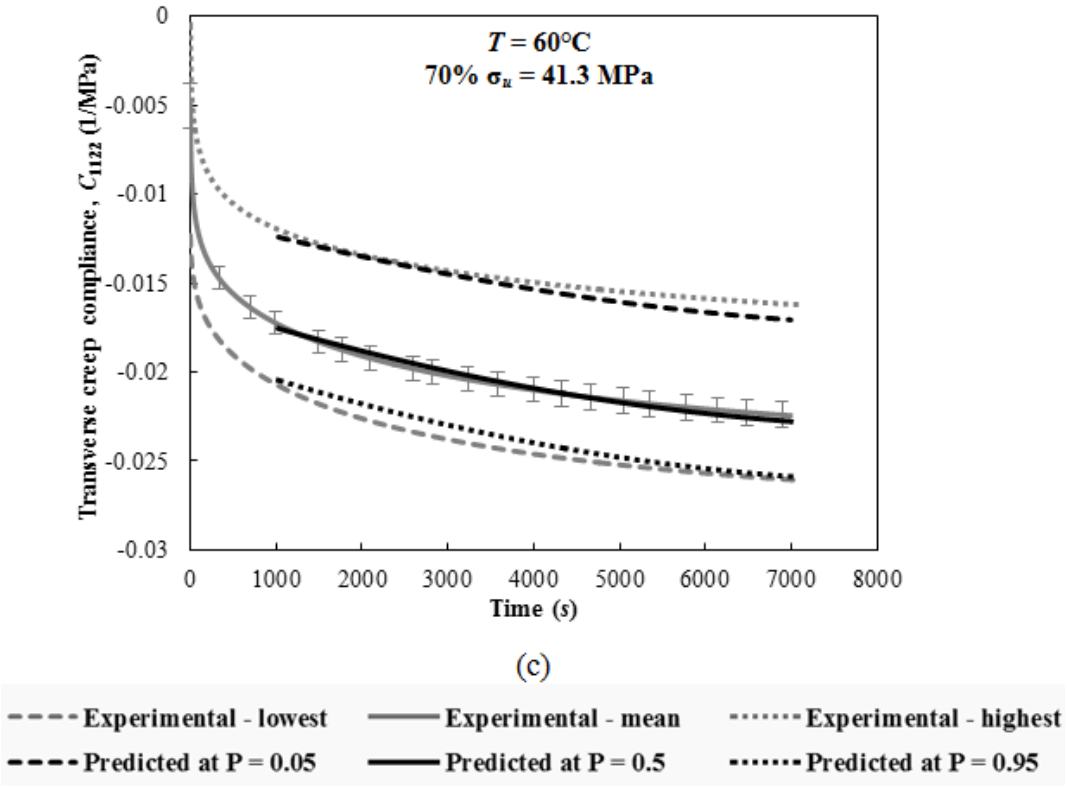

(c)

Figure D.3 (Continued)